**Ministry of Higher Education and Scientific Research**
**University of Baghdad**
**Institute of Laser for Postgraduate Studies**

# Investigation of modified CR39 surface by ArF laser as an SERS sensor

**A Thesis Submitted to the Institute of Laser for Postgraduate Studies, University of Baghdad in Partial Fulfillment of the Requirements for the Degree of Doctor of Philosophy in Laser / Electronic and Communication Engineering**

**By**

## Rana Mohammed Taha AlBayatti

B.Sc. Laser and Optoelectronics Engineering- 2001
M. Sc. Laser and Optoelectronics Engineering- 2004

**Supervisors**
**Asst. Prof. Dr. Hussein Ali Jawad**

**2017 AD** **1439 AH**

بسم الله الرحمن الرحيم

قالُواْ سُبْحَانَكَ لاَ عِلْمَ لَنَا إِلاَّ مَا عَلَّمْتَنَا إِنَّكَ أَنتَ الْعَلِيمُ الْحَكِيمُ

صدق الله العظيم

البقرة الاية/ ٣٢

## *Certification*

I certify that this thesis was prepared under our supervision at the Institute of Laser for Postgraduate Studies, University of Baghdad, in a partial fulfillment of requirements for the degree of a Doctor of Philosophy in Laser/Electronic and Communication Engineering.

Signature:
Name: **Dr. Hussein Ali Jawad**
Title: Assistant Professor
Address: Institute of laser for postgraduate studies,
University of Baghdad
Date: / / 2017

(Supervisor)

In view of the available recommendation, I forward this thesis for debate by Examining Committee.

Signature:
Name: **Asst. Prof. Dr. Shelan Khasro Tawfeeq**
Title: Head of the Scientific Committee.
Address: Institute of Laser for Postgraduate Studies,
University of Baghdad.
Date: / / 2017

# Examination Committee Certificate

We certify that we have read this thesis "Investigation of modified CR-39 surface by ArF laser as SERS sensor" and as examination committee we examined the student in its contents and in our opinion it is adequate with standards as a thesis for the degree of Doctor of Philosophy in Laser/ Electronic and Communication Engineering.

Signature:
Name: **Dr. Abdul Hadi M. Al-Janabi**
Title: Professor
Address: Institute of Laser for Postgraduate Studies, University of Baghdad.
Date: / / 2017
(Chairman)

Signature:
Name: **Dr. Bassam Ghalib Rasheed**
Title: Professor
Address: College of Engineering, Al-Nahrain University.
Date: / / 2017
(Member)

Signature:
Name: **Dr. Anwar Abdul satar**
Title: Assistant Professor
Address: College of Engineering, Al-Nahrain University.
Date: / / 2017
(Member)

Signature:
Name: **Dr. Zainab Fadhil Mahdi**
Title: Assistant Professor
Address: Institute of Laser for Postgraduate Studies, University of Baghdad.
Date: / / 2017
(Member)

Signature:
Name: **Dr. Tahreer safaa Masour**
Title: Assistant Professor
Address: Institute of Laser for Postgraduate Studies, University of Baghdad
Date: / / 2017
(Member)

Signature:
Name: **Dr. Hussein Ali Jawad**
Title: Assistant Professor
Address: Institute of Laser for Postgraduate Studies, University of Baghdad
Date: / / 2017
(Supervisor)

Approved by the deanship of Institute of Laser for Postgraduate Studies, University of Baghdad,

Signature:
Name: **Prof. Dr. Abdul Hadi M. Al-Janabi**
Title: Dean
Address: Institute of Laser for Postgraduate Studies, University of Baghdad.
Date: / / 2017.

# Dedication

*To the memory of my father and my mother who I still miss them every day. To Ali, my amazing husband whose scarified care for me and our children, made it possible for me to complete this work. To my two brothers and my sister for all their supports. To my sons Saif and Zain who are indeed a treasure from the lord.*

# Acknowledgment

I would like to express my sincere appreciation and thanks to my supervisor **Assistant Prof. Hussein Ali Jawad** for his thoughtful guidance, continuous support and unwavering encouragement during this work.

I would also like to thank the dean of the institute of Laser for postgraduate studies **Prof. Abdul hadi M. Al-Janabi** for his help and support during the PhD courses and after.

I would also like to thank my **co-supervisor Prof. Parviz Parvin** for their outstanding academic support during my stay in Iran and all members of photonics group at Amirkabir University of technology especially my friend **Dr. Refah Zadeh** for sharing their extensive knowledge with me.

**Also,** Special thanks to all members in my institute, especially my friend **Hiba**, who inspired me to pursue a PhD degree.

**Finally**, I am deeply grateful to my husband **Ali** for all his support and encouragement over the years.

**Abstract**

The development of highly sensitive biosensor that susceptible of detection and identification of a trace levels of biomedical contaminants in nature has become an efficient field of researches. Raman spectroscopy is a powerful technique for molecular characterization. Unfortunately, its signal is inherently weak. A surface enhancement Raman scattering has facilitated molecular detection since it provides a remarkable enhancement of weak Raman signal.

In this work, a two- dimensional finite element model is performed for a better understanding of the involved physical approach in laser-polymer ablation process followed by an experimental demonstrations to produce a surface enhancement Raman scattering substrate through laser ablation process.

A 193 nm ArF Excimer laser with a maximum pulse energy of 275 mJ, 15 ns pulse duration and a repetition rate of 1 Hz is utilized to irradiate CR39 polymer samples. Thiophenol and Methylene blue are used for surface enhanced Raman scattering characterization and biosensing application respectively.

A surface enhanced Raman scattering substrate is engineered upon laser irradiation that induces a periodic surface structures, commonly known as Laser Induced Periodic Surface Structures of three different morphologies (nanochains, contours, grooves) on surface of CR39 polymer with a periodicity of 630 - 822 nm at a fluence range above the investigated ablation threshold (250 $mJ/cm^2$). The ablation threshold is found to match considerably well with simulation results for the case of repetitive laser pulses. Then the produced nanostructured surface is coated with gold layer of various thickness.

The capability of the produced substrate for surface enhanced Raman scattering is evaluated through thiophenol as an analyte molecule. It is observed that the Laser Induced Periodic Surface Structures of grooves

like nanostructures coated with a gold layer of 30 nm thickness gives a best enhancement factor in the range from $0.9*10^8$ to $2*10^8$ which is suitable for a single- molecules sensitivity.

The potential of the produced substrate as a surface enhanced Raman scattering biosensor is investigated through Methylene blue. The biosensor sensitivity is characterized by detecting low concentration of Methylene blue with a detection limit of 0.1 μM.

# *LIST OF CONTENTS*

# *LIST OF SYMBOLS*

| SYMBOLS | DESCRIPTION | UNITS |
|---|---|---|
| $E$ | Electric field of the incident laser light. | V/m |
| $E_0$ | Amplitude of the oscillating electric field | V/m |
| $f_0$ | Frequency of the incident laser light. | Hz |
| $t$ | time | s |
| $P$ | Electric dipole moment | C.m |
| $\alpha$ | polarisability of the molecule | $C.m^2.V^{-1}$ |
| $\alpha_0$ | equilibrium polarisability | $C.m^2.V^{-1}$ |
| $q_0$ | vibrational amplitude | $m/s^2$ |
| $\Delta q$ | displacement | cm |
| $f_m$ | frequency of the vibrational mode | Hz |
| $I_R$ | Intensity of Raman active band | $W/cm^2$ |
| $I_0$ | Intensity of the incident laser light. | $W/cm^2$ |
| $P_R$ | Induces Raman dipole | C.m |
| $E_{loc(w_l)}$ | local electric field | V/m |
| $M_{loc}$ | Local intensity enhancement | - |
| $M_s$ | Scattering enhancement | - |
| $AEF$ | analytical enhancement factor | - |
| $I_{SERS}$ | SERS intensity | $W/cm^2$ |
| $I_{RS}$ | normal Raman scattering intensity | $W/cm^2$ |
| $C_{RS}$ | Concentration of normal Raman | M |
| $C_{SERS}$ | Concentration of SERS | M |
| $SSEF$ | SERS substrate enhancement factor | - |
| $N_{vol}$ | Average molecular number in the scattering volume | mol |
| $N_{SERS}$ | Number of adsorbed molecules on the optically probed SERS substrate | mol |
| $A$ | laser spot area, | $cm^2$ |
| $h$ | path length, | cm |
| $\rho$ | density of the analyte | $g/cm^3$ |
| $M$ | molecular weight of the analyte | g/mol |
| $C$ | Molar concentration | M |
| $V$ | Volume of analyte solution respectively | L |
| $S$ | Geometrical area of analyte casting film | $cm^2$ |
| $\varepsilon(w)$ | Dielectric function | - |

| SYMBOLS | DESCRIPTION | UNITS |
|---|---|---|
| $w_P$ | plasma frequency of the free electron | Hz |
| $\gamma$ | Characteristics collision rate | Hz |
| $n$ | Electron density | $1/m^3$ |
| $e$ | Elementary charge | Col. |
| $m$ | Electron mass | g |
| $\varepsilon_0$ | Free space permittivity | F/m |
| $d(F)$ | Ablation rate | nm/pulse |
| $\alpha_{eff}$ | Effective absorption coefficient | $cm^{-1}$ |
| $F$ | Laser fluence | $J/cm^2$ |
| $F_{th}$ | Ablation threshold fluence | $J/cm^2$ |
| $c_p$ | Specific heat | J/Kg.K |
| $k$ | Thermal conductivity | W/m.K |
| $Q(z,t)$ | Distribution of the absorbed laser fluence | $W/cm^3$ |
| $T$ | Temperature | K |
| $I_s\,(t)$ | Temporal laser irradiance | $W/cm^2$ |
| $R$ | Reflectivity | - |
| $\alpha_1$ | Absorption coefficient | $cm^{-1}$ |
| $z$ | Distance | cm |
| $\Lambda$ | Periodicity | nm |
| $\lambda$ | wavelength | nm |

# *LIST OF ABBREVIATIONS*

| ABBREVIATION | DESCRIPTION |
|---|---|
| SERS | Surface Enhancement Raman Scattering (SERS) |
| EM | Electromagnetic field |
| MNPs | Metallic nanoparticles |
| ArF | Argon Fluoride |
| LIPSS | Laser induced periodic surface structures |
| FEM | finite element model |
| UV | Ultraviolet |
| IR | Infrared |
| Au | Gold |
| Ag | Silver |
| EFs | Enhancement factors |
| CE | Chemical enhancement |
| LSP | Localized surface Plasmon's |
| SPPs | Surface Plasmon polaritons |
| LSPPS | Localized SPPS |
| PSPPS | Propagating SPPS |
| AEF | Analytical enhancement factor |
| SSEF | SERS substrate enhancement factor |
| NIR | Near Infrared |
| PMDS | polydimethylsiloxane |
| NSL | Nanosphere lithography |
| EBL | Electron beam lithography |
| Ar | Argon |
| Kr | Krypton |
| Xe | Xenon |
| F | Fluorine |
| Cl | Chlorine |
| ADC | Allyl diglycol carbonate |
| PI | Polyimide allyl diglycol carbonate (ADC), |
| PMMA | Poly(methyl methacrylate) |
| PS | Polystyrene |
| PC | Polycarbonate |
| LSFL | Low spatial frequency LIPSS |
| TP | Thiophenol |
| SAM | Self-assembled monolayer |

| ABBREVIATION | DESCRIPTION |
|---|---|
| MB | Methylene blue |
| F2 | fluorine laser |
| PET | Polyethylene terephthalate |
| KrF | Krypton fluoride |
| Pt | platinum |
| Nd:YAG | Neodymium Yttrium Aluminum Garnet |
| PLLA | poly(lactic acid) |
| PHB | polyhydroxybutyrate |
| FBG | fiber Bragg grating |
| FTIR | Fourier Transform Infrared |
| SEM | Scanning electron microscopy |
| AFM | Atomic Force Microscopy |
| DI | Deionized water |
| TGA | Thermogravimetric analysis |
| ATR | Attenuated total reflectance |
| NA | Numerical aperture |
| $R_a$ | surface roughness |
| N | Number of pulses |
| $T_g$ | Glass transition temperature |
| $T_m$ | Melting temperature |
| 3-D | Three- dimensional |

# *LIST OF TABLES*



# *LIST OF FIGURES*

# CHAPTER ONE

## Introduction and Basic Concepts

## 1.1 Introduction

Ultrasensitive detection of biological and chemical species is significant in a wide range of technological and scientific fields ranging from biomolecular diagnostics, materials and analytical chemistry [1-5] to the monitoring of pollutant, pharmaceutical drugs and explosives [6-8]. Among many analytical techniques, Surface Enhancement Raman Scattering (SERS) is the most promising technique in detection of traces of molecules due to its high molecular specificity and high sensitivity [9-17]. SERS is a plasmonic phenomenon whereby molecules at or near surface of a metallic nanostructures encounter a spectacular increase in the incident electromagnetic field (EM) [18]. It is probable that many of "hot spots" are created between neighboring material particles leading to the SERS capability. As a result, the weak Raman signal is enhanced by many order of magnitude and leads to prominent sensitivities that reach the limit of detecting a single molecule and enable SERS substrates for use in enormous biological inspections, biosensor or environmental analysis [10, 19-21].

Since the discovery of SERS effect, an extensive studies have been promoted for producing substantial substrate structures. The commonly used techniques comprise metallic nanoparticles (MNPs) in suspension, roughened metallic electrodes and metallic structure substrate. While all produced SERS capable surfaces, they either depend on random processes or expensive producing equipment leading to prevent cost effective commercialization [22-24]. An alternative technique is to utilize a laser based nanostructuring resulting in the generation of Laser Induced Periodic Surface Structures (LIPSS). LIPSS was studied since 1965s [25]. It is a phenomenon that may happen by illumination of solid surfaces by intensive pulses of laser. It originates from the interference of the incident/ refracted laser light with the scattered or diffracted light near the surface. The periodicities of resulting structures is exceedingly related to the irradiating laser wavelength [26]. These structures can be generated on many types of

materials such as metals [27], semiconductors [28], and polymers [29] with lasers of various pulse durations from nanosecond (ns) to femtosecond (fs) and with various wavelengths from Ultraviolet (UV) to Infrared (IR) [30-32]. A leading technology used for this purpose is the excimer laser. The advantage of Excimer laser treatment over the other lasers types is the capability to process surfaces only within the sub micrometer scale without any damage to the bulk of the material. For most polymers, this is possible which is due to the fact that most of it reveals a high absorption for UV light and have low heat conduction properties [33].

In this thesis, the capability of a complex nanostructured substrate that consist of a polymeric substrate (nanostructured by pulsed laser ablation to induce a periodic surface structure (LIPSS) followed by coating with metal layer for SERS will be investigated.

## 1.2 Raman Spectroscopy

Raman spectroscopy is a vibrational spectroscopic and imaging technique based on an effect discovered by C. V. Raman and his collaborator K. S. Krishnan in 1928 [34]. The fundamental process of Raman effect is the transfer of energy between light and matter. This effect is observed when light is scattered from molecules in different vibrational and rotational states of a material and is characterized by corresponding energy exchange between the incident and scattered light [35]. When a laser light of frequency $f_0$ and electromagnetic field E interact with a sample, both elastic and inelastic scattering occur as shown in Fig.1.1 but most of the scattering that takes place is elastic with no energy loss and therefore no change in frequency, this is known as Rayleigh scattering. However, a small fraction of the scattered light subjects to inelastic or Raman scattering. The Raman effect involves two distinct types of scattering, known as stokes and anti-stokes scattering. The stoke scattering is the most likely to occur where the incident photon gives up energy to sample molecule. In this case, photon is

scattered with a red - shifted frequency. Anti- stokes scattering is the less probable and weaker effect, which happens when photon interacts with a molecule that is already in a vibrational excited state where the output has a blue - shifted frequency [36].

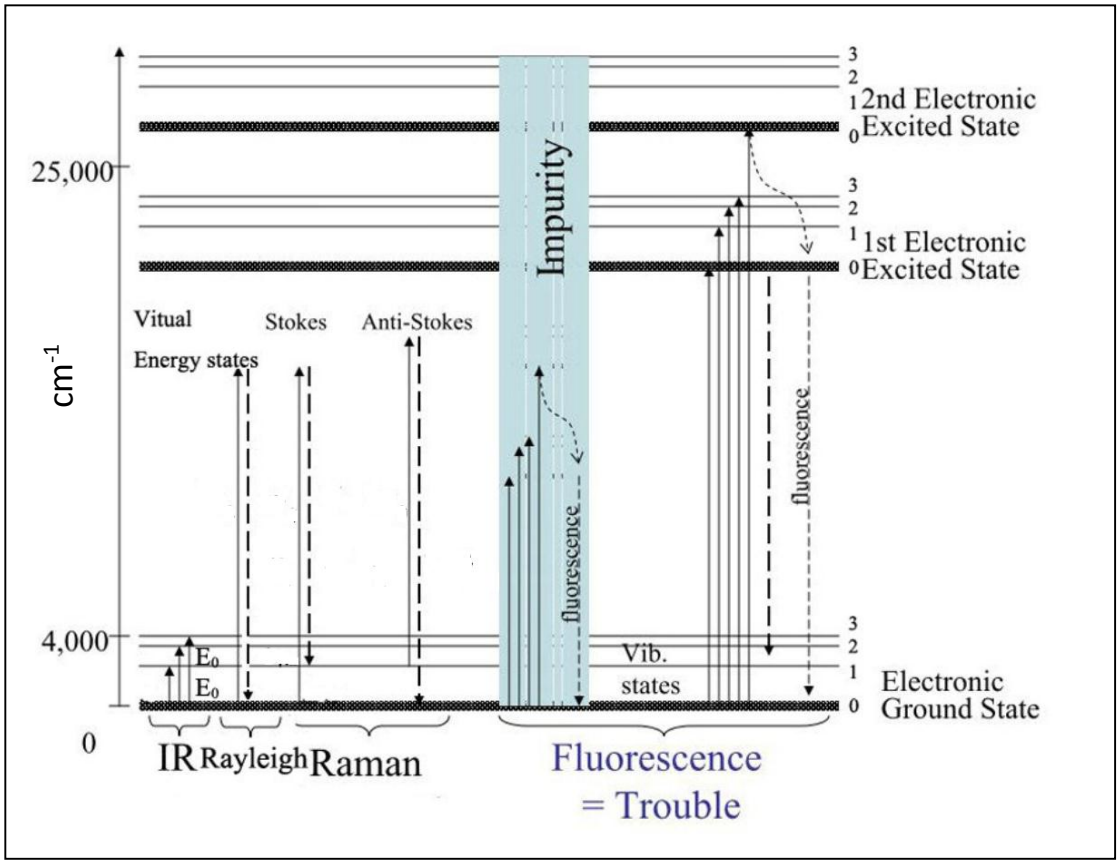


**Fig.1.1: Energy level diagram representing IR, Rayleigh, Raman and fluorescence processes [36].**

The frequency shift between the incident and the scattered photon represents the key to use Raman scattering for investigation of physiochemical structure of a material [37]. In most cases, the collected and analyzed photons in Raman scattering are stokes photons, denoted as stokes lines. However, a much weaker anti-stokes lines resulting from rarity anti-stokes photons are sometimes preferred in analysis due to absence of fluorescence interference which represents a big problem for stokes lines [36]. It is important to mention that fluorescence is much different from

Raman scattering. In fluorescence, the molecule is totally absorbed the incident photon which causes a change in electronic energy state. Subsequently, the molecule relaxes back to a lower energy state releasing a fluorescence photon [38] whereas Raman scattered photon is released instantaneously [36].

### 1.2.1 Measurement of Raman spectrum

The electric field of the incident laser on the sample is given by the following equation [35]:

$$E = E_0 \cos(2\pi f_0 t) \tag{1.1}$$

Where $E_0$ is the amplitude of the oscillating electric field.
The electric field will prompt an electric dipole moment $P$ in the sample molecule that is given by [35]:

$$P = \alpha E \tag{1.2}$$

where $\alpha$ is the polarisability of the molecule. It is a material property that depends on the structure of the material and the bond nature, it can be expanded around the equilibrium of the vibrating molecule with a small amplitude of vibration. It is given by [35]:

$$\alpha = \alpha_0 + [\frac{\partial \alpha}{\partial q}]_0 \Delta q + \text{-----} \tag{1.3}$$

Where $\alpha_0$ is the equilibrium polarisability, $q_0$ is the vibrational amplitude and $\Delta q$ is the displacement of the normal coordinates of vibrating molecules about their equilibrium position due to a specific vibrational mode and it is expressed by [35]:

$$\Delta q = q_0 \cos(2\pi f_m t) \quad (1.4)$$

*Where* $f_m$ is the frequency of the vibrational mode.

$$p = \alpha_0 E_0 \cos(2\pi f_0 t) + \frac{1}{2}\left[\frac{\partial \alpha}{\partial q}\right]_0 q_0 E_0 \left[\cos(2\pi\{f_0 - f_m\}t) + \cos(2\pi\{f_0 + f_m\}t)\right] \quad (1.5)$$

This equation performs an oscillating dipole which radiates three different frequencies of photons where the first term represents Rayleigh scattering that happens at the excitation frequency $f_0$. The second and third terms identifying stokes $(f_0 - f_m)$ and anti-stokes $(f_0 + f_m)$ Raman scattering respectively. The change in the frequency between the incident and scattered light is called Raman shift.

### 1.2.2 Existing of Raman Effect

For Raman spectroscopy, it is clearly that the Raman effect is occurred only if $\left[\frac{\partial \alpha}{\partial q}\right]_0 \neq 0$ which means that the molecular transitions from which a Raman shift happens can only be achieved optically if the corresponding vibration of the molecule change polarisability [39]. The intensity of Raman active band $(I_R)$ is determined by molecule polarisability, power and frequency of incident laser light. It is given by [35, 37]:

$$I_R = K I_0 (f_0 - f_m)^4 \left[\frac{\partial \alpha}{\partial q}\right]_0^2 \quad (1.6)$$

Where $K$ is the proportionality constant and $I_0$ is the intensity of the incident laser light. The frequencies of the vibrational modes are very small in comparison with the frequency of the excitation light, therefore the term

$(f_0 - f_m)^4$ is modified to $(f_0)^4$or $(\lambda)^{-4}$. This means that the intensity of Raman signal is inversely proportional to the forth power of the incident laser wavelength. Thus, a strong Raman signal can be achieved with shorter laser wavelength.

### 1.3 Enhancement of Raman Scattering

As mentioned earlier, Raman scattering is inherently a weak process in that only one in every $10^6$-$10^{10}$ photons is scattered inelastically [34, 37, 40]. The name SERS denotes that it provides the same information that produced from normal Raman scattering, simply with a highly enhanced signal [41]. SERS effect was discovered in 1974 by Fleischmann et al [23], they noticed an enhancement of Raman signal of pyridine adsorbed on roughened silver (Ag) surface. Since then, a series of experiment regarding this effect were published and confirmed that a dramatic enhancement of Raman signals of analytes with an enhancement factors (EFs) as high as $10^8$ can be produced using films of noble metal with roughened surface or nanoscale patterns where the EM field is more confined on this type of surface compared to smooth surface [42, 43]. This enhancement of Raman signal are belonged to two mechanisms: an electromagnetic (EM) enhancement mechanism and chemical enhancement (CE) mechanism [44, 45]. These two mechanisms can coexist and give rise to a cumulative effect where the enhancement can be produced by inducing a net change in the induced dipole moment. Since the intensity of Raman signal is proportional to the square of the induced dipole moment, thus the enhancement can be achieved by increasing the electric field (EM enhancement) or polarisability of the molecule (CE enhancement) or both of them [46]. In theory, EM enhancement is independent on analyte while CE enhancement is analyte dependent and it is required to sort a chemical interaction to the metal surface [47].

### 1.3.1 Electromagnetic enhancement (EM enhancement) mechanism

The EM enhancement is the dominant contribution in SERS [48]. The basic of EM enhancement mechanism is the amplification of EM field produced by coupling of incident radiation field with localized surface Plasmon's (LSP) of the metal. According to this mechanism, when the laser light hits a surface of metal, the electromagnetic field in the proximity of this surface get a strong alteration. This is due to the oscillation of free electrons in the conduction band with respect to the fixed positive ions [49]. The phenomenon of collective oscillation of metal conduction electrons at the interface with a dielectric is called Surface Plasmon. As these charge density waves (Plasmon) cannot occur without being correlated with transverse EM wave (photon) and according to this energy sharing, therefore, they should be called surface Plasmon polaritons (SPPs). This SPPS can be divided into two different types according to metallic substrate and resonance conditions [50]:

**1-** Localized SPPS (LSPPS).

**2-** Propagating SPPS (PSPPS).

These two types of SPPS are described in Fig. (1.2).

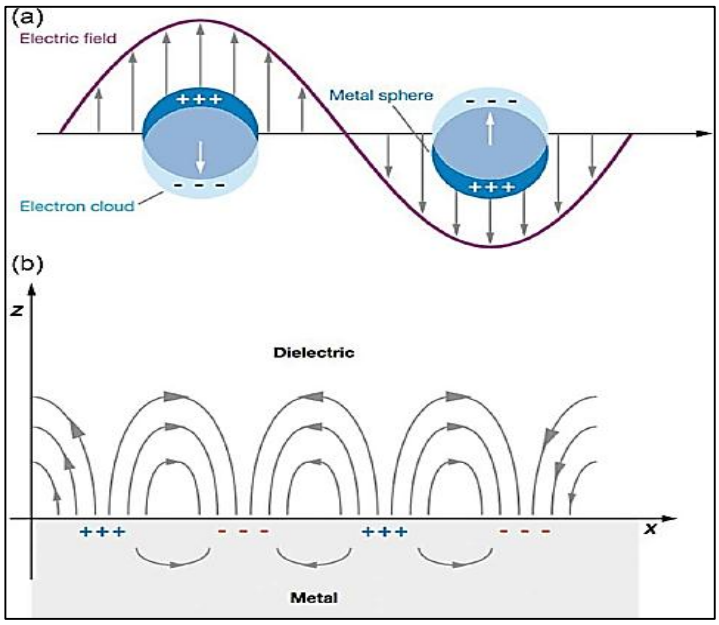


**Fig. 1.2: Schematic representation of (a) Localized surface Plasmon polaritons and (b) Propagating surface Plasmon Polaritons [50].**

In the case of PSPPs, the SPPs is propagating in the X and Y directions along the metal dielectric interface (for example, on the surface of a grating) [51, 52]. This propagation extends for distances on the order of hundreds micrometers in X & Y directions and exponentially decayed in the z direction. While for LSPPs, EM light interacts with metallic structures much smaller than the incident λ that leads to the generation of localized Plasmon oscillation within nanoparticles (for example, on the surface of a spherical particle). When the frequency of the incident EM radiation matches the frequency of LSPPs, a resonance state is achieved that referred to Localized Surface Plasmon Resonance (LSPR) [53, 54]. This resonance state will give rise to two main consequences. The first consequence is the selectively absorption of the light wavelength by nanoparticles. The second consequence is the EM field's enhancement that provide from the nanoparticles surfaces. The enhancement is mostly proportional to $|E|^4$ [41]. For the mathematical description of EM enhancement factor (EF), the simplest approach that gives the most prudence into the effect of SERS is the classical EM theory with the same depiction of Raman scattering, that is discussed later in this chapter, while, a two considerable modifications in the field description are introduced due to the existence of nanostructured metal surface.

- At the position of molecule, the EM field is altered (local field enhancement).
- The properties of the Raman dipole radiation are altered (radiation enhancement).

For the local intensity enhancement, the local field $E_{loc}$ can be much larger than the incident field $E_0$ and can dramatically varying with position, this induces Raman dipole that is given by [55]:

$$P_R = \alpha_R \, E_{loc(w_l)} \tag{1.7}$$

Which radiates in free space with power proportional to $|P_R|2$ and is enhanced due to local field EF [55]:

$$M_{loc} = \frac{|E_{loc\,(w_l)}|^2}{|E_0|^2} \tag{1.8}$$

In the case of scattering enhancement, the scattering enhancement factor can be defined as [55]:

$$M_s = \frac{|E_{loc\,(w_R)}|^2}{|E_0|^2} \tag{1.9}$$

Since the Raman shift is small, thus $W_R = W_l$. This assumption give rise to the well-known $|E|^4$- approximation factor [55].

$$EF = \frac{|E_{loc\,(w_l)}|^4}{|E_0|^4} \tag{1.10}$$

### 1.3.2 Chemical enhancement (CE enhancement) mechanism

The existence and definition of CE are the subject of many argumentation in literature [56]. It is almost impossible to separate these effects from a system that supports EM enhancement. In any case, its contribution in enhancement process is believed to be much smaller than the EM enhancement.

There are a few other factors in addition to EM and CE enhancements that influence SERS enhancement. Some of these factors are listed in the following:

- Laser excitation characteristics such as wavelength, angle of incidence, polarization, etc.

- Setup of detection, particularly: Scattering configuration, collection solid angle, etc.
- SERS substrate, such as materials, shape of roughness, dimensionality of substrate, etc.
- Adsorption properties of analyte such as concentration of analytes, adsorption efficiency, distance from the surface, etc. [18].

### 1.3.3 SERS enhancement factors

In most of SERS experiments, it is very difficult to exactly characterize the source of the enhancement mechanism (as EM or CE enhancement). An analytical enhancement factor (AEF) is used by many researchers to determine the EF by comparing both the SERS and normal Raman scattering (RS) intensity [47].

$$AEF = \frac{I_{SERS}}{I_{RS}} \frac{C_{RS}}{C_{SERS}} \tag{1.11}$$

Where I is the signal intensity at concentration C.

According to the above definition of AEF, an assumption that $I_{SERS}$ & $I_{RS}$ scales linearly with power density of the incident beam and the concentration of analyte is considered while it is ignored the fact that SERS is a surface spectroscopy and only the part that adsorbed will participate in SERS signal. In order to mend this issue, a SERS substrate enhancement factor (SSEF) can be used [47]

$$SSEF = \frac{I_{SERS}}{I_{RS}} \frac{N_{vol}}{N_{SERS}} \tag{1.12}$$

Where $N_{vol}$ is the average molecular number in the scattering volume and $N_{SERS}$ is the number of adsorbed molecules on the optically probed SERS substrate that can be acquired from the following equations [57].

$$N_{vol} = \frac{Ah\rho}{M} \tag{1.13}$$

And

$$N_{SERS} = \frac{cVA}{S} \tag{1.14}$$

Where $A, h, \rho, M$ are the laser spot area, path length, density and molecular weight of the analyte respectively. Also $S, c,$ and $V$ are the geometrical area of analyte casting film, the molar concentration and volume of analyte solution respectively.

The above expression of SERS EF is deemed as the best estimation of average enhancement factor for a given substrate and has been used extensively in SERS experiments [18, 58-60].

## 1.4 Existing of SERS substrate

Generally, the term "SERS" is used for describing any nanostructured metallic platform that supports Plasmon resonance and produce SERS enhancements. Moreover, as SERS enhancements are robustly wavelength dependent thus a given SERS substrate will manifest a good enhancements in a specific range of excitation wavelength. According to that, SERS substrate are intended to work with an excitation wavelengths in the visible-NIR range of spectrum which is the most interesting range of molecular Raman scattering experiments [18]. As a rule of thumb, an effective achievement of the technique is arising from a metallic structures with dimensions less than~100nm. Although a simple flat metallic surface can serve as Raman signals amplifier for an analyte deposited on it but with a much lower level of amplification that achieved in metallic nanostructures.

In general, Au and Ag metals are widely used for plasmonic and SERS according to their inherent optical properties that ensures resonance in visible-NIR range of spectrum. In fact, the optical properties bulk materials are characterized by their dielectric function. The Drude model of the dielectric function of a free electron gas represent a good model for depiction the metals conduction electrons [18, 61].

$$\varepsilon(w) = 1 - \frac{{w_P}^2}{\mathrm{w}^2 + \mathrm{i}\gamma\mathrm{w}} \tag{1.15}$$

Where γ is the characteristics collision rate responsible for damping of electron oscillation and $w_P$ is the plasma frequency of the free electron system, it is given by [18]:

$$w_P = \sqrt{\frac{ne^2}{m\varepsilon_0}} \tag{1.16}$$

Where n is the electron density, e is the elementary charge, $\varepsilon_0$ is the free space permittivity and $m$ is the electron mass. The plasma frequency plays a main role in the depiction of metals optical properties as it is the characteristics frequency of electron oscillation. The complex dielectric function can be separated into real and imaginary parts. It is given by [18]:

$$\varepsilon(w) = Re\big(\varepsilon(w)\big) + i\, Im\big(\varepsilon(w)\big) \tag{1.17}$$

Where

$$Re\big(\varepsilon(w)\big) = 1 - \frac{{w_P}^2}{w^2 + \gamma^2} \tag{1.18}$$

$$Im\big(\varepsilon(w)\big) = \frac{\gamma {w_P}^2}{w(w^2 + \gamma^2)} \tag{1.19}$$

The real and imaginary part represent the reflecting and absorbing properties of molecules respectively. According to equation (1.18, 1.19).

SERS effects can be observed in metals that satisfies the condition that: A negative real part and a relatively small imaginary part of dielectric function in the Vis.- IR region of spectrum. Fig. (1.3) shows the real and imaginary parts of dielectric functions of Ag and Au in the UV to near IR region of spectrum. The plasmonic resonance for the two nanostructured metals lie in two different spectral regions (~ 400nm for Ag and~ 520nm for Au). The extinction band of plasmonic can be modified in a spacious spectral range, from UV - Vis. to the near IR, through modification of the metal morphology of nanostructure and dimension. The importance of this tunability is not only for matching with the wavelength of laser excitation but also for detection of in accurate spectral range (for example where fluorescence is not present) for various molecules [55]. Ag is considered a good nominee for LSPR but it has a poor stability and lower compatibility due to their oxidation issue. Au is a better choice for LSPR, in contrast to Ag, due to its ease of manipulation, especially for nanostructures fabrication, excellent biocompatibility and chemical stability [18, 62]. Also, SERS has been tried on a spacious range of metals structures such as platinum or copper but they presented a lower amplifications than that accomplished with Au and Ag [18].

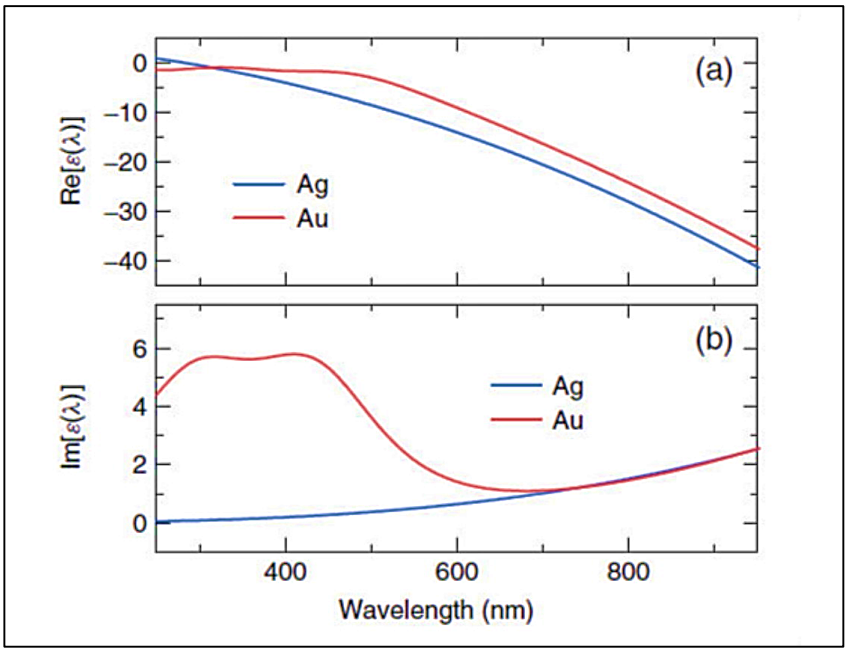


**Fig.1.3: a) Real and b) imaginary part of silver and gold dielectric function [62].**

## 1.5 SERS substrates classification

SERS can be classified in a many different ways. Herein, they are classified into three main classes:

- Metallic nanoparticles (MNPs) in suspension such as colloidal solutions: It is the simplest SERS substrate, predominantly made of Ag and Au nanoparticles where SERS experiment are performed in the presence of certain analyte concentration (Raman probe molecule). Metallic colloids are produced by various chemical reduction processes [22, 63] or by laser ablation from solid metals [64, 65]. Metallic colloids are of historic importance that related to SERS development as the first detection of single molecule were reported using colloidal substrate [10, 66]. Most researchers are yet interested in colloid -based SERS rather than more developed substrates because colloids are simple in production and resort to produce large factors of enhancement. On the other hand, the aggregation of metal nanoparticles may disturb the reproducibility of SERS spectra. In addition to this and as it was mentioned previously, MNPs suspension must be mixed with the analyte solution and due to their sampling requirements, it may limited for some applications [41].
- Roughened metallic electrode: It is the most primal SERS substrate that was discovered by Fleischmann et al [23]. Typically, these substrates are produced in electrochemical cell containing metallic salt solution by running the redox cycle [47]. In this case, gold and silver electrodes provide a relatively low enhancement factors in comparing with another SERS substrate but they have the utility of modifying their surface potential to understand the charge transfer phenomenon between the molecule of the target and the metal surface [67, 68].
- Metallic structure substrate, such as a random deposited or an arrays of metallic nanoparticles/nanostructures created on planner and other related substrates. In colloidal metallic particles, it is possible to perform

SERS spectrum of a single molecule. Although, it is often challenging to reproduce such a high performance SERS feature. To overcome this issue, a variety alternative methods have been introduced. Metal island films that includes a configuration of a metallic nanoscale particles deposited on a substrate. It is produced by deposition of colloidal solution onto the substrate (Fig.1.4) [69, 70].

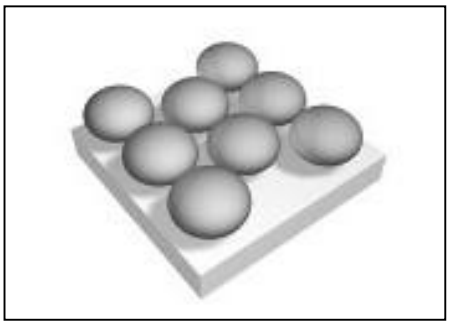

**Fig.1.4: Colloidal metal on a substrate [70].**

Colloidal solution depend on the interaction between two or more metal particles (forming trimmers, dimmers, etc.) to produce high signal counts and they can have high reproducibility of the particle size [71, 72]. Although, large distinctions in the SERS enhancement can result as there is no flat approach to assure if the interaction occurs. Substrate can be planner surfaces like quartz, glass or polydimethylsiloxane (PMDS), etc. or nanoparticles (polystyrene, silica beads, etc.) established surfaces (Fig.1.5) [70].

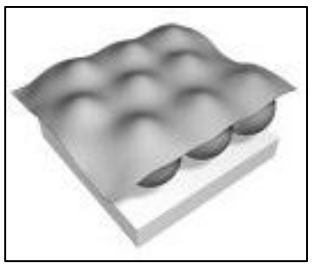

**Fig.1.5: Film on nanosphere [70]**

Lithographic ones present the potential to manufacture periodic array with specific shape, orientation and placement of the particles. The two most

common examples are nanosphere lithography (NSL) and electron beam lithography (EBL) [73-75]. The difficulty with NSL technique is that it depend on micro- or nanospheres ordering themselves into a monolayer. While there are many different methods that can support this process. Additionally, it is difficult to manufacture large areas of these surfaces which sets limitations on the possibility for large scale manufacturing [70]. EBL is a highly accurate technique for generation of a nanoparticles with arbitrary shape, size and spacing. In this method, an electron beam is utilized to write directly the deposition mask into a film of polymer then the metal is deposited through the mask. The film is removed to leave the remaining nanoparticles pattern on the substrate. Although, EBL, is expensive, time consuming and inefficient for large scale substrates [50]. The goal of more widespread use of SERS is to generate substrates with a high enhancement/ sensitivity and high reproducibility. Additional eligible features include easy maintenance, simple operation and robust system to reduce down time. Laser Induced periodic Surface Structure (LIPSS) onto polymer substrate followed by deposition of gold film used as SERS substrate present a solution to all of these issues.

### 1.6 Excimer laser induced LIPSS on polymer

As previously discussed, LIPSS is a regular wavy surface structure which can be progressed on the surface of any material by laser ablation. Excimer laser ablation of polymers is a multilateral method for polymers structuring with good resolution.

#### 1.6.1 Laser ablation

Since the invention of laser in 1960, powerful light beam have been directed to solid materials for diversity of uses [76]. Generally, laser ablation is the process of material removal from solid surface by intense laser beam [77]. The impact of the incident laser beam onto a solid material is that the

EM energy is absorbed by the surface of material and then transfers into thermal, mechanical, chemical and electronic energy. The ejected ablative debris, in the form of plume, including electrons, ions, atoms, molecules, and agglomerations or fragments of the irradiated substrate. In the whole process, the shape and the molecular structure of the material is altered in various ways [78].

### 1.6.2 Excimer laser ablation of polymers

Recently, the development of manufacturing technology of gas lasers has extremely advanced in terms of reliability and in most cases has enabled the transformation from laboratory environmental to industrial applications [79]. Excimer lasers have been used in several pulsed laser ablation experiments. The excimer laser radiation is absorbed in a very cursory region near the surface of the irradiated polymer and that is due to the fact that most polymers show strong absorption for UV- wavelength light. Accordingly, the excimer laser demonstrated to be an effective tool for producing photothermal and photochemical polymer ablation in order to produce a precise surface patterning and micromachining [80].

### 1.6.3 Ablation parameters

The fundamental parameters used to characterize the ablation of polymers are the ablation rate (which is defined as the slope of a linear fit for a plot of ablation depth versus number of pulses for a given laser fluence or the depth of ablation crater after one laser pulse at a given fluence) and the effective absorption coefficient ($\alpha_{eff}$ ) where it is a kind of measure to depict the depth of penetration of the laser during the ablation process. The third important parameter is the ablation threshold fluence $F_{th}$ below which no removal of material by the laser pulse can occurred. The relation between these three ablation parameters can be described by the following empirical correlation [81, 82]:

$$d(F) = \frac{1}{\alpha_{eff}} \ ln\frac{F}{F_{th}} \tag{1.20}$$

The ablation rate dependence on the irradiation fluence can't be realized with a single set of parameters. Therefore, for each range of fluence, one set of parameters has to be defined where a different effects control the ablation process and impact the ablation rate. The ablation rate dependence on the laser fluence is stated in Fig. (1.6), which is typical for most polymers [83].

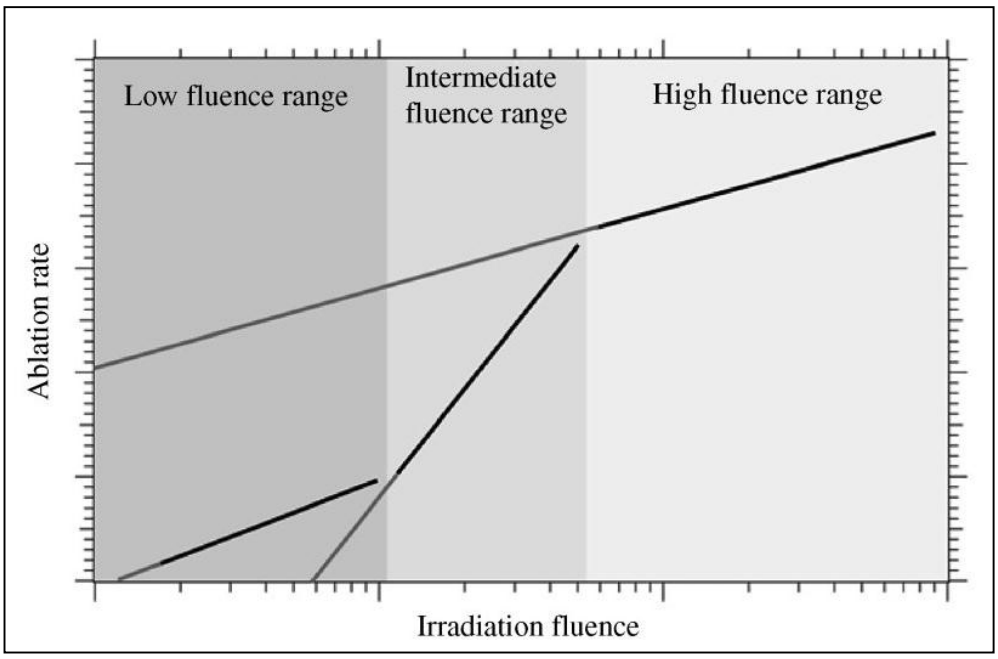


**Fig.1.6: Schematic plot of ablation rate dependence on the laser fluence [83].**

From the low fluence range, the ablation threshold can be defined. In the mid fluence range, the slope of the ablation rate is increased. This effect belongs to a decrease of the effective absorption coefficient and may be interpreted by releasing of heat during the ablation process (e.g. exothermic decomposition of polymer) while the ablation rate is decreased in the range of high fluence, this decrease corresponds to screening of laser irradiation by liquid, gaseous and solid ablation products. This procures a similar ablation rates for many polymers at high fluences [84].

### 1.6.4 Excimer lasers

Excimer lasers are a type of pulsed UV laser. The term "Excimer" is an acronym for "Excited dimers" [80]. It describes very short lifetime molecules that consisting of one rare gas atom (Argon Ar, Krypton Kr, or Xenon Xe) and one halogen atom (Fluorine (F) or Chlorine (Cl)) [77]. Under the appropriate conditions of high pressure and electrical simulation, a rare gas-halogen combinations is obtained which can only occur in an electronic excited states, and then dissociate into atoms in the ground states after a few tens of nsec. [85]. This transition gives rise to laser light in the UV range. The output wavelength of excimer laser is defined by rare gas- halogen combinations and can be modified by choosing different rare gas and halogen pair [78]. The wavelengths of some excimer lasers are given in Table 1.1

**Table 1.1: Wavelengths of excimer lasers [85].**

| Rare Gas-Halogen Combination | Wavelength (nm) |
|---|---|
| ArCl | 175 |
| ArF | 193 |
| $F_2$ | 157 |
| KrCl | 222 |
| KrF | 248 |
| XeBr | 282 |
| XeCl | 308 |
| XeF | 351, 353 |

Typically, the maximum pulse energies of excimer laser are from 0.25 to 1 joule with a repetition rates are from 1 Hz to few hundred Hz. The output powers are in the range 10-100 W and the pulse duration is generally between 10-30 nsec. As a result, the peak power may reach tens of Megawatts [78].

## 1.7 Polymers

Polymers are materials with a very high molecular weight that preferred for many applications. Usually, they consist of many structural units bound with each other by covalent bond Polymers are acquired via a chemical reaction of small molecular compounds called monomers. In order to form polymers, monomers either have reactive functional groups or double or triple bonds whose reaction supplies necessary linkage between repeat units. Polymeric materials usually have high strength, possess a glass transition temperature, exhibit rubber elasticity, and have high viscosity as melt and solutions. In fact, the investment of many of these unique properties has made polymers so useful to mankind [86, 87].

### 1.7.1 Polymers classifications

One of the popular ways of classifying polymers is based on their response to heat. According to this system, there are two types of polymers: thermoplastics and thermosets. In the former, polymers melts on heating and solidify on cooling. The cycle of heating and cooling can be applied many times without affecting the properties. On the other hand, thermoset polymers, melt only the first time they are heated. During the initial heating, the polymer is cured, subsequently, it does not melt on reheating but degrades [88].

- **Allyl diglycol carbonate (ADC) or CR39 polymer**

Allyl diglycol carbonate (ADC) or CR39 polymer is a plastic polymer. It is transparent in visible wavelengths range and almost completely opaque in UV. Because of the presence of two allyl functional group, CR39 s monomers can not only polymerize but also cross-link with each other which outcome a thermoset plastic distinguished by being hard, infusible and insoluble in all solvents [89]. The structure of CR39 monomer is shown in Fig. 1.7.

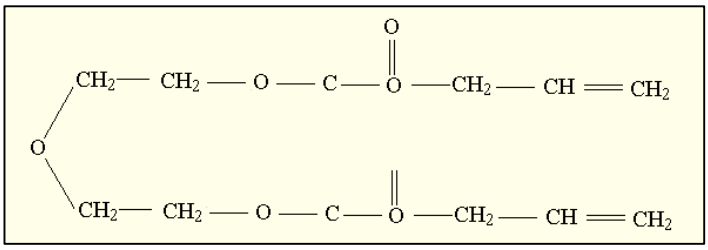

**Fig.1.7: Structure of allyl diglycol carbonate [89].**

CR39 has various applications in many fields and technologies. One of the most important application is in nuclear physics Also, CR39 has a high abrasion resistance, half the glass density, with a refractive index that is slightly lower than that of crown glass, which make it as the most appropriate material for eyeglass and sunglass lenses [90].

## 1.8 Mechanism of excimer Laser ablation of polymers

Mechanism of laser ablation of polymers is one of the most important motivation of researches. Even after 35 years of these researches, the ablation mechanism is still ongoing discussion. In this case, the polymer surface materials is not just thermally evaporated. Through numerous studies, , it has been emphasized that in laser ablation and even for thermally robust polymers, spacious fragmentation of the main chains take places which indicating that strong intra- chain covalent bonds are broken [91]. Ablation is also known to be stimulate, with material being ejected from the surface on a time-scale similar to the laser pulse duration [92]. This so-called bond-breaking mechanism, particularly with deep UV lasers, has aroused much attention and speculation. It is mostly accepted that laser photons energy is used for excitation of electronic states in a first step. The subsequent steps are still under discussion. It has been suggested that the mechanism is either photochemical or photothermal, or photophysical [92, 84, 93]. The different models can be summarized as follows:

- **Photochemical model:** In Excimer laser ablated polymer surface, the absence of considerable thermal damage can be interpreted by the fact that the incident laser photons have appropriately high energy for breaking the bonds of main chain through initiating many chemical reactions such as crosslinking, chain scission and radical formation [91, 94, 95]. According to this model, the excited electronic states of polymer, due to absorption of laser energy, to the energy levels which are above the energies of bond dissociation leading to decomposition reaction. In this process, the abundant decomposition productions required a large free volume, thus repulsive forces among these products would lead to their fast expulsion from the surface [91, 96]. The delivered photon energies by some commercial lasers are shown in Fig. 1.8, and Fig.1.9 illustrates the bond energies of some molecular bonds [94].

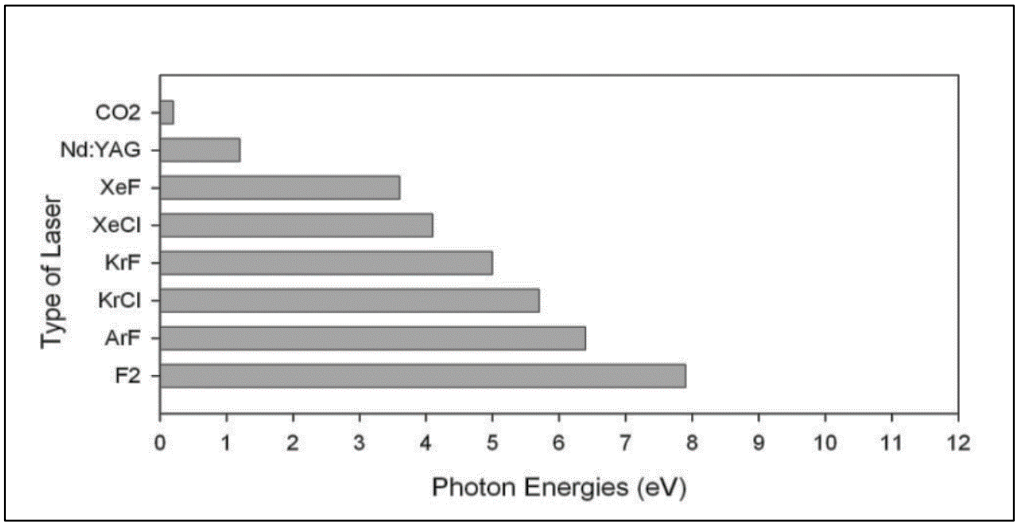


**Fig.1.8: Some common lasers photon energies [94].**

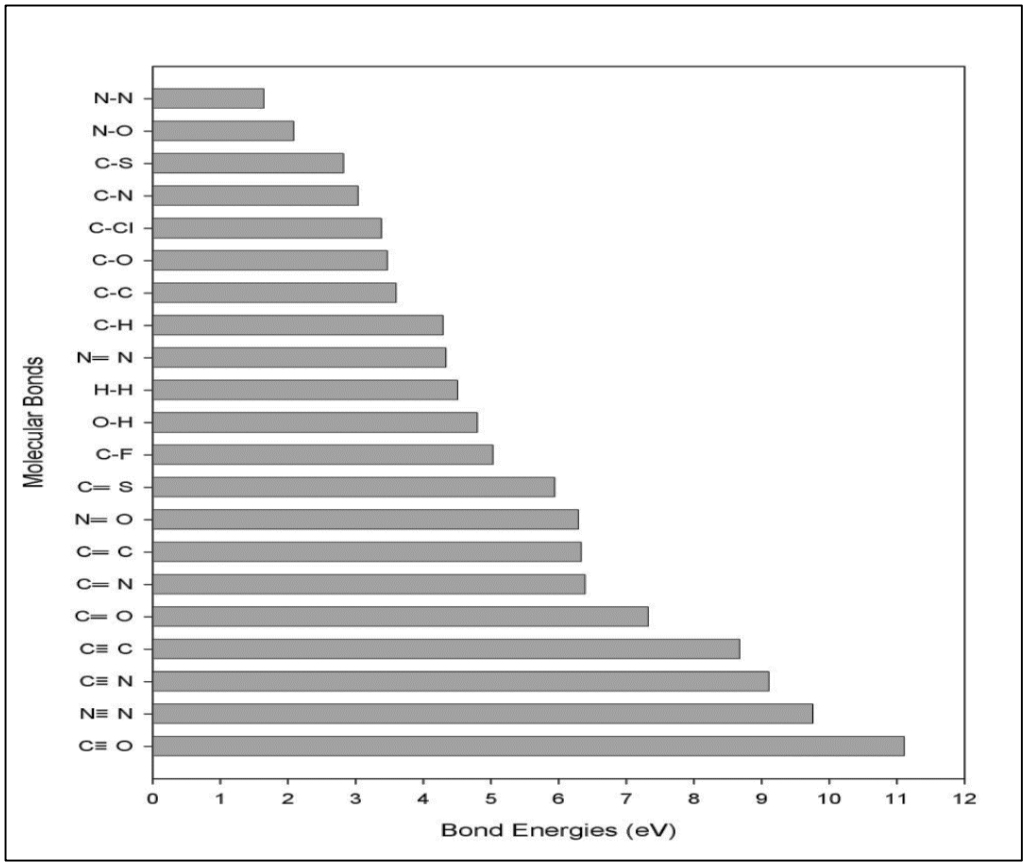


**Fig.1.9: Strengths of some common molecular bonds [94].**

- **Photothermal model:** A number of investigations have emphasized that a purely thermal process can produced an efficient ablation of polymer [97, 98]. This model indicates that the excitation of the electronic state by laser energy is thermalized on a psec. timescale which means that the transformation of electronic to vibrational energy states is fast compared to the rate of polymer removal which then results in thermal bond breaking [83]. Numerous models have been improved to describe the thermal aspects influence on the ablation characteristics. Arrhens-type rate expressions [99], thermal diffusion [100], and a model assuming one dimensional heat transfer after the two -level chromophore absorption [92].
- **Photophysical model:** From experimental observations during Excimer laser ablation of polymers, both photothermal and photochemical model

play an important role in which two independent channels of bond breaking [101, 102] or different energies of bond breaking for ground state and electronic excited states chromophore are applied in this model. Ablation happens if the number of bonds broken directly or via thermal decomposition exceeds a threshold [83].

### 1.8.1 Basic of heat transfer

In principle, a three different mechanisms are used to describe the heat transfer: conduction, convection and radiation (Fig.1.10). In conduction, only thermal energy is transported while in convection, a mass transport is connected with heat transfer. Finally, matter emits EM radiation according to its temperature where higher temperature matter emits more energy. Consequently, there is a net heat transfer from higher temperature matter to lower temperature matter [103].

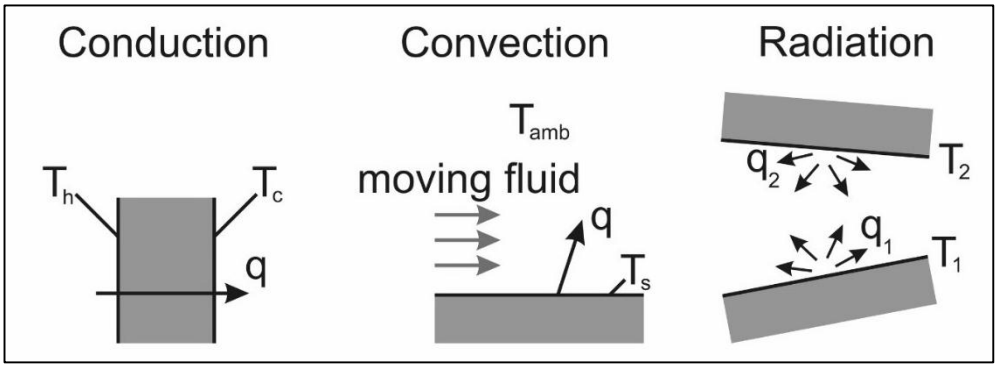


**Fig.1.10: Schematic illustrating mechanisms of heat transfer, ($T_h$) hot temperature, ($T_c$) cool temperature, ($T_s$) surface temperature, ($T_{amb}$) ambient temperature [103].**

A mathematical model based on the linear heat transfer equation could be used to estimate the temperature distribution and ablation depth in polymers during laser ablation process. In the absence of convective and radiative energy transport, a two dimensional heat conduction equation is given by [84]

$$\rho\, c_p \frac{\delta T(x,z,t)}{\delta t} = \nabla.[k\, \nabla T(x,z,t)] + Q(z,t) \qquad (1.21)$$

Where ρ, $c_p$ and κ are the mass density, specific heat at constant pressure and thermal conductivity of sample material respectively, *T* is the temperature which is a function of time and coordinates. The source term Q (*z*,*t*) describe the distribution of the absorbed laser fluence within the sample and is given by [84]

$$Q(z,t) = I_s(t)(1-R)\,\alpha_1 \exp(-Bz) \qquad (1.22)$$

Where $I_s$ *(t)* is the temporal laser irradiance at the sample surface. *R*, $\alpha_1$ are the reflectivity and absorption coefficient of the target material and *z* is in the direction normal to the sample surface.

## 1.9 Surface Modification

The excimer laser ablation of polymer surfaces exhibit not only a removal of material but also various physical and chemical modifications in the irradiated regions. Many research group have published numerous studies regarding the morphological changes of a large diversity of polymers such as Polyimide (PI), Poly(methyl methacrylate) (PMMA), allyl diglycol carbonate (ADC), Polystyrene (PS), polycarbonate (PC) upon excimer laser irradiation [104-109, 76]. The domination of these modification has become a field of considerable technical importance. The nature of the developed surface structure depends on the type excimer, laser irradiation conditions and nature of polymer morphology. Unfortunately, the relationships between these parameters and resulted surface structure is not perfectly established yet [110].

### 1.9.1 Chemical modifications

In general, when an excimer laser irradiated polymers surface in atmospheric environment, some fraction of the polymer hydrocarbon group ($CH_x$) may be modified in terms of its chemical structure such as hydroxyl (-OH) and carbonyl (-C=O) group due to reactions with the environment [110]. Oxygen is considered as the most important reagent in atmosphere. The laser radiation can initiate and accelerate photo- and thermal-oxidation. The oxidation leads to the degradation / decomposition of the polymer by bond dissociation, cross linking and chain scission [111]. Occasionally, high fluence laser radiation can induce direct bond breakage of polymer chain without oxidation [112]. In addition, a thermal oxidation may be combined with photo- oxidation reactions leading to photo- thermal oxidation [113].

### 1.9.2 Physical modifications

In addition to chemical modifications, UV laser ablation of polymers is often accompanied by modification of the surface morphology in the irradiated area. A variety of surface microstructures have been observed over the years. In general, these microstructures include cones and the so- called LIPSS (Laser Induced periodic Surface Structures) that have been observed on a variety of polymers using excimer laser [85, 77, 78, 91, 92, 96]. The generally accepted view on the formation of LIPSS is that the incident laser light interferes with a wave scattered off the sample surface, initially produced due to the natural roughness of surface, which results in a heterogeneous light intensity distribution on the surface. Irradiation with multiple laser pulses enhances the effect by a feedback mechanism that is needed for LIPSS generation [26, 114]. The most LIPSS, as surface ripples can be induced with a polarized laser light within a narrow fluence range below the ablation threshold [31, 115-118]. These ripples show a periodicity

Λ that depends on the wavelength and on the incidence angle of the laser light through the following relation [119]:

$$\Lambda = \frac{\lambda}{n - sin\theta} \tag{1.23}$$

Where n is the effective refractive index.

The interference causes a modulated distribution of intensity, which is imprinted into the material. The ripples having these properties are usually referred to as low spatial frequency LIPSS (LSFL). Recently, a new kind of LIPSS has been observed with a periodicity larger than the laser wavelength. These LIPSS usually looks like a "grooves" [120].

## 1.10 Polymer LIPSS applications

It is possible to produce LIPSS with various shape and sizes, making these substrates suitable for different applications.

### 1.10.1 Surface Enhanced Raman Scattering (SERS) substrate for sensing

The many thousands of Raman active molecules are improving research toward a new applications of SERS. Also, it can be applied to the system that could not be visualized with normal Raman scattering**.** SERS is known as an efficient method for environmental monitoring, biomedical research and chemical analysis [19-21, 122]. The technique have been successfully performed for both sensing of biofluids at higher concentrations and for detection of chemicals and biologicals traces (pharmaceuticals, explosives, environmental contaminations etc.) [123-127]. It is particularly well-suited to these tasks because of the signal amplification accompanied with high sensitivity, the "fingerprint" ability to produce distinct spectra

from molecules similar in structure and function that observed when the molecule of interest is very close or lies on the surface of appropriate plasmonic nanoparticles or nanostructured materials [128]. Recently, SERS has attracted considerable attention for new biosensor. In general, biosensor is a self- contained integrated device capable of selective detection of biological and chemical analytes .It consists of a bioselective layer that react with a target biomolecules and a transducer to transform the biological interaction into physical signal (electrical, optical, chemical, thermal, etc.) [129]. A biosensor with optical transducer are considered as a powerful alternatives to conventional analytical techniques. It exploits light absorption, luminescence, fluorescence, reflectance, refractive index and Raman scattering [130].

The technology of nanomaterial presents a promise to solve the biocompatibility and biofouling problems in biosensor [131].Thiophenol (TP) ($C_6H_6S$) (Fig.1.11) is chosen as an analyte SERS molecule because it produce a strong Raman scattering with a well-defined spectral lines. Thiol (sulfur-hydrogen group) tipped molecules are known to bond with noble metal (e.g. gold, silver and copper) surfaces through sulfur bond [132].

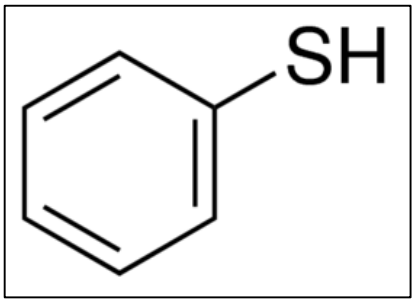


**Fig.1.11: Thiophenol molecule [132].**

The mechanism behind the adsorption of molecules to the surface is believed to be cleaving of the S-H bond to form S-Au bond (Fig. 1.12) [133]. Additionally, Thiol molecules also form a stable self-assembled monolayer (SAM) on the SERS substrates. The adsorption rate of thiophenol onto Au

indicate a coverage of over 90% is realized after at most five minutes [134,135]. To measure SERS signal, the molecules of analyte must deposit on the surface of SERS substrate (nanostructured polymer surface), as close as possible to the hot spots molecules.

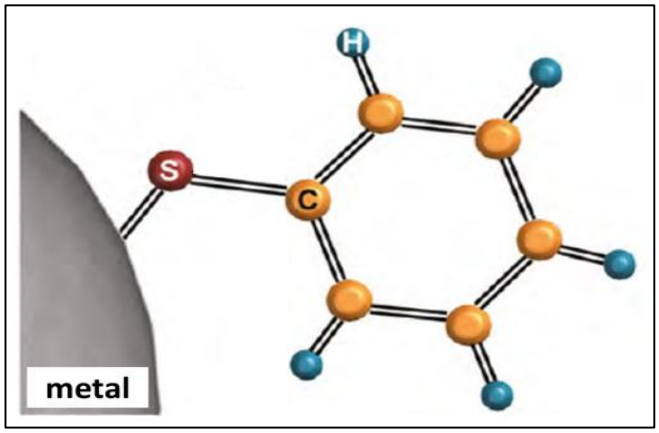


**Fig. 1.12: Thiophenol molecule bound to metallic surface. Figure adapted from ref [133].**

### 1.10.1.1 Detection of environmental contaminants

Natural and artificial organic compounds that used, synthesized and disposed are largely distinguished as environmental contaminants. [136]. The existence of these compounds in the environment has significant effect on humans, wildlife and aquatic ecosystems. Usually, these environmental agents interfere with the endogenous steroid hormones of vertebrates through interfacing with hormone receptors which leads to negatively vary the entire endocrine system [137]. Environmental appearance of these pollutants are at very low levels of concentration, sometimes ranging from parts per billion to sub parts per trillion. Since, at these levels of concentration, few analytical techniques have been developed to detect these compounds [138] then, analytical challenges exist the call for technical improvement that capable for trace levels detection of such environmental contaminants. To explore the application of the fabricated SERS substrate in monitoring environmental organic pollutants, methylene blue (MB) is used

in this work as a water pollution (Fig.1.13). It is a dark green powder, have a good solubility in water, where it yields a deep blue solution [139]. MB has many important applications in fields of medicine, microbiology, diagnostic [140]. It is utilized for malaria treatment, blood disorder and neural problems [141-143]. Also it has many industrial applications such as dyeing, textile, leather, printing, food processing and others [144].

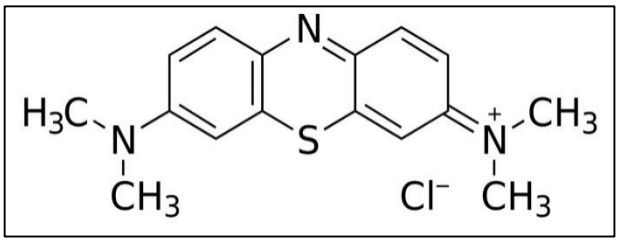


**Fig.1.13: Methylene Blue molecule, Figure adapted from ref [139].**

## 1.11 Literature Survey

In ***2006***, Rebollar et al. [145] reported the effect of molecular weight on morphological and chemical modifications induced by Krypton fluoride ( KrF) Excimer laser ablation of PMMA & PS films doped with NapI and phenI. They demonstrated a strong dependence of the extent and duration of the induced morphological change on polymer molecular weight as well as on the optical absorption coefficient of polymer at the irradiation wavelength.

In ***2008***, Slepicka et al. [146] studied fluorine laser (F2) modifications of Polyethylene terephthalate (PET) with different angles of incidence. They showed that the formation of periodic structures on PET was angle dependent.

In ***2010***, Siegel et al. [147] investigated the properties of Au coatings sputtered onto ripples structures that induced by F2 and KrF Excimer laser irradiation. They concluded that the morphology of Au layer was distinctly different for gold sputtered onto ripples induced by F2 laser, which were narrower and considerably shallower than the KrF laser induced features.

In ***2011***, Heitz et al. [148] described the formation of photonic microstructures originating from relaxation stress fields in surface of polyethylene terephthalate (PET) polymer due to laser irradiation and nanostructures ripples induced by interference of the incident beam with the scattered light at the surface of PET induced by ArF Excimer laser for applications in cell biology. They demonstrated that both types of structures were able to motivate an alignment of living biological cells cultured thereon.

In ***2012,*** Kim et al. [149] performed 355 nm DPSS Nd: $YVO_4$ laser ablation of polyimide (PI) film to change the morphology of surface for the application as an electrochemical electrode, they concluded that the sensitivity of the ablated PI coated with platinum (Pt) is higher than that of plain PI/Pt due to increasing of surface area by laser ablation

In ***2013***, Perez et al [150] reported on a systematic study about the formation of periodic surface structures on biopolymers films using linearly polarized ArF, KrF and 4th harmonic Nd: YAG lasers. They observed that the periods of the induced nanostructures was similar to the laser wavelength and parallel to the laser polarization direction.

In ***2013***, Dorronsor et al [151] reported on the formation of a periodic surface structures in a copolymer upon ArF laser irradiation above the ablation threshold. They discovered a new type of surface structures with a period much larger than those characteristic for LIPSS and features nanchains instead of ripples.

In ***2014***, Barb et al. [152] observed coherent structures on PET & PS polymers upon irradiation with linearly polarized KrF Excimer laser. They demonstrated that the induced nanostructures can be used for nanoparterning of relative large areas on synthetic polymers commonly used as cell cultures substrates and can be modified into Au nanowires by means of evaporation under an inclined angle .

In ***2014***, Jacob et al. [153] studied and analyzed the thermal effects during KrF laser ablation of negative photoresist E-1020 polymer in different gaseous environment such as air, nitrogen, argon, hydrogen and helium, they observed that hydrogen gas enhanced both the surface quality and ablation rate significantly.

In ***2015***, Shakeri Jooybari et al. [154] investigated the ablation and conical structure formation on CR39 as a result of ArF Excimer laser irradiation. They suggested that the formation of microcones was due to perturbations on surface of laser irradiated polymer.

In ***2015,*** Michaljanicova et al. [155] focused on the investigation and comparison of poly(lactic acid) (PLLA) and surface modification due to irradiation with two Excimer lasers (ArF and KrF), they confirmed that and with the same irradiation condition, ArF laser caused more significant alteration on surface morphology, surface chemistry and pattern formation on the polymers under investigation.

In ***2016***, Behrouzinia et al. [156] investigated the surface modification of PET polymer due to 193nm ArF laser irradiation, they concluded that in addition to considerable morphological changes on the polymer surface , changes in the hydrophobic arises from the chemistry modification of the surface which depends on the energy of the incident photon and the number of laser pulses.

In ***2017***, Pospori et al. [157] reported the first polymer optical fiber Bragg grating (FBG) engraved with one 15nsec KrF laser pulse that recorded in a single-mode PMMA optical fiber having a core doped with benzyl dimethyl ketal for photosensitivity enhancement. They found that the produced FBG providing a reflectivity of 98.4% which is appropriate for sensing applications.

## 1.12 Aim of the work

Performing a computer simulation program to determine the effect of ArF laser on various ablation parameters of CR39 polymer. Then conducting and investigating a SERS biosensor based on generation of LIPSS on surface of CR39 polymer through ArF laser ablation followed by coating with gold layer.

# CHAPTER TWO

## Simulation and Experimental Work

## 2.1 Introduction

In this chapter, a simulation program is performed for a better understanding of the involved physical approach in laser- polymer ablation process. Also, the materials, main experimental methods and apparatus that utilized to accomplish the present work are presented. Specific details of the used parameters are determined. Addressed here, are the characterization of unirradiated CR39 polymer sample through UV- visible spectroscopy and thermogravimetric analysis, the basic details for generation of nanostructured CR39 polymer through 193nm ArF laser ablation and the chemical properties of unirradiated and irradiated polymer surface by Fourier Transform Infrared (FTIR) spectroscopy. Also, the coating method of that surface with thin layer of gold metal and investigation of the complex nanostructured surface morphology through Scan Electron Microscopy (SEM) and Atomic Force Microscopy (AFM) are described. Finally, the enhancing properties of the SERS substrate (complex nanostructured surface) are given for studying of the effectiveness of the whole structure in detection through Thiophenol (TP) as an analyte molecule and for biosensing of water contamination via methylene blue (MB).

## 2.2 Simulation program

It is essential to build an effective simulation that can reflect effects of polymer thermal diffusion, laser fluence, beam geometry and number of pulses during laser- polymer ablation process. For polymers in general, it has been proposed that laser irradiation causes heating of the upper layer of the polymers. The corresponding temperature increase can be estimated by solving the heat conduction equation. Accordingly, a two dimensional finite element model (FEM) is performed to predict temperature distribution and ablation depth in CR39 during 193nm ArF laser ablation process.

### 2.2.1 Finite Element Modeling (FEM)

In this work, ablation process is simulated using ANSYS 11 [158], elements of plane 55 with a two dimensional thermal conduction capability are used for analysis, each element has four nods with a single degree of freedom, temperature, at each node. The element is applicable to steady state or transient thermal analysis. Fig. 2.1 shows the modeling approach layout. Sequentially, the time dependent problem is solved for an ArF laser with a top- hat beam profile of 15nsec. pulse duration and 1 Hz pulse repetition rate.

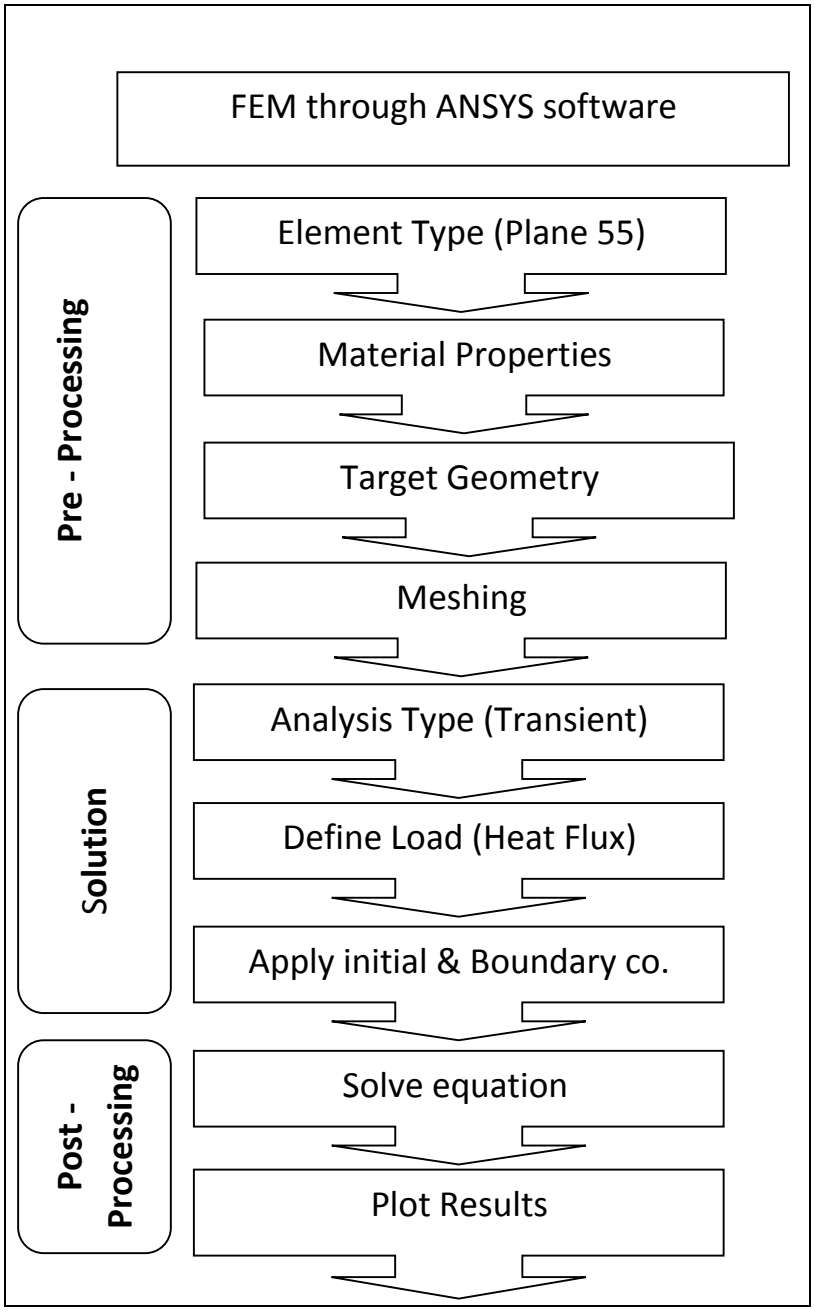


**Fig.2.1: FEM of laser- polymer ablation**

### 2.2.2 Sample description

The geometry of sample with dimensions of 10 mm x1.5 mm is shown in Fig.2.2.

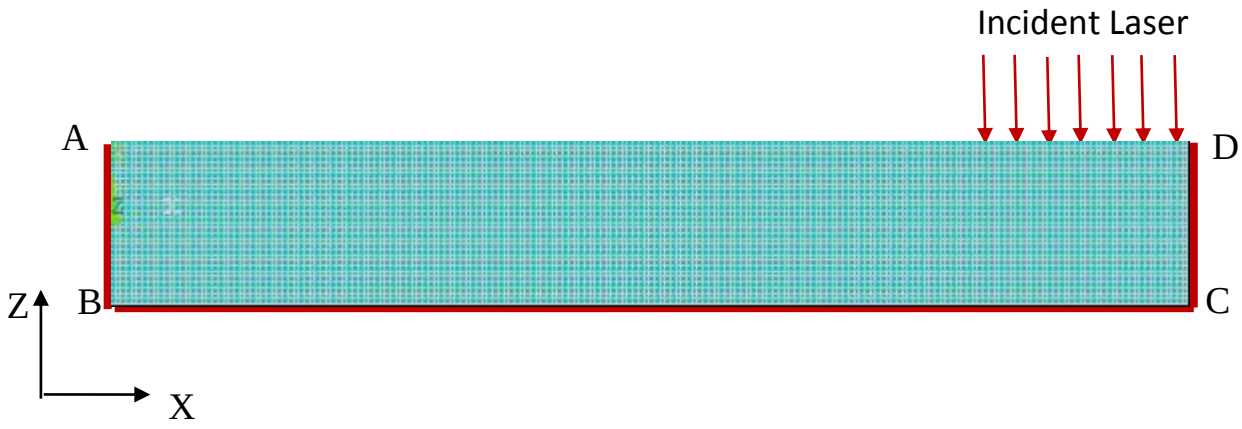


**Fig.2.2: Sample Geometry**

The size of each element is assumed to be 50 µm x 50 µm which is small compared with size of laser irradiation region. To reduce the program processing time, and due to symmetry along center of the beam, one half of the rectangular sample is simulated. The analysis time is too short, so heat transfer with surrounding air is ignored. Also, the convective heat transfer is not affected the temperature change.

The boundary conditions of Fig.2.2 are given by the following equations:

$T(x,t)|_{z=0} = T_\circ$ along boundary BC (2.1)

$T(x,t)|_{x=0} = T_\circ$ along boundary AB (2.2)

$-K(T) = \frac{\delta T}{\delta Z}|x = 10mm$ along boundary CD (2.3)

Where $T_0$ is the sample initial temperature.

### 2.3 Laser ablation experimental setup

For generating Laser Induced Periodic Surface Structure (LIPSS) on surface of CR39 polymer via ablation process, a Lambda Physik Excimer laser (LPX 220i) operated at wavelength of 193 nm is used. The ArF laser

produces a maximum output energy of 275 mJ/pulse with 15 ns pulse duration that is spatially distributed over 9mm x 25 mm beam area with 1 and 3 mrad full angle beam divergence in narrow and long dimensions respectively. The beam profile is uniform in x- direction and top- hat in y-direction. The repetition rate is set at 1 Hz to avoid unwanted heat accumulation on the surface. Fig 2.3 shows configuration of laser ablation experimental setup. In order to obtain identical irradiation areas, the excimer laser beam cross section is masked to a rectangular shape of 9 x 20 $mm^2$ using a homemade aluminum mask at a distance of 15 cm from the output aperture and is focused on samples through $MgF_2$ cylindrical lens with 25cm focal length and 30 x 25 $mm^2$ dimensions .The lens sample distance is adjusted to achieve the desired laser fluence where the sample is inserted in a computer assisted 3D translational mount with 1 μm spatial resolution. The measurements of absolute pulse energy is performed using a calibrated pyroelectric energy detector. The corresponding laser fluences are calculated through dividing the laser pulse energy on the ablated area of sample. Production is performed in air at ambient atmospheric with 10, 100 and 1000 pulses and laser fluences range 240 $mJ/cm^2$ to 2000 $mJ/cm^2$ range.

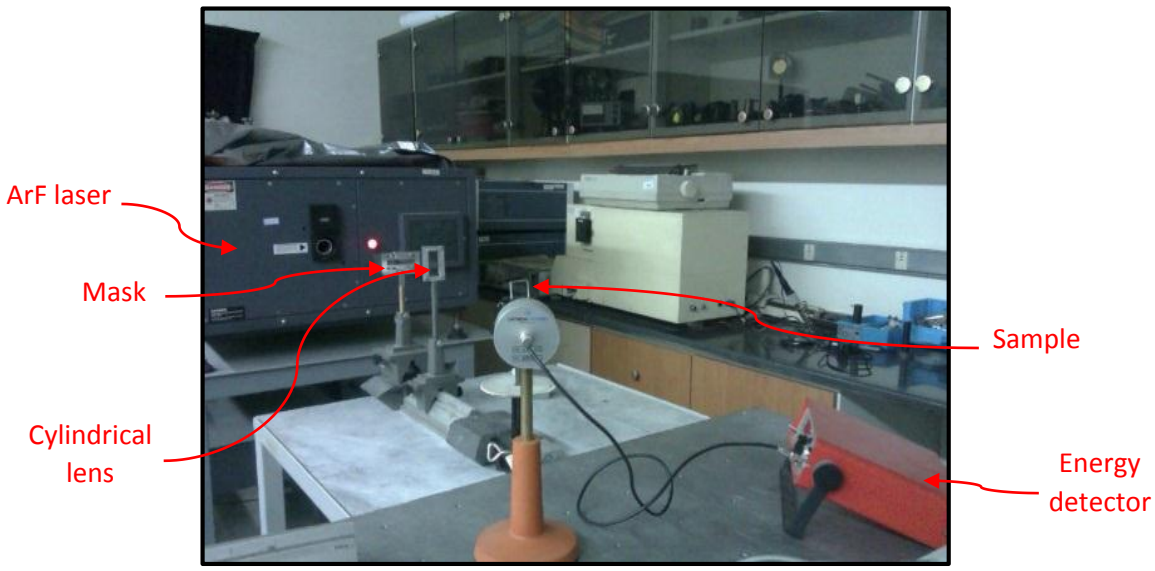


**Fig.2.3: Experimental setup of Excimer laser ablation experimental.**

## 2.4 Materials

The polymer chosen for this study is CR39 with dimensions of 10 x 10 x 1.5 $mm^3$. Table 2.1 lists the necessary thermal parameters of pristine CR39 that used in this work, the other unknown parameters are measured experimentally as will be shown later in the present chapter.

**Table 2.1: Thermal parameters of CR39.**

| Thermal conductivity, K (W/m.K) | Specific heat, $C_\rho$ (J/Kg.K) | Density, ρ ($kg/m^3$) |
|---|---|---|
| 0.2 [159] | 2300 [159] | 1320 [160] |

For the experiment conducting, the nanostructured substrates are coated with gold (99.99% purity, Quorum Technologies) layer with thickness range from 5 – 50 nm. For SERS characterization, thiophenol (TP) ($C_6H_6S$) (99%, sigma-Aldrich) with a molecular weight of 110.19 g/mol and a density of 1.08 $g/cm^3$ is chosen as an analyte molecule. In order to measure SERS signal, the molecules of analyte must deposit on the surface of SERS substrate (nanostructured polymer surface), as close as possible to the hot spots molecules. Consequently, a drop of 100 μL solution of thiophenol diluted in ethanol (100%, Hayman specialty products) is poured onto SERS substrate and dried in air. Typically, 100 nM, 100 μM and 100 mM concentrations of thiophenol solution in ethanol followed by rinse with ethanol to remove unboned molecules then the average of spectra is measured at three random locations on the SERS substrate for each concentration of thiophenol. For biosensing applications of the produced SERS substrate, methylene blue (MB) ($C_{16}H_{18}CIN_3S$) solid from central drug house India with a molecular weight of 319.85 g/mol is used in this work as a water contaminant. To perform that, a drop of 100 μL solution of 100 μM, 10 μM, 1 μM and 0.1 μM concentrations of MB diluted in Deionized water (DI) is poured onto SERS substrate and dried in air followed by rinse with ethanol to remove any debris then the average of spectra is

measured at three random locations on the SERS substrate for each concentration of MB.

## 2.5 Material characterization

### 2.5.1 UV- Vis. Spectroscopy

The UV-Vis. analysis of a pristine CR39 sample of 1000 μm thickness is carried out using UV- Vis. shimadzu Spectrophotometer (UV-1800) to obtain the sample spectra. Information are recorded in the absorbance mode in the wavelength range 190 -1100 nm.

Based on UV- Vis. Spectrum of CR39 polymer shown in Fig. 2.4, CR39 apparently has low absorption at wavelengths in the range 350- 1100 nm but significant absorption below ~225 nm. At 193 nm the linear absorption coefficient ($\alpha_{lin}$) is estimated to be 26.976 $cm^{-1}$ suggesting that CR39 has a good absorption in the deep UV. As will be seen later CR39 can be ablated with fluence of ~ 250 $mJ/cm^2$ at 193 nm. For ablation at the longer wavelength of 248 nm KrF Excimer laser, where CR39 has a low absorption (estimated at ~ 11.07 $cm^{-1}$), ablation threshold is shifted to a much higher value of 6 $J/cm^2$ [161]. From the calculated value of $\alpha_{lin}$ at 193 nm, the related extinction coefficient and reflectivity are determined.

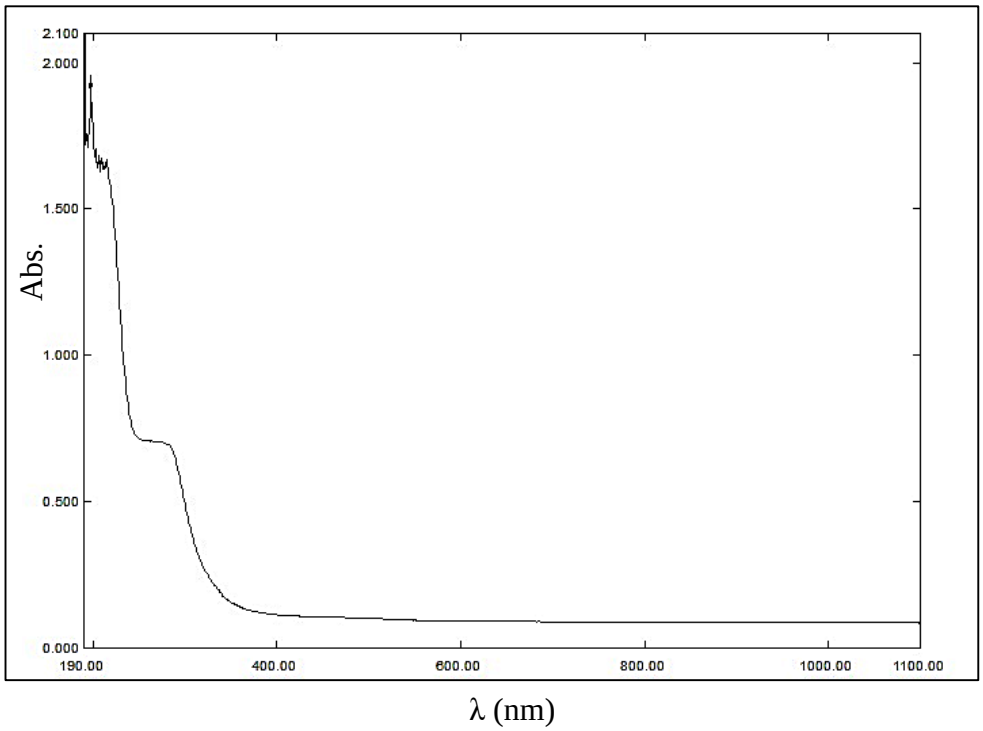


**Fig. 2.4: UV- Vis. Spectrum of CR39.**

### 2.5.2 Thermogravimetric analysis (TGA)

The decomposition temperature of a 23.4 mg of pristine CR39 sample at low heating rates (10 $^{o}$C/min) is investigated by thermogravimetry at quasi equilibrium condition. Linseis (STA PT1000) is a simultaneous thermal analyzer with an exchangeable measuring systems TG – DTA/DSC

In terms of the thermal stability, the CR39 polymer sample is decomposed at 189 $^{o}$C (463 K) and 233 $^{o}$C (507 K) as indicated by the temperatures for 10 and 20% mass loss acquired from a thermogravimetric analysis (Fig.2.5). CR-39 is a thermosetting plastic and cannot be melted in general. But when laser pulses interact with sample, a lot of processes due to photothermal, photochemical occurs and consequently leads to depolymerization of polymer into mixtures of monomers just on the surface of sample and finally change the optical and the thermophysical properties. However, the exact nature of the decomposed product is not well analyzed yet but the products of laser induced decomposition are available in liquid [162]. A correlation between behavior of pulse laser heating and quasi

equilibrium behavior is not trivial but would be very assistant. A special designed setup and sophisticated data analysis are required for characterization on time scale of pulse laser experiment. Comparison on time scales of quasi equilibrium are in contrast a standard measurement procedure. In this work, thermal decomposition for the applied laser pulse is assumed to start at temperature similar to the start of decomposition in thermogravimetry.

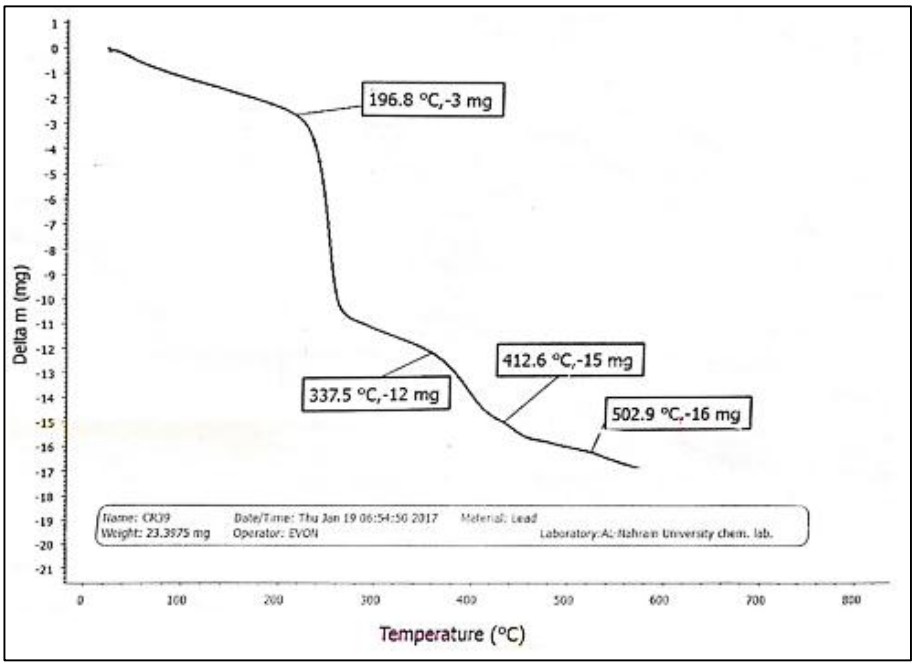


**Fig. 2.5: TGA plot of CR39 polymer**

All the obtained and determined parameters of CR-39 polymer are summarized in table 2.2.

**Table 2.2: Parameters of CR-39 polymer**

| $T_{10\%\ loss}$ [K] | $T_{20\%\ loss}$ [K] | $\alpha_{lin}$ [$cm^{-1}$] at 193 nm | K[-] at 193 nm | R[-] |
|---|---|---|---|---|
| 463 | 507 | 26.976 | $414.3x10^{-7}$ | 0.547 |

### 2.5.3 FTIR Spectroscopy

FTIR spectroscopy with attenuated total reflectance (ATR) accessory is used to investigate the chemical modifications of sample surface due to

Excimer laser ablation experiment. The IR transmission spectra of both unirradiated and irradiated samples are recorded using a Thermo scientific (Nicolet IR100) FTIR spectrometer and spectra – tech foundation speculATR attachment in range 500-4000 $cm^{-1}$ with a spectral resolution of 4 $cm^{-1}$.

## 2.6 Metal layer deposition

As previously mentioned, the SERS effect depends on the interaction between a molecule and a nanoscale metal particle. This works concentrates on the formation of nanostructured polymer substrate therefore it must be coated with metal to function as a SERS biosensors. Moreover, coating are also required to prevent charging effect when using SEM. Prior to metal coating, all samples are ultrasonically cleaned with ethanol and deionized water then dried in ambient air to remove any residual debris. The Quorum high resolution turbomolecular- pumped coating system (Q150T ES) is utilized to deposit a thin layer of gold metal onto the nanostructured polymer surface. The system is equipped with layer Thickness Monitor (FTM) which control thickness of the deposited layer.

## 2.7 Analysis of nanostructured surface

The commonly used techniques to investigate the morphology of LIPSS are to implement a direct microscope imaging of the surface by techniques like SEM or AFM. The nanostructures visualization in real space is advantageous since it allows direct assessment of the pattern morphology. A CamScan (MV2300) SEM is used to examine nanostructured surface morphology precisely with secondary electron imaging mode and an accelerating voltage of 20 KV.

The average roughness of nanostructured surface is measured by contact mode of Angstrom advanced (A3000 AFM). The imaging are

analyzed with a digimizer image analysis software to measure the periodicity and height of the produced nanostructured surface due to laser ablation.

## 2.8 Surface Enhanced Raman Scattering (SERS) measurements

The second part of the main thesis aim is to investigate the convenience of the fabricated nanostructured polymers surface for the SERS in biosensing applications. For SERS measurements, a few steps are required:

1- Raman spectrometer with a suitable laser wavelength for analyte excitation, collecting of scattered Raman signal and identification by intensity measurements at different wavelengths.
2- Analyte that achieves Raman scattering.
3- SERS substrate which enhances the weak Raman signal.

A Holmarc (HO-ED-S06) laser Raman spectrometer is utilized for Raman measurement. The excitation source is emit a 40mW at 532 nm Diode Pumped Solid State (DPSS) laser. Raman spectra are acquired in a 90◦ scattering with an objective of 0.09 Numerical aperture (NA). SERS measurements of TP and MB are performed from three different places across the whole nanostructured area and the averaged value is adopted.

# CHAPTER THREE

## Results and Discussion

## 3.1 Introduction

In this chapter, the simulation and experimental results of 193 nm ArF laser ablation of CR39 polymer are presented and discussed. In addition, the mentioned data for Fourier Transform Infrared (FTIR) Spectroscopy, UV-visible spectroscopy, Scanning Electron Microscope (SEM), and Atomic Force Microscopy (AFM) are shown. Finally, the performance of the produced SERS substrate are given through Thiophenol (TP) as an analyte molecule and methylene blue (MB) as a water contaminant.

## 3.2 Simulation program results

Based on heat transfer model which is implemented using ANSYS 11 program, the CR39 polymer surface is supposed to be heated with a single and repetitive 193 nm ArF laser pulses for range of fluences. The simulation results for temperature profile across depth of sample is shown in Fig. 3.1. The ablation depths acquired from the analysis for a single laser pulse with fluences of 750 and 2000 mJ/cm$^2$ are 51.5 and 127 nm respectively while for repetitive laser pulses with the same fluences values, the obtained ablation depths are 457 and 1101 nm respectively. The size of the removed material is enlarged as the laser fluence is increased for both cases (single & repetitive laser pulses). For a top-hat beam, the profile of the ablated surface is almost flat except at the edge of the beam cross- section, due to heat conduction in the lateral direction, the profile of the edge seems to be curvature. It is evident that the maximum reached temperature through CR39 polymer tends to decrease with depth increasing.

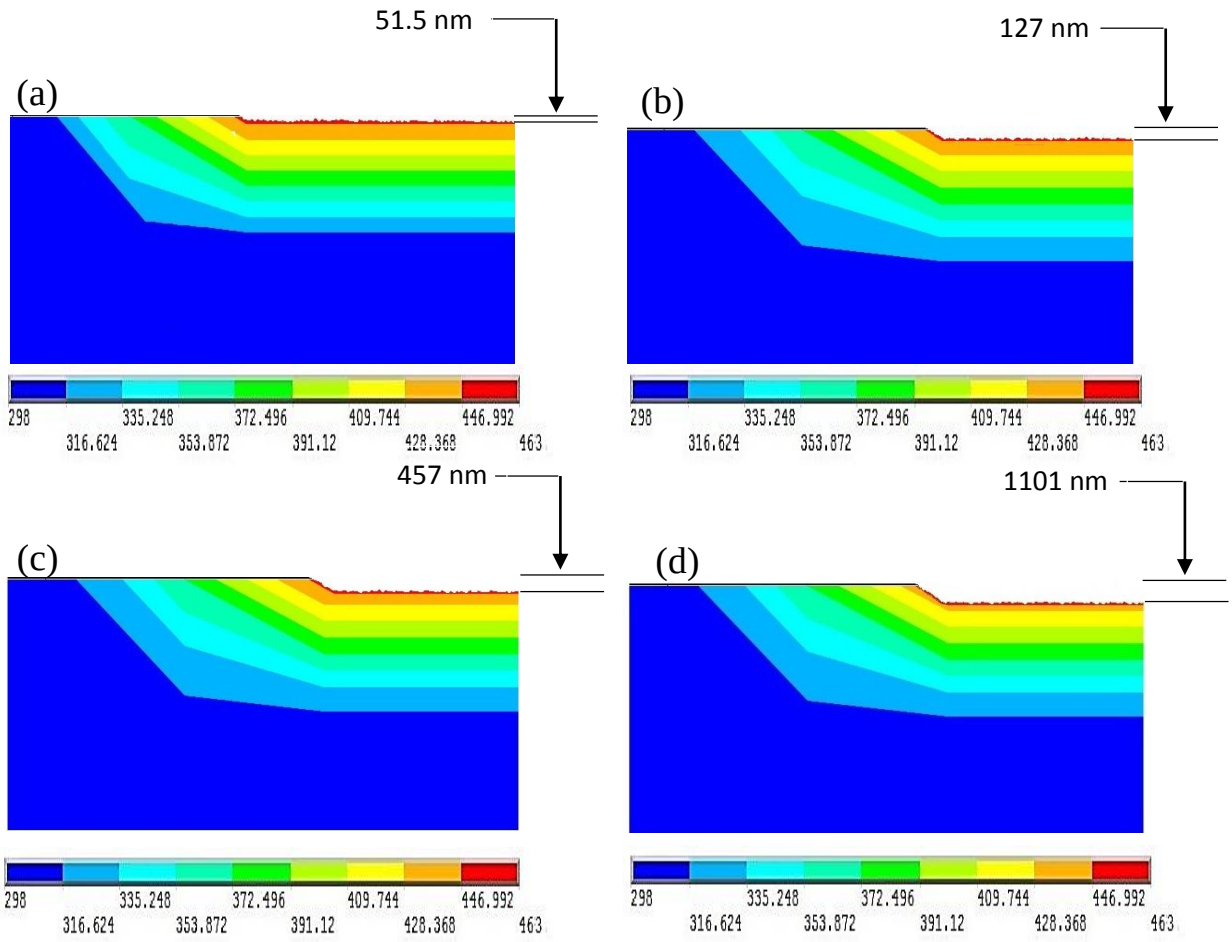


**Fig. 3.1: Temperature profile of CR39 polymer for single pulse [a- 750 mJ/cm$^2$ & b- 2000 mJ/cm$^2$] and repetitive pulses [c- 750 mJ/cm$^2$ & d- 2000 mJ/cm$^2$] (Temperature scales in kelvin (K)).**

The variation of the surface temperature of samples as a function of number of laser pulses under different laser fluences is obtained, the result is plotted in Fig. 3.2. From this figure, at low laser fluences, the rate of surface temperature increases with the pulse numbers is comparatively low since less amount of energy is obtainable. As the fluence increased to a value equal or more than 1000 mJ/cm$^2$, the rate of temperature elevation with pulse number is also increased.

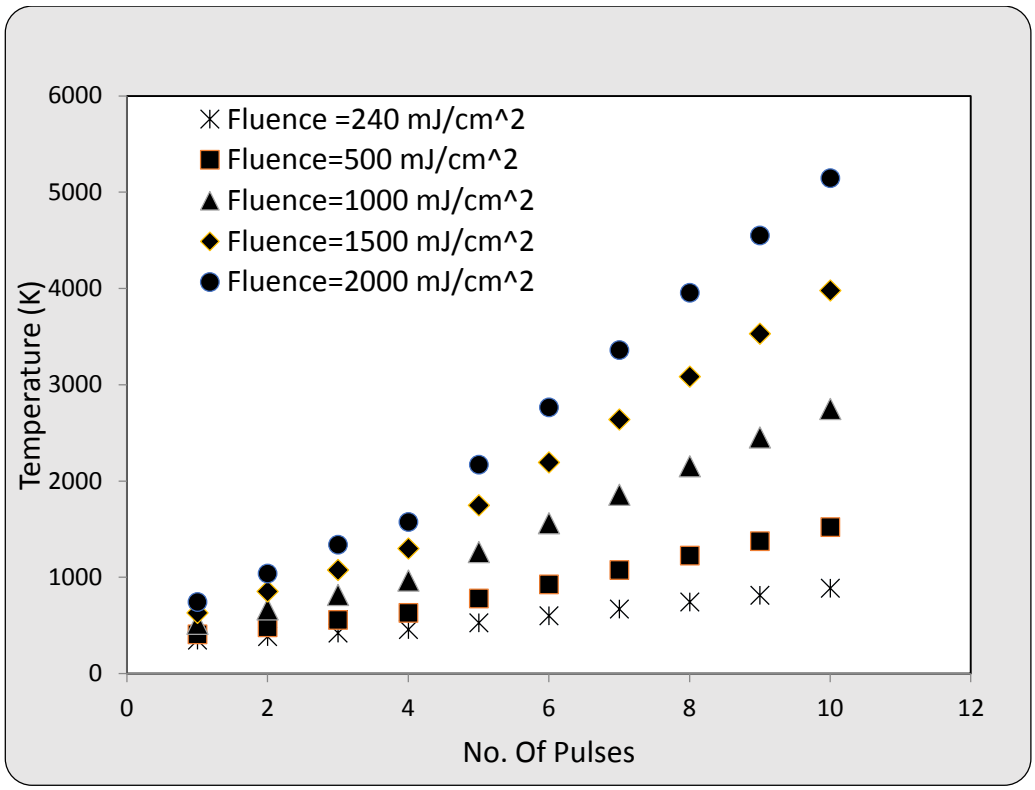


**Fig. 3.2: Surface temperature as a function of number of ArF laser pulses for CR39 polymer.**

The crater depth for single and repetitive laser pulses as a function of laser fluence for CR-39 polymer irradiated with 193 nm single laser pulse is presented in Fig. 3.3. It is observed that the ablation threshold occurs at laser fluence of 750 mJ/cm$^2$. At a fluence greater than 1000mJ/cm$^2$, a slight increment in ablation depth is noticed, it may be due to increment of thermal contribution in ablation process. In the case of a repetitive laser pulses, the ablation threshold is dropped to a value of 240 mJ/cm$^2$. For a fluence equal or more than 750 mJ/cm$^2$, the thermal influence become significant together with photochemical effects and the ablation depth showed an abrupt increase. Many studies of excimer laser ablation of polymers have been confirmed that at low fluences, thermal effects are negligible where photochemical models appears to work well while at higher fluences, thermal effects become significant [82, 101, 163].

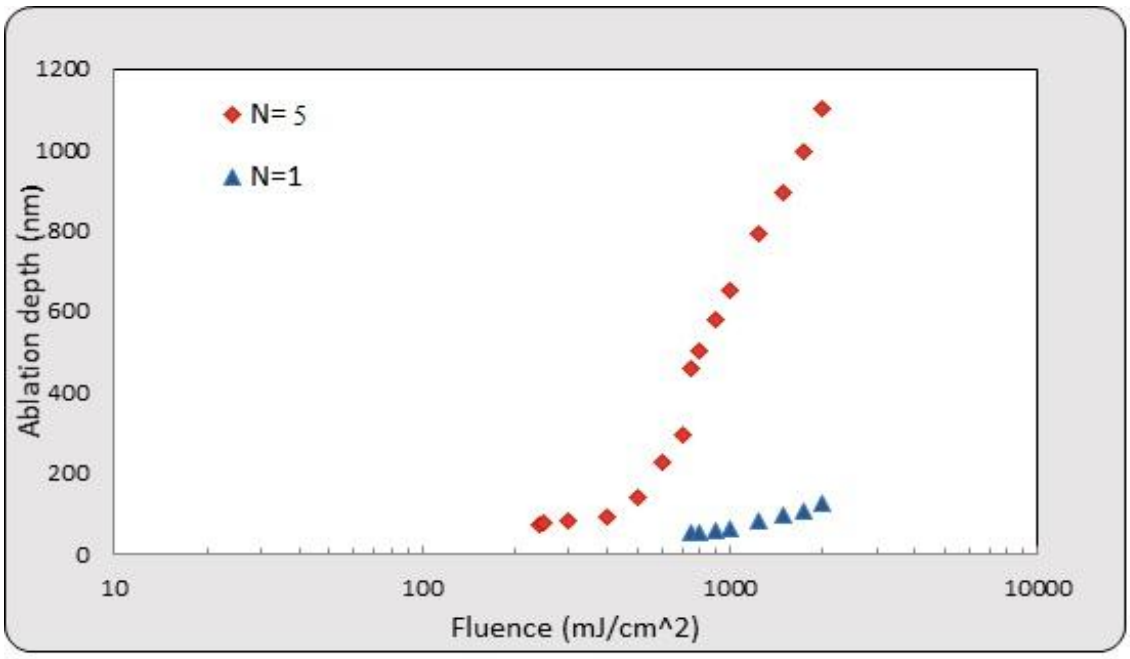


**Fig.3.3: Ablation depth versus laser fluence for CR39 polymer.**

Accordingly, the threshold fluence is presented in response to number of laser pulses as shown in Fig. 3.4, where the ablation threshold is modified from 750 mJ/cm$^2$ in case of a single laser pulse to a value of 240 mJ/cm$^2$ for five laser pulses.

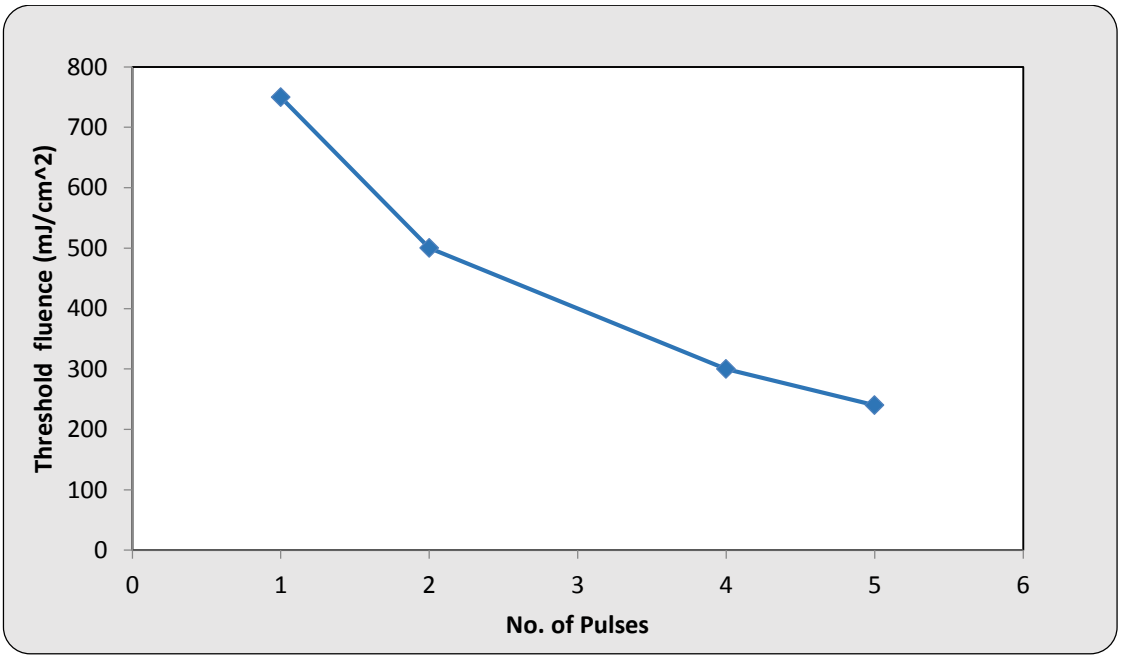


**Fig. 3.4: Threshold fluence dependence on number of laser pulses for CR39 polymer.**

### 3.3 ArF laser ablation

The ablation sites produced in CR39 polymer upon 193 nm ArF laser irradiation is quantitatively characterized utilizing the SEM micrographs. The side view of obtained sites gave ablation depth information allowing estimates of the etch rates and ablation threshold of CR39 polymer ablated at 193 nm ArF Excimer laser. Fig. 3.5 shows both the simulation and experimental results of ablated crater depth versus logarithmic laser fluence at 10 laser pulses.

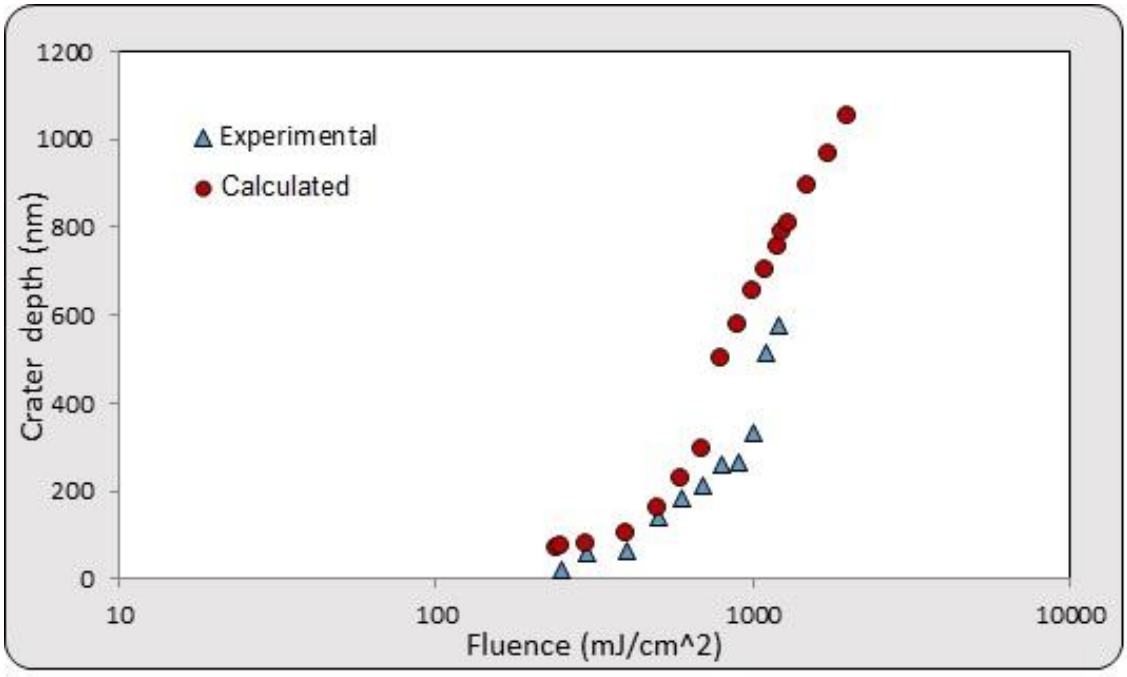


**Fig. 3.5: Calculated and experimental results for crater depth versus log laser fluence at 10 laser pulses.**

The crater depth given by the simulation is in a good agreement with the experimental results. However, simulation results show an increase in the crater depth with the incident laser fluence, while, practically is not, as the number of laser pulses increase the beam focusing position with respect to sample is varied so that the fluence is varied also which affect the resulting depth of the crater. The ablation threshold fluence ($F_{th}$) and the effective absorption coefficient($\alpha_{eff}$) are obtained by fitting the ablation rate versus

laser fluence line (Fig. 3.6) using eq. 1.21. The ablation threshold of 250 ± 10 mJ/cm$^2$ obtained for CR39 sample appears close to that reported for the same polymer with different laser irradiation setup, where the ablation threshold is about 300 mJ/cm$^2$ [164]. The obtained ablation threshold is found to match considerably well with simulation results for the case of repetitive laser pulses.

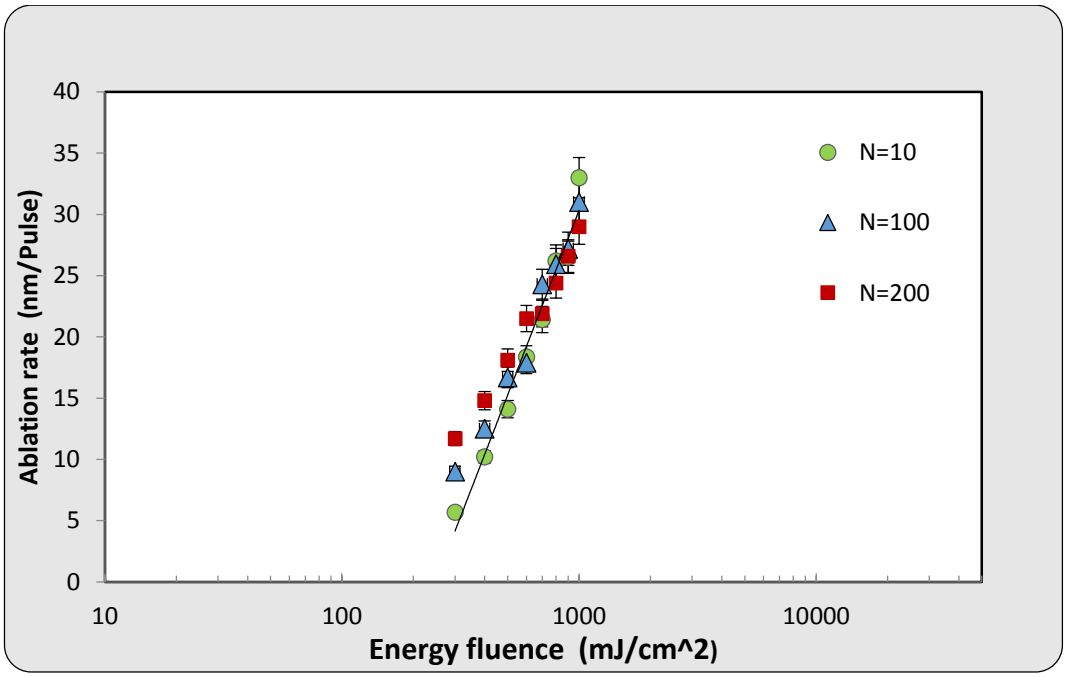


**Fig. 3.6: Ablation rate (nm/Pulse) versus log laser fluence at 10, 100, 200 laser pulses respectively.**

The effective absorption coefficient is calculated to be 3.9 ±0.3*10$^5$ cm$^{-1}$. It is different from linear absorption coefficient ($\alpha_{lin}$) of the polymer, it`s value is 26.976 cm$^{-1}$, that determined from the transmission behavior of UV –Vis. absorption spectrum of CR39 polymer under low irradiation fluence, which suggests that during the ablation process the laser light penetrates the polymer less than that expected from the linear absorption coefficient. It has been reported that $\alpha_{eff}$ could be many order of magnitude higher than ($\alpha_{lin}$) [165].

## 3.4 Physical modifications

### 3.4.1 Surface modifications prior and during ablation

The morphology and topography of CR39 polymer surface is investigated by SEM and AFM respectively. Fig. 3.7 shows the SEM micrograph of a non- irradiated sample.

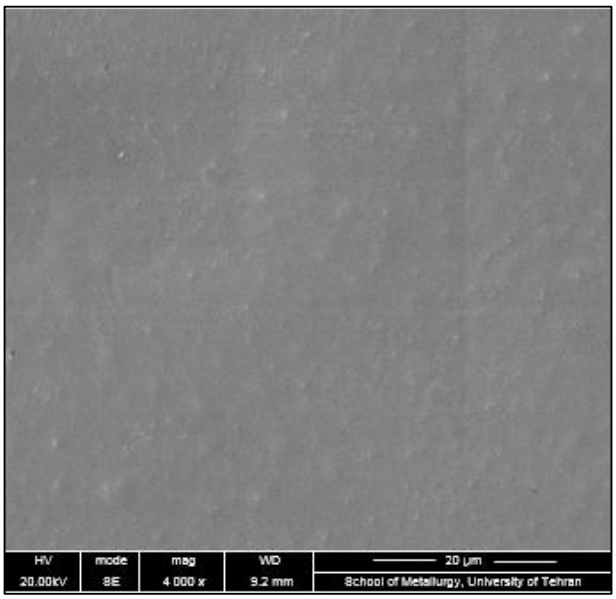


**Fig. 3.7: SEM micrograph of a non-irradiated CR39 polymer**

It can be observed that the sample surface is almost smooth and the corresponding surface roughness ($R_a$), as determined by AFM, given by deviations of arithmetic average in height from the sample center plane is around 2.5 nm.

The rectangular ablation site with an area of 5.923 $mm^2$ due to 193 nm ArF Excimer laser ablation using 50 pulses at a fluence of 400 $mJ/cm^2$ is shown in Fig. 3.8. The surface around the ablated area is seen to be clean with no evidence of debris or thermal damage which indicating that the photochemical ablation process is dominant and a good quality surfaces can be produced when ablating CR39 polymer at this laser wavelength.

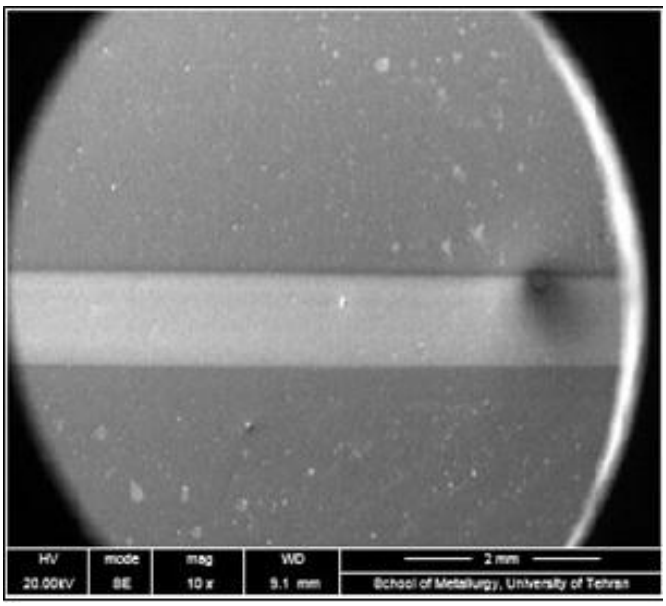


**Fig. 3.8: SEM micrograph of irradiated CR39 sample using 50 pulses at 400 mJ/cm$^2$.**

For CR39 irradiation with fluences below the threshold of ablation, no remarkable alteration on surface morphology more than a grains spread on the surface even if the number of pulses is reached up to 2000. Fig. 3.9 shows an SEM image of CR39 at fluence of 100 mJ/cm$^2$ with 2000 laser pulses.

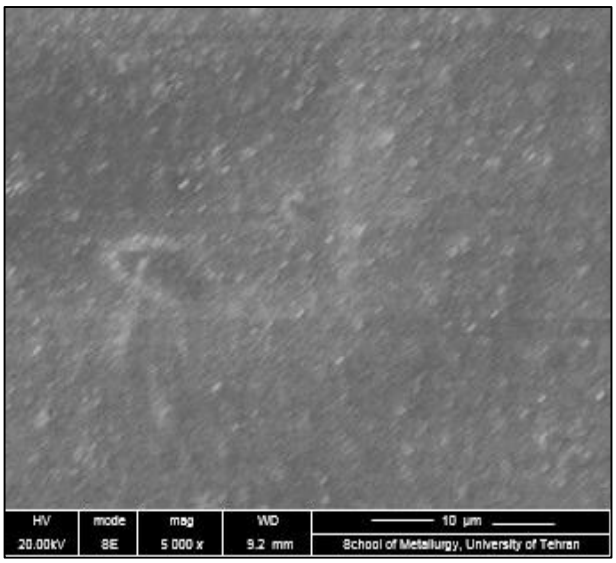


**Fig. 3.9: SEM micrograph of CR39 at a laser fluence of 100mJ/cm2 with 2000 laser pulses.**

This results agreed with other references stated that CR39 is resistant to present a morphological alteration at low UV irradiation while an obvious modification of its properties carry out over high UV irradiation [161]. Actually, CR39 is a threshold dependent polymer that exhibits a progressive formation of various micro- and nano- structures after a successive number of ArF laser pulses.

### 3.4.2 LIPSS formations

The treated areas above ablation threshold reflect major morphological changes as shown by SEM images depicted in Fig. 3.10 (a) – (f) at a laser fluence of 650 mJ/cm$^2$ while holding the laser parameters unchanged whereas the number of pulses (N) vary as 200, 400, 750, 1200, 1500 and 3000 respectively, In particular, the morphology comprised of three types of laser induced periodic surface structures (LIPSS): entangled nanochains microstructures at low energy dose (2.4 – 150 J/cm$^2$) and contours having a progressively increasing radius with energy dose at moderate level (200 - 500 J/cm$^2$) then the grooves patterns are gradually aligned at energy dose > 500 J/cm$^2$. It is worth emphasizing that these surface structures are formed at the crater bottom of the CR39 sample. It is commonly accepted that the interference between the incident laser beam and the surface- scattered wave play an important role in LIPSS formation [116,119] and this interfacing resulting in a modulated distribution of the energy on the surface. For polymers, some authors have been proposed that the modulated energy disposal on the surface induces a similarly modulated substrate heating [116, 166]. For CR39 polymers, the subsequent gradients of temperature allow diffusion of polymeric chains and, as consequence, entangled nanochains microstructures is evolved on the polymer surface. After repeated cycles of heating and cooling, due to increasing number of pulses, accumulation of polymer motion leads to the formation of grooves pattern.

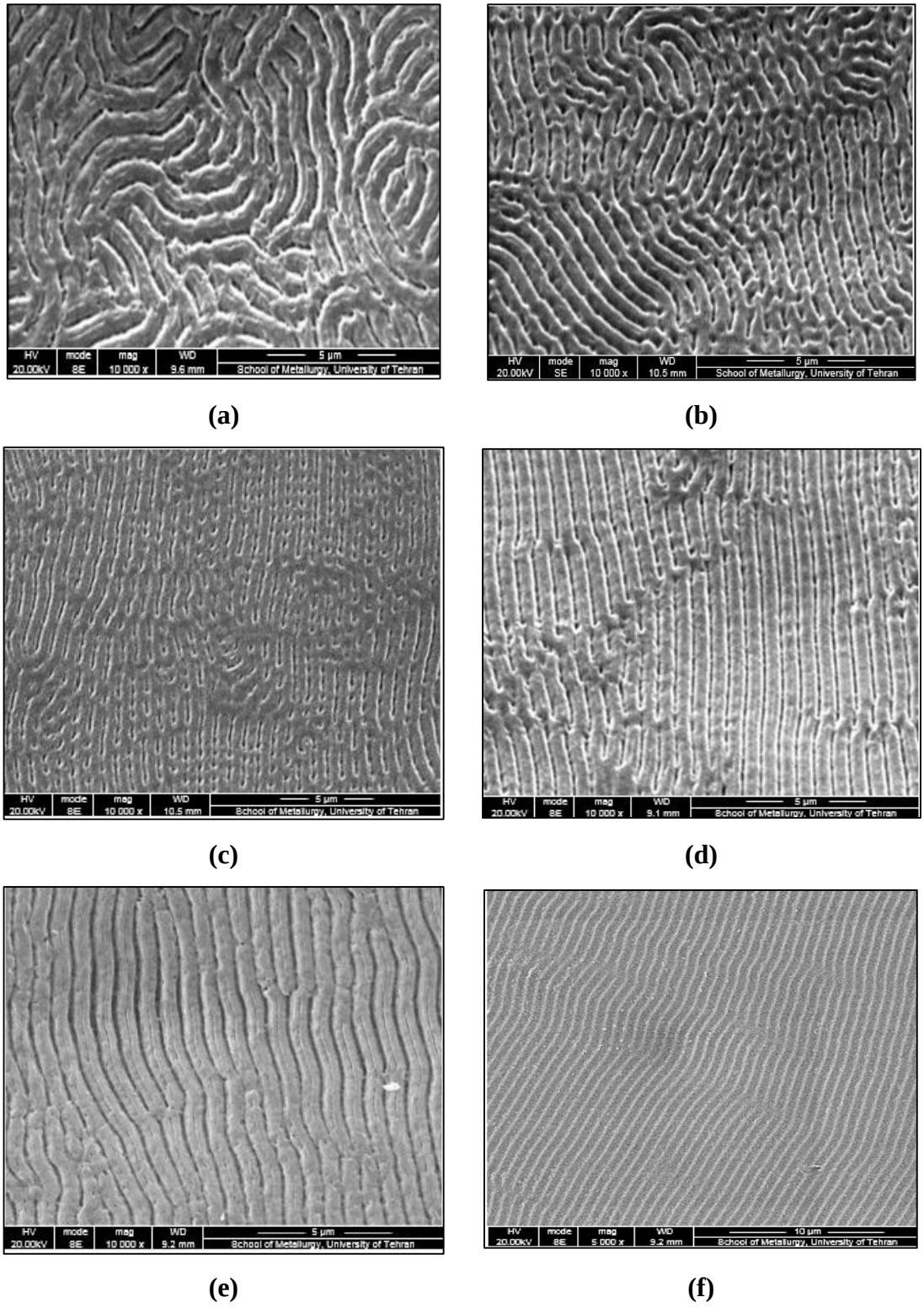


**Fig. 3.10: SEM micrograph of irradiated CR39 samples with 650 mJ/cm$^2$ at a) N= 200, b) N= 400, c) N= 750, d) N= 1200, e) N= 1500, f) N= 3000 coated with gold layer.**

Although there is no laser ablation below $F_{th} \approx 250$ mJ/cm$^2$, however the LIPSS produced after five to ten laser pulses. Recently, some publications have reported that in order to obtain LIPSS in amorphous polymers a minimum fluence value is necessary to ensure that the surface temperature exceeds the characteristic glass transition temperature ($T_g$) of the polymer therefore allowing polymer chain to rearrange [29, 115, 150]. In the case of semicrystalline polymers, not only the glass transition temperature is governed the thermal properties but also the melting temperature ($T_m$). It means that, to obtain LIPSS, the temperature of sample surface must be higher than $T_m$ and as a result superficial crystallites are melted which provides enough polymer dynamics [114] and the redistribution of the material [167]. The same model may be employed for CR39 polymer too since it is considered as semicrystalline polymer [168]. According to simulation results, it is shown that for CR39 irradiated with a fluence of 240 mJ/cm$^2$ at single laser pulse, the highest attained surface temperature is 351 K, which is below the decomposition temperature of CR39. However, for irradiation at the same fluence but with five laser pulses, a layer of around 19 nm heats to a temperature above decomposition temperature. Accordingly, to obtain LIPSS in CR39 polymer, it is suggested that the minimum required number of laser pulses, at a fluence of 250 mJ/cm$^2$, is about five to ensure that the surface temperature overcomes the decomposition temperature.

### 3.4.3 Measurement of Roughness, periodicity and height

In order to investigate roughness of the ablated surface and the relevant alteration of periodicity and height of the produced LIPSS, a three-dimensional (3-D) AFM images of CR39 samples is depicted as shown in Fig. 3.11. The topography images is acquired in the center of the ablation area.

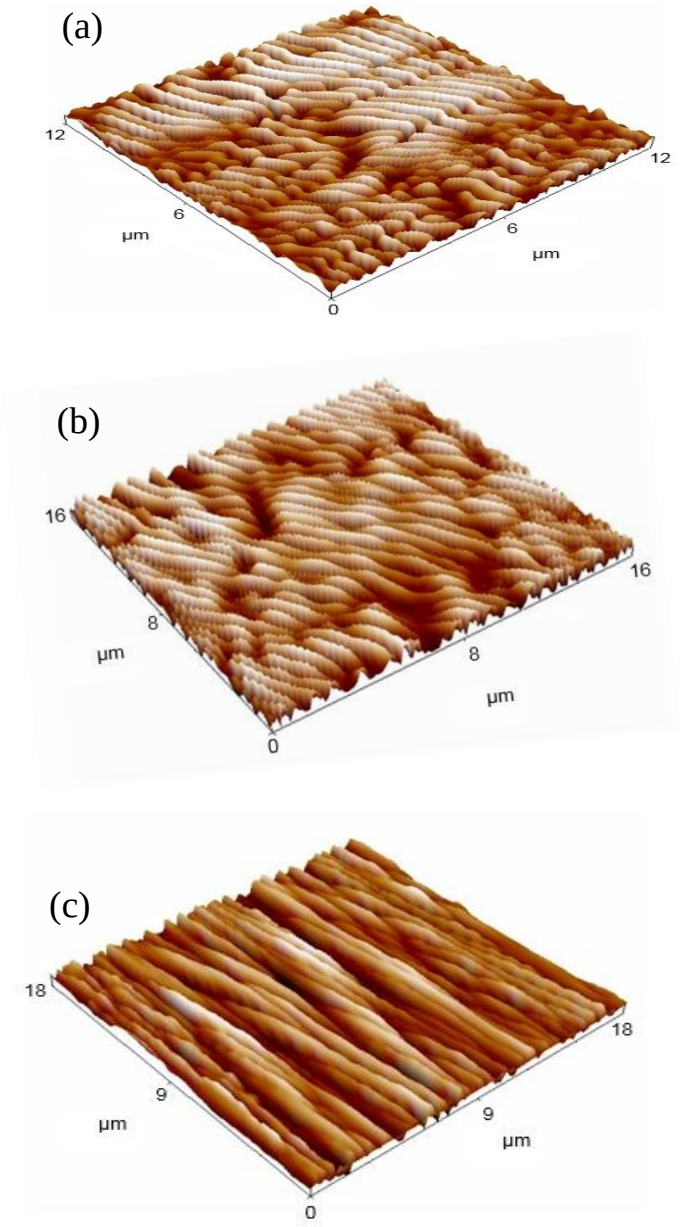


**Fig. 3.11: 3-D AFM images of irradiated CR39 samples at 1200 laser pulses with a fluence of a) 300mJ/cm2, b) 750 mJ/cm2, c) 1250 mJ/cm2.**

Generally, a number of laser parameters can be used to modify the periodicity of LIPSS in polymers [169, 151, 115]. For CR 39, LIPSS with a period of 630- 822 nm can be obtained by changing the laser fluence from 300- 2000 mJ/cm$^2$ at 1200 laser pulses (Fig. 3.12). It is observed that the periodicity increases in the fluence range 300- 1000 mJ/cm$^2$ then remains

nearly constant up to 2000 mJ/cm$^2$.The height of the LIPSS follows a similar tendency as a function of laser fluence, increasing up to 186 nm at 1000 mJ/cm$^2$ and then it gets plateau as shown in the inset of Fig. 3.12.

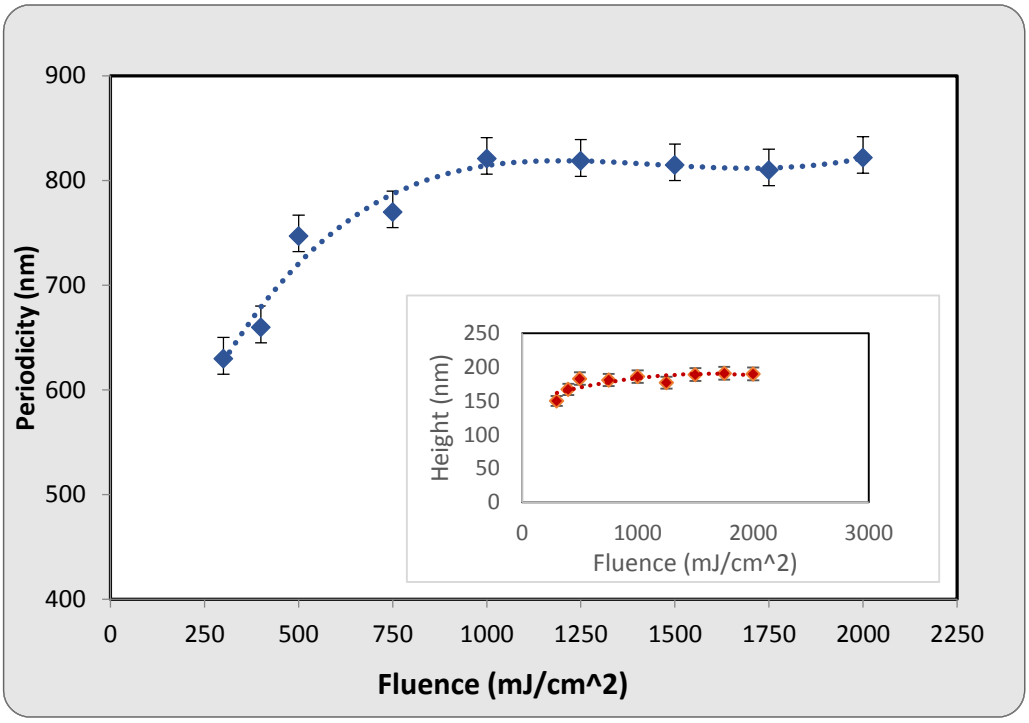


**Fig. 3.12 Variation of periodicity (nm) of LIPSS versus incident laser fluence (mJ/cm2) for 1200 laser pulses.**

The period of LIPSS also exhibit dependence on number of pulses, as reported by studies [170, 29]. Fig.3.13 shows a linear increase in the periodicity of LIPSS for a range of number of pulses from 750- 2500 at a fluence of 650 mJ/cm$^2$. Regarding LIPSS height, (shown in the inset of Fig. 3.13), similar to what is observed in the dependence of periodicity with number of laser pulses, it increases up to 186 nm for 2500 pulses.

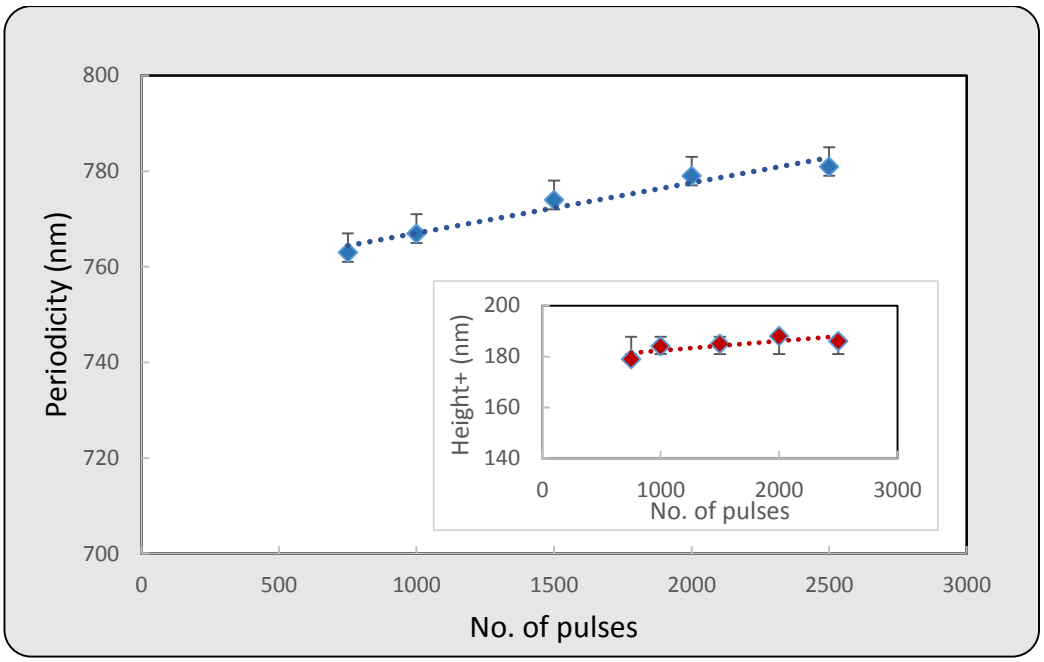


**Fig. 3.13: The periodicity of LIPSS (nm) versus number of pulses at a fluence of 650 mJ/cm$^2$.**

The results indicate that the periodicity of the produced LIPSS is not depending on the wavelength of the incident laser where the produced LIPSS shows a periodicity about four times greater than incident laser wavelength. Only a few studies on the formation of LIPSS with a periodicity larger than the laser wavelength are reported by researchers. These LIPSS usually referred to as "grooves" [171] were observed in metals [172], semiconductors [171] and polymers [151,164]. To the best of our knowledge, there are a few papers proposed grating coupling as an explanation for groove formation [172]. From a practical point of view, it is concluded that these structures can be written reproducibly, homogeneously over a large area with a period can be selected in the range from 630-822 nm. Also, the roughness of the produced LIPSS, $R_a$, given by the arithmetic average of the deviation in height from the center plane of polymer sample is measured and its dependence on the laser fluence for 1200 laser pulses is plotted in Fig. 3.14. It is observed that for a laser irradiation below ablation threshold, typically 125 mJ/cm$^2$ gives $R_a$ equal 3.7 nm, there are no

significant change neither in morphology nor in surface roughness in comparison to unirradiated polymer surface. For the fluencies above ablation threshold, pronounced difference in surface roughness is revealed till it reached to a 1500 mJ/cm$^2$ where a slight increase in surface roughness is observed. A similar results are obtained for the dependence of surface roughness on incident laser fluence, upon KrF Excimer laser irradiation of polymeric fiber, was reported [173].

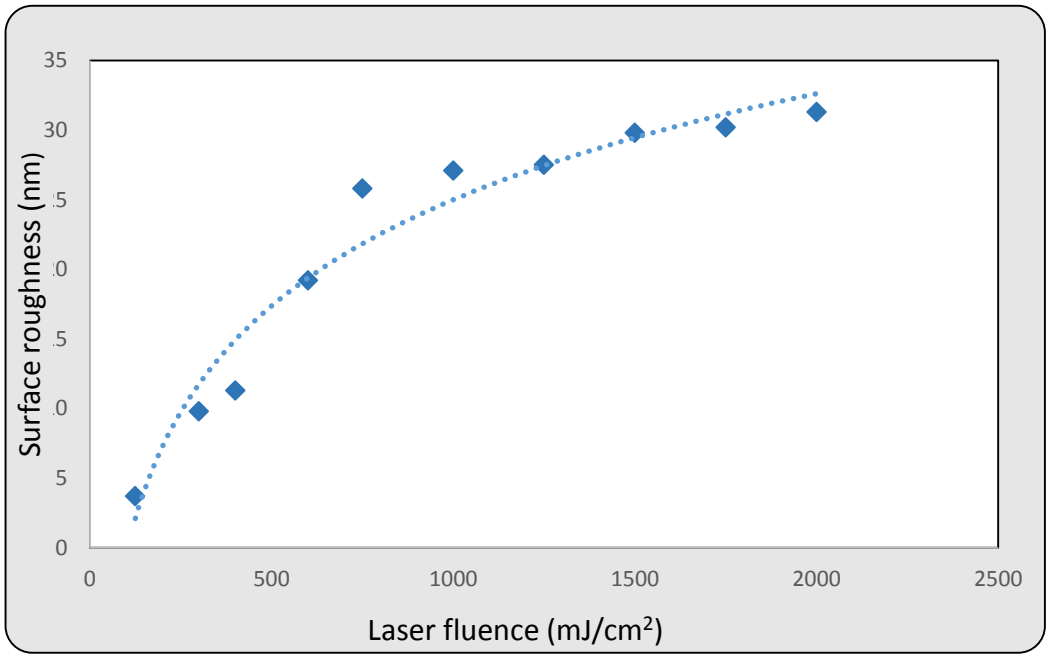


**Fig.3.14 The surface roughness (nm) versus laser fluence (mJ/cm2) for 1200 laser pulses.**

## 3.5 Chemical modifications

Together with the physical modifications induced due to 193 nm laser irradiation, chemical modifications can take place also. The analysis of unirradiated and irradiated CR39 polymer with a fluences smaller than $F_{th}$, 125 mJ/cm$^2$ at 100 and 400 pulses and with a fluence greater than $F_{th}$, 800 mJ/cm$^2$ at 100 and 200 pulses by ATR- FTIR spectroscopy is shown in Fig. 3.15.

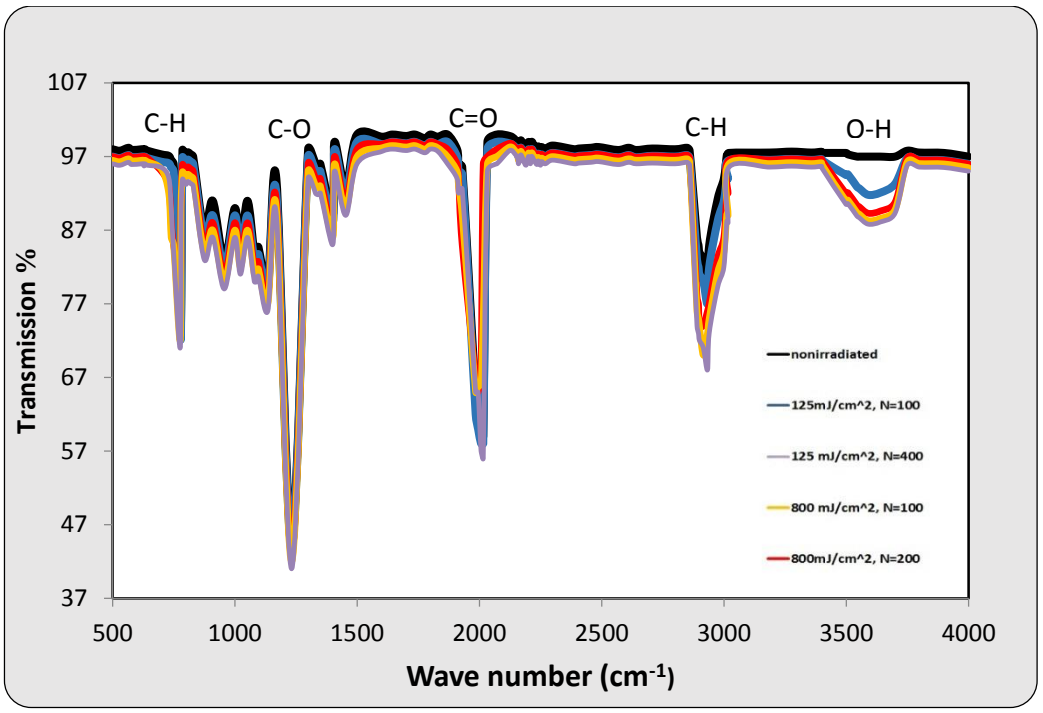


**Fig. 3.15 FTIR spectrum of unirradiated and irradiated CR39 Polymer at 125 mJ/cm$^2$ with N=100 and 400 and 800 mJ/cm$^2$ at N= 100 and 200.**

For the irradiated sample at 125 mJ/cm$^2$ with 100 pulses, it is observed that the transmission is decreased over the whole mid- IR region and decreased more upon irradiation at the same fluence with 400 laser pulses. This decrease in transmission is assigned to an accumulation of carbonaceous species in and around irradiated area [174,175]. While for irradiation at 800 mJ/cm$^2$ with 100 pulses, the transmission is increased over the whole mid- IR region and is continuing in increasing upon pulse number increasing and a slight shift in the band at 2940 cm$^{-1}$ toward a lower wavenumber is also observed. This modifications is attributed to bond scission and cross- linking process that finally produce a new composition [90]. Also, a new band in the region 3500- 3700 cm$^{-1}$ (OH band) is formed upon 193 nm irradiation and even below ablation threshold. It has been reported that for several polymers the oxygen concentration can change upon irradiation in air with low fluences [169, 176,177] and in the particular case

of LIPSS formation, surface oxidation has also been reported for irradiation of different polymers with UV pulses in the nsec. regime [118].

### 3.6 SERS characterization

The SERS enhancing properties of nanostructured CR-39 polymer surface coated with gold (Au) metal layer have been tested using Thiophenol (TP) as a probe molecule. TP used as a model system, which has widely been studied to evaluate the conductivity between metallic electrodes and the body of conjugated molecules [178].

#### 3.6.1 Detection of Thiophenol (TP) analyte

The Raman spectrum of the supplied TP liquid in a cuvette and the spectrum of a drop of TP poured onto unirradiated CR39 substrate and dried in air substrate is shown in Fig. 3.16.

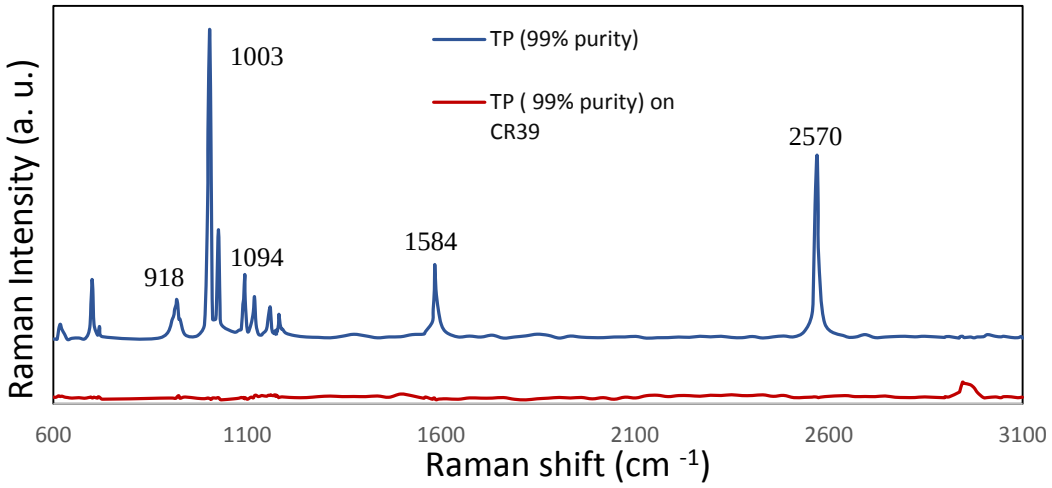


**Fig. 3.16: Raman spectra of Thiophenol (TP) (99% purity) in liquid and on CR39 substrate. The spectrum has been shifted vertically for clarification.**

The spectrum of TP as supplied exhibits the characteristic bands that are belonged to its molecular vibrations [179,180]. For the TP poured on the surface of CR39 sample, no Raman signal of TP is recognized and only a band in 2945 $cm^{-1}$ that attributed to CR39 sample is detected [181].

Self- assembled monolayers of pure and functionalized alkylthiols on metals, especially on gold, have been practically widely investigated [134, 182,183]. At the molecular level, these systems have facilitated investigations and added extensive fundaments insight to this field. This approach is used here to generate a monolayer of thiophenol (TP) to estimate the SERS activity of the produced substrate. In particular, the interaction of TP with gold surface causes variations in the Raman bands of the TP in terms of frequency shift, change of relative intensity or disappearance of some of the bands with respect to the spectrum in solution which is related to the surface enhancement mechanism and molecular orientation [184, 26,185]. Most prominently, bands recognized in the spectrum of TP liquid at 918 and 2570 $cm^{-1}$ that ascribed to the stretching and binding vibrations of the S-H bond respectively are disappeared in the spectrum of gold coated nanostructured CR39 substrates. This observation suggests that TP is chemisorbed dissociatively on the substrate surface by rupture of the S-H bond as mercaptide ($C_6$ $H_5S^-$) [179, 186]. This effect, together with intensity enhanced of bands shifted from 1094 to 1074 $cm^{-1}$ and from 1584 to 1572 $cm^{-1}$ (Fig. 3.16 blue line), belonged to a change of the adsorbed molecules environment, give supporting evidence of the bonding of TP anion to the gold surface through the sulfur atom, indicating the formation of a monolayer at the surface [179].

Fig. 3.17 compare the Raman spectra obtained for a TP (100μM concentration) acquired on 30 nm gold coated irradiated CR39 substrates with 650 $mJ/cm^2$ at 100, 200, 1200, 1500 and 3000 laser pulses respectively. As expected, the SERS intensity is dramatically improved due to the existence of LIPSS on polymer substrate underlying the gold layer and this

enhancement is depending on the variation of the morphology of polymer substrate. It has been reported that gold nanoparticles coating nanostructured polymer film that prepared by spin coating on silicon wafer enhanced the Raman signal around ten order of magnitude while a negligible Raman signal is obtained for TP concentration of 9 M on silicon wafer [187]. The enhancement of the Raman signal can be attributed to the electromagnetic enhancement mechanism which is direct consequence of hot spots created by agglomeration of the deposited gold nanoparticles [188].

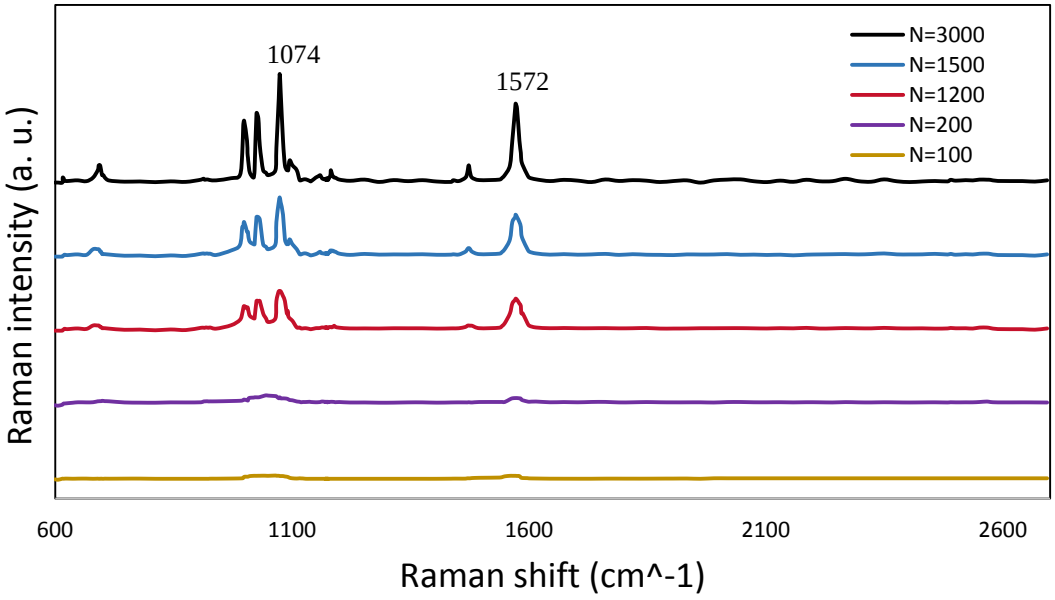


**Fig. 3.17: SERS spectra for TP at a concentration of 100 µM on gold coated irradiated CR39 substrate with 650 mJ/cm2 at 100, 200, 1200, 1500 and 3000 laser pulses respectively. Spectra have been consecutively shifted vertically for clarification.**

### 3.6.2 SERS- enhancement factor (EF) for TP

The SERS enhancement factor is determined by using equation (1.13). To estimate values of signal intensity for both SERS ($I_{SERS}$) and normal Raman scattering ($I_{RS}$), the SERS intensity of the strongest TP band at 1074 $cm^{-1}$ is compared with the corresponding band measured from liquid TP, as

proposed [189]. For normal Raman measurement, the number of contributing molecules ($N_{vol}$) is calculated by determining the number of molecules situated in the focal volume which is about $4.74*10^{21}$ molecules. For SERS measurement, the number of molecules contributing is calculated by estimating the number of molecules in the focal spot, which is about $0.86*10^{14}$ molecules for 100 µM concentration of TP. The Enhancement Factors of SERS substrates for TP at 100 µM concentration are compared on different LIPSS morphology that produced using ArF laser pulses and coated with 30 nm gold (Fig. 3.18).

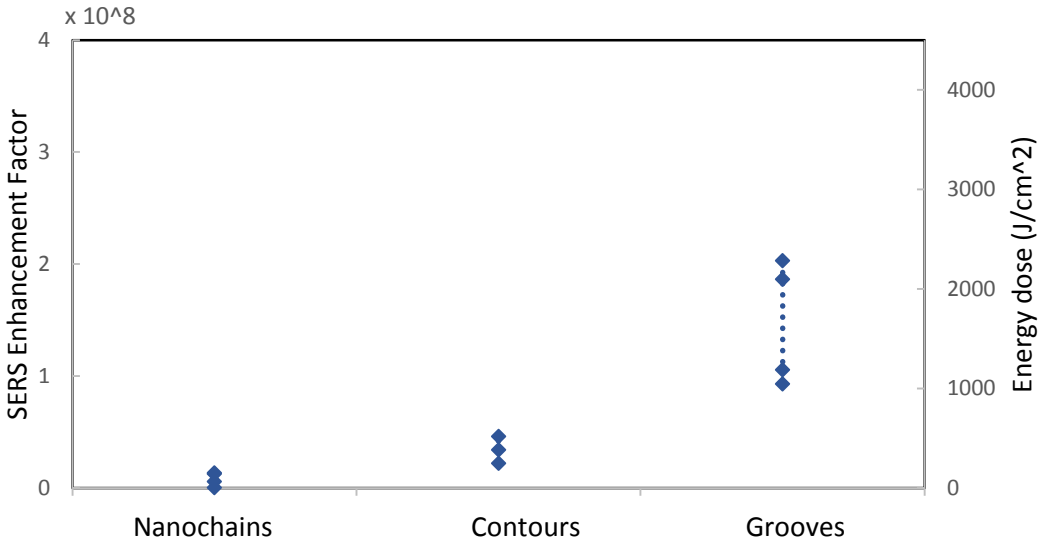


**Fig. 3.18: Enhancement factor of SERS substrate for TP at a concentration of 100 µM on 30 nm gold coating as a function of LIPSS morphology.**

An accurate speculation of enhancement factor of SERS is not easy to determine. The SERS equations that stated in (section 1.3.3) calculate the EF by comparing the normal Raman scattering and SERS signal counts for the number of contributed molecules. When measuring the normal Raman signal from a solution, an acceptable accurate speculation of the total number of contributing molecules is made through calculation of the system focal volume. However, for SERS signal, it is quite challenging to find the exact

number of molecules that adsorbed on the nanostructured surface. Instead of that, a speculation of number of contributing molecules that might suit into the focal plane is utilized. Nevertheless, for the goal of completeness, the EF for SERS substrate is speculated and the highest obtained values are for LIPSS of grooves like structure. It is found to be in the range from $0.9*10^8$ to $2*10^8$ which is four times greater than that reported for gold coated LIPSS that generated on thin PTT film upon 193 nm ArF laser irradiation [190]. A comprehensive study on SERS enhancement factor demonstrated that the EF only need to be $10^7$ for a single- molecules sensitivity [191].

### 3.6.3 Effect of LIPSS parameters on SERS intensity

To get a better understanding of the effects of morphological alterations of polymer surface, upon laser irradiation, on the enhanced Raman signal. Fig. 3.19 exhibited the variation of SERS intensity of the strongest Raman band of TP at 1074 $cm^{-1}$ for a concentration of 100 μM as a function of surface roughness, periodicity and height of the LIPSS that obtained through irradiation at a fluences of 300, 400, 750, 850 and 1000 $mJ/cm^2$ with 1200 laser pulses. These results suggest that, the LIPSS with highest values of surface roughness, periodicity and height gave the highest Raman enhancement.

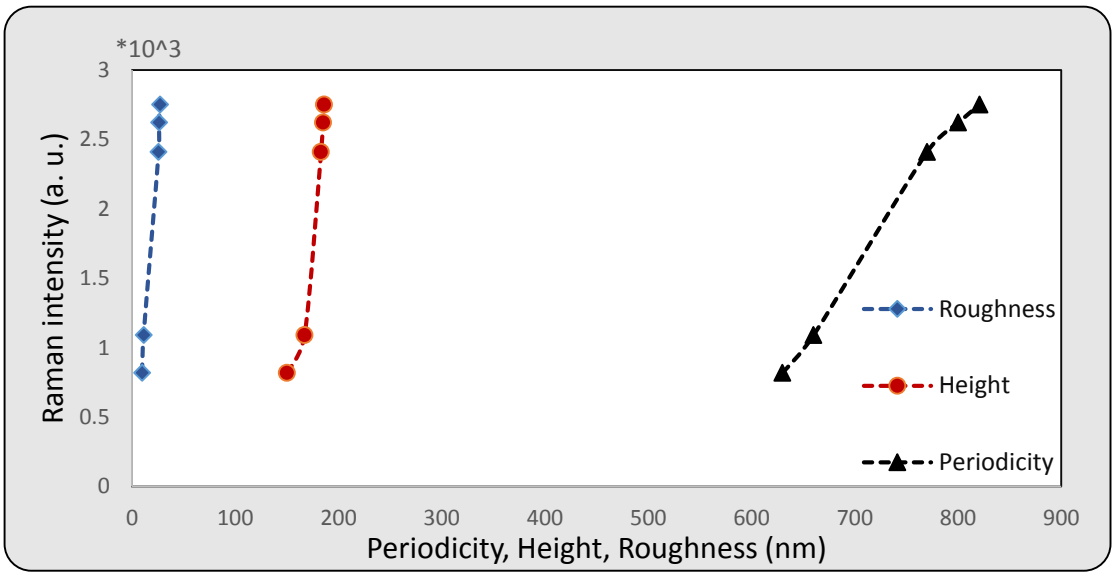


**Fig. 3.19: Relation between SERS intensity of the strongest Raman band of TP at 1074 cm-1 for a concentration of 100 µM and surface roughness, periodicity and height of the LIPSS that obtained through irradiation at a fluences of 300, 400, 750, 850 and 1000 mJ/cm2 with 1200 laser pulses.**

### 3.6.4 Effects of gold layer thickness on SERS activity

The SERS intensity increases with Au layer thickness deposited on ripples has been demonstrated [192,193]. To explore if there is any relation between SERS activity of the produced LIPSS and thickness of coated gold layer, SERS measurements of the strongest Raman band of TP at 1074 $cm^{-1}$ with a concentration of 100 µM acquired on gold coated LIPSS, that produced due to irradiation at a fluence of 1000 $mJ/cm^2$ with N= 1200, are performed for various thickness of Au (Fig. 3.20). It is showed that the Raman signal of TP is dramatically enhanced with increasing of thickness of Au layer. This may be in a good agreement with the fact that with small thickness of gold layer, nanoparticles layer are obtained and with thickness increasing the distance between these nanoparticles are decreased. Research studies on silver and gold nanoparticles have shown that as the gap between the particles decreases, there is an increase in the EM intensity, a large number of hot spot is existed, which leads to enhancement of Raman signals

[194-196]. However, the Raman signal decreases rapidly when the thickness of gold layer is more than 30 nm and this may be attributed to transformation of nanoparticles layer to continues or large particulates which signifies a lower amount of hot spot.

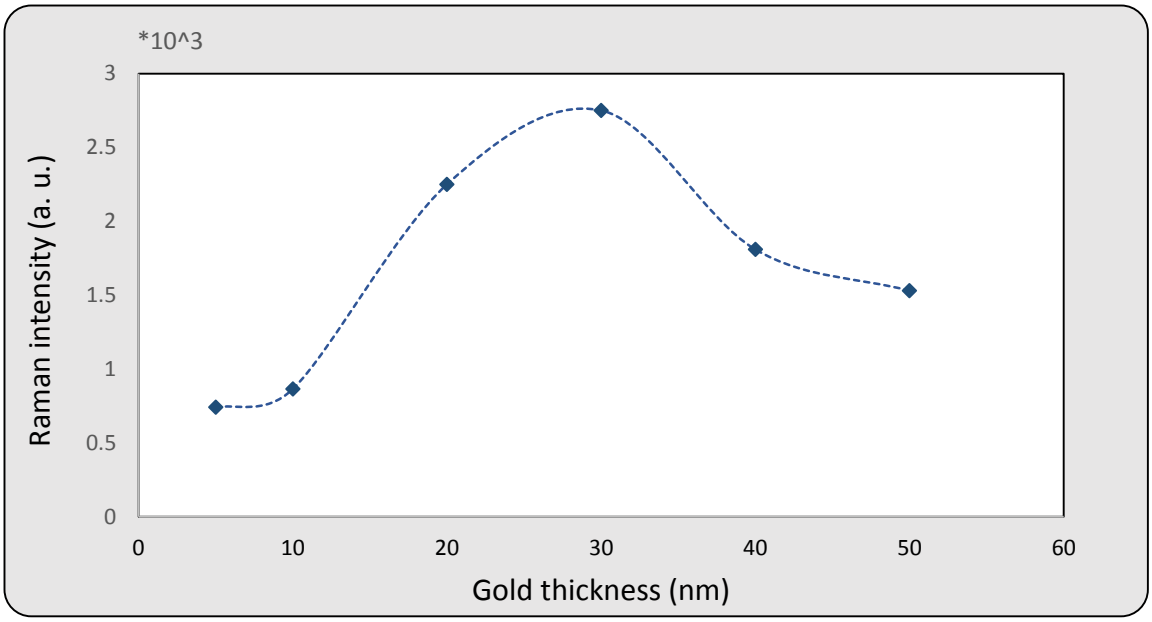


**Fig. 3.20: Comparison of SERS intensities of TP at 1074 cm-1 with 100 µM concentration acquired on gold coated LIPSS, that produced due to irradiation at a fluence of 1000 mJ/cm2 with N= 1200, are performed for various thickness of gold coating .**

### 3.6.5 Sensitivity of SERS substrate

The Sensitivity is an important figures of merit for SERS substrates and to evaluate the Raman enhancing capability of the produced LIPSS substrate as SERS sensor. Solution of TP with different concentrations are used to study the SERS sensitivity of the LIPSS substrates. Fig. 3.21 shows the Raman intensity of TP at 1074 $cm^{-1}$, acquired on gold coated LIPSS substrates that obtained through irradiation with 2000 $mJ/cm^2$ and 1200 laser pulses, versus TP concentration. These results clearly show the ability of the produced substrate to exhibit a measurable Raman signal even with a TP concentration of 10 nM.

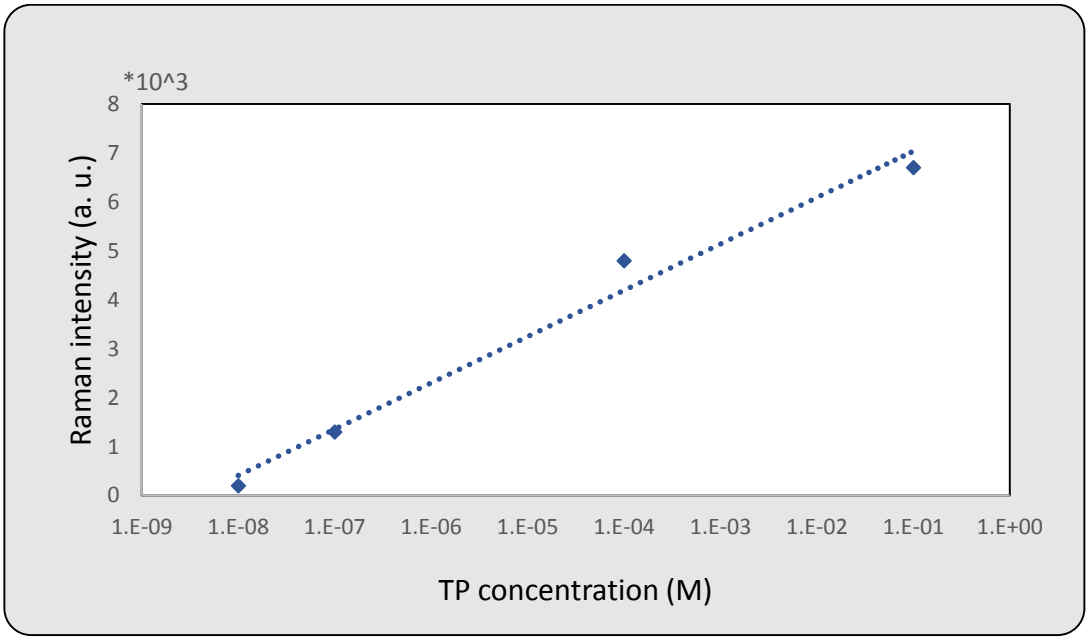


**Fig. 3.21: SERS intensity of TP at 1074 $cm^{-1}$, acquired on gold coated LIPSS substrates that obtained through irradiation with 2000 mJ/cm2 and 1200 laser pulses, as a function of TP concentration.**

## 3.7 Applications of SERS substrate

### 3.7.1 Detection of Methylene Blue (MB) traces in water

One of the important applications of SERS is for detection of contaminants in drinking and agricultural water. Unlike other techniques such as IR absorption spectroscopy, SERS is comparatively insensitive to the presence of water molecules. As such, contaminants can be specified from the collected spectrum**.** Accordingly, a test is performed to determine if the produced SERS substrate may detect Methylene blue traces in water. Figure 3.22 exhibits the normal Raman spectrum of 1mM methylene blue aqueous solution. It can be seen that, only a part of Raman bands are recognized, such as at 449, 502, 772, 1181, 1395 and 1623 $cm^{-1}$. Both the bands at 449 and 502 $cm^{-1}$ are belonged to C-N-C skeletal bending vibrations. While the other bands are belonged to C-H out of plane bending

vibration, C-N stretching, $CH_3$ deformation and C-C ring stretching respectively [197].

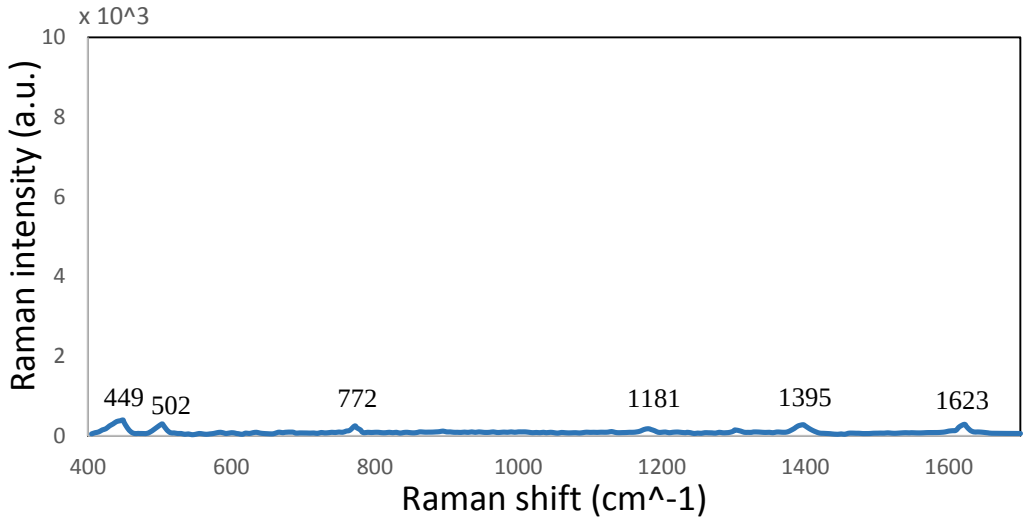


**Fig. 3.22: Normal Raman spectrum of 1mM methylene blue (MB) aqueous solution.**

Among many SERS substrates that produced during this study, the SERS substrate of 30 nm gold coated LIPPS of grooves like nanostructures, produced due to irradiation of 2400 J/cm$^2$ energy dose, gives the strongest enhancement effect and is elected here for detection of MB traces in water as shown in Figure 3.23. It exhibits the SERS spectra of MB adsorbed on the substrate with a concentration ranging from 100 down to 0.1 μM. In comparison with normal Raman spectrum of methylene blue aqueous solution (Fig. 3.22), good quality and high well-resolved SERS spectra are achieved for MB adsorbed on the substrate where the characteristic bands of MB at 449, 502, 1395 and 1623 cm$^{-1}$ are recognized at concentration as low as 0.1 μM. No MB features is identified for 0.01 μM concentration. The major bands of SERS and normal Raman scattering of MB are consistent where there are no blue or red shift detected in the SERS of MB but there are an alterations in the relative intensities of the characteristic bands of SERS in comparison with normal Raman scattering. These relative intensities alterations of characteristic bands is belonged to interaction of MB molecules with active metal surface.

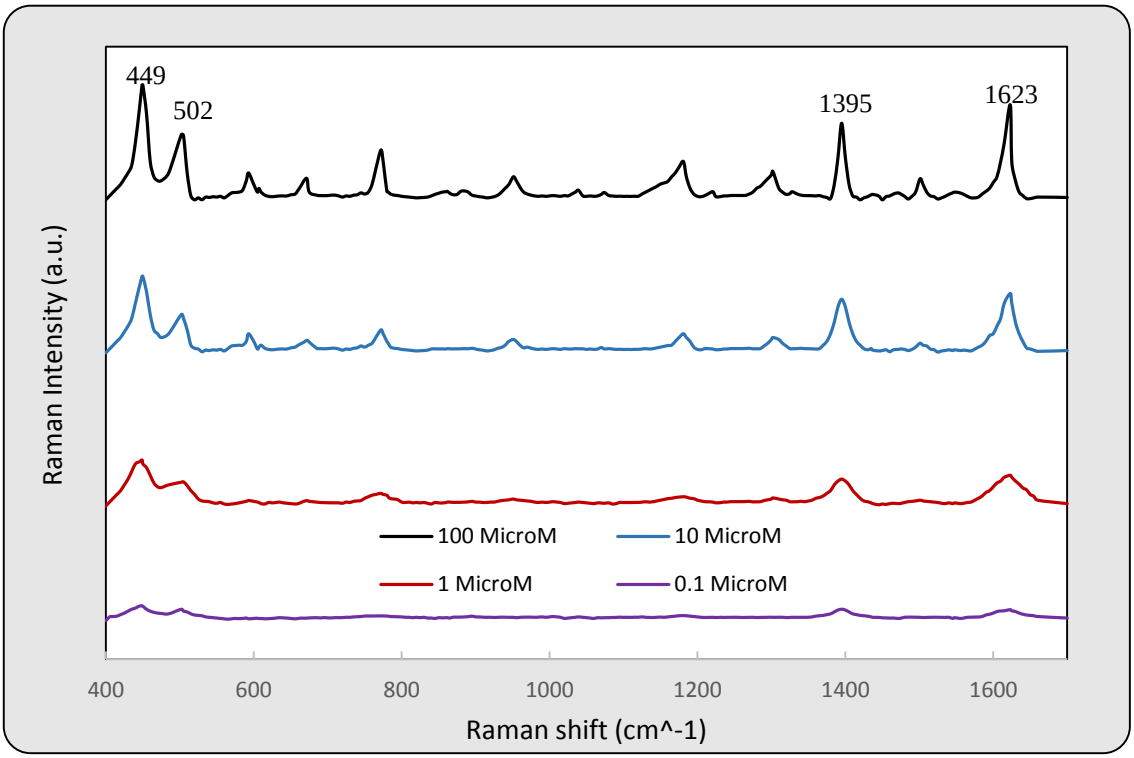


**Fig. 3.23: SERS spectra for MB at a concentration of 100, 10, 1 and 0.1 µM on 30 nm gold coated LIPPS of grooves like nanostructures produced due to irradiation of 2400 J/cm2 energy dose . Spectra have been consecutively shifted vertically for clarification.**

The relative intensity of major characteristic bands of SERS at 449, 502, 1395 and 1623 $cm^{-1}$ is increased as MB concentration is increased as shown in Fig. 3.24. It is evident that there is a high linear relationship between intensity of each of the four characteristic bands and MB concentration, indicating that it is probably to quantify MB in water through the produced SERS substrate.

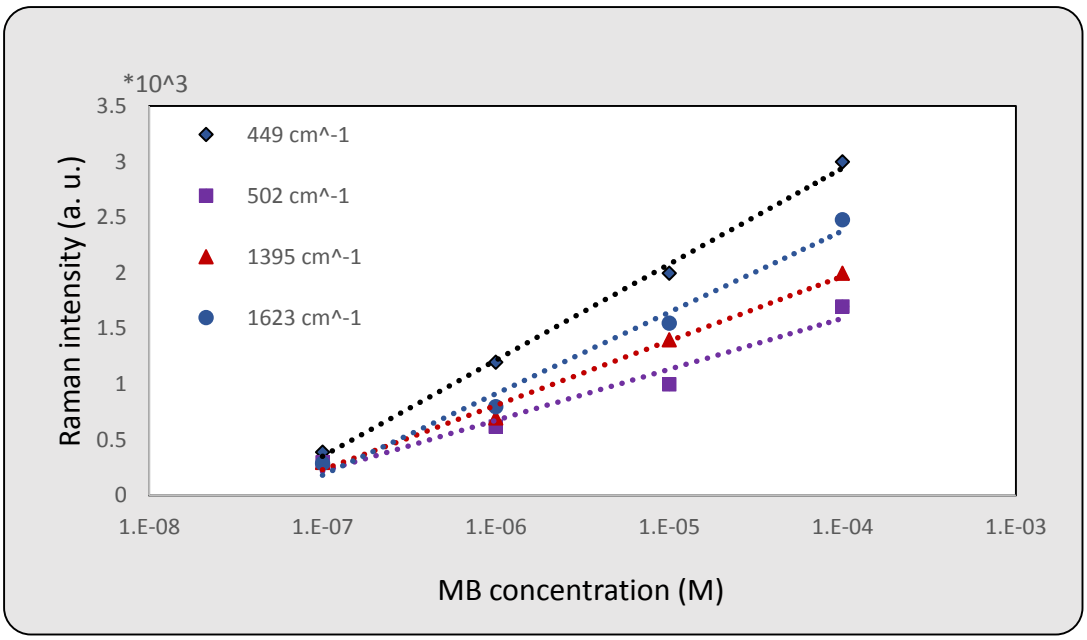


**Fig. 3.24: The relationship between relative intensities of major characteristic bands of SERS at 449, 502, 1395 and 1623 cm-1 and MB concentration.**

### 3.7.2 Cell adhesion and proliferation

It is established that the modified surface properties due to formation of LIPPS on polymer surface have the ability to induce an alignment of living biological cell cultured thereon [148]. Regarding that, there is a trial to investigate the capability of the produced LIPSS for cell culturing but it is postponed for future work.

# CHAPTER FOUR

## Conclusions and Suggestions for Future Works

## 4.1 Conclusions

The main conclusions of the present work are summarized according to the uniting theme:

- The thermal contribution have an important role in 193 ArF laser ablation of CR39 polymers where the formation of LIPSS at bottom of the ablated crater is achieved only when the polymer surface temperature overcomes the decomposition temperature.
- The obtained ablation threshold of 250 mJ/cm$^2$ is found to match considerably well with simulation results for the case of repetitive laser pulses in which it is much lower than that reported using 248 KrF laser that gives $F_{th}$ as 6 J/cm$^2$ [161].
- The intensity enhancement appears to be more related to the roughness and height of the LIPPS than the periodicity and that is due to an increase in effective area which leads to a large number of light enhancing nano- particles and more scattering of TP molecules bound to the gold.
- The produced SERS substrate has the capability to be utilized as a SERS biosensor and it`s sensitivity is characterized through detection of MB at concentration as low as 0.1 μM.

## 4.2 Suggestions for future work

The work presented in this thesis can be extended in the future to cover the following research trends:

- Investigating the ability of the produced LIPSS as a notch filter for optical communication systems.
- Investigating the capability of the produced LIPSS for cell culturing.
- Studying the effect of utilizing ultra-short pulses duration for ablation of CR39 polymer.
- Examining the ability of SERS biosensor to characterize other biomaterials.

- Utilizing different types of lasers for irradiation of CR39 to investigate effect of various wavelengths on the produced LIPSS.

## References


1. P. M. Kosaka, V. Pini, J. J. Ruz, R. A. da Silva, M. U. González, D. Ramos, M. Calleja and J. Tamayo, "Detection of cancer biomarkers in serum using a hybrid mechanical and optoplasmonic nanosensor". Nat Nanotechnology Vol. 9, No. 12, P. 1047–1053, 2014.
2. Sh. O. Kelley, C. A. Mirkin, D. R. Walt, R. F. Ismagilov, M.Toner and E. H. Sargent, "Advancing the speed, sensitivity and accuracy of biomolecular detection using multi-length-scale engineering", Nat Nanotechnology, Vol. 9, No. 12, P.969–980, 2014.
3. C. Y. Zhang, H. C. Yeh, M. T. Kuroki and T. H. Wang, "Single-quantum-dot-based DNA nanosensor" , Nat Mater Vol. 4, No.11, P. 826–831, 2005.
4. J. E. Reiner, A. Balijepalli, J. W. F. Robertson, J. Campbell, J. Suehle and J. J. Kasianowicz, "Disease detection and management via single nanopore-based sensors", Chem Rev., Vol. 112, No. 12, P. 6431–6451, 2012.
5. J .Homola, "Surface plasmon resonance sensors for detection of chemical and biological species", Chem Rev, Vol. 108, No. 2, P. 462–493, 2008.
6. E. J. Reiner, R. E. Clement, A. B. Okey, C. H. Marvin, "Advances in analytical techniques for polychlorinated dibenzo-p-dioxins, polychlorinated dibenzofurans and dioxin-like PCBs" , Anal Bioanal Chem, Vol. 386, No. 4, P. 791–806, 2006.
7. B. R. Baker , R. Y. Lai , M. S. Wood , E. H. Doctor , A. J. Heeger and K. W. Plaxco, "An electronic, aptamer-based small-molecule sensor for the rapid, label-free detection of cocaine in adulterated samples and biological fluids", J Am Chem Soc., Vol. 128, No. 10, P.3138–3139, 2006.

**8.** M. B. Pushkarsky, I. G. Dunayevskiy, M. Prasanna, A. G. Tsekoun, R. Go and C. K. N. Patel, "High-sensitivity detection of TNT", Proc Natl Acad Sci USA, Vol. 103, No. 52, P. 19630–19634, 2006.

**9.** S. Nie, S. R. Emory, "Probing single molecules and single nanoparticles by surface enhanced Raman scattering", Science, Vol. 275, No. 5303, P.1102–1106, 1997.

**10.** K. Kneipp, Y. Wang, H. Kneipp, L. T. Perelman, I. Itzkan, R. R. Dasari, and M. S. Feld, "Single molecule detection using surface-enhanced Raman scattering (SERS)", Phys Rev Lett, Vol. 78, No. 9, P.1667–1670, 1997.

**11.** Y. C. Cao, R. Jin , C. A. Mirkin, "Nanoparticles with Raman spectroscopic fingerprints for DNA and RNA detection", Science, Vol. 297, No. 5586, P.1536–1540, 2002.

**12.** M. Moskovits, "Surface-enhanced spectroscopy", Rev Mod Phys, Vol. 57, No. 3, P. 783–826, 1985.

**13.** J. N. Anker, W. P. Hall, O. Lyandres, N.C. Shah, J. Zhao and R. P. Van Duyne, "Biosensing with plasmonic nanosensor", Nat Mater, Vol. 7, No. 6, P. 442–453, 2008.

**14.** J. F. Li, Y. F. Huang, Y. Ding, Z. L. Yang, S. B. Li, X. Sh. Zhou, F. R. Fan, W. Zhang, Z. Y. Zhou, D. Y. Wu, B. Ren, Z. L. Wang and Z. Q. Tian, "Shell-isolated nanoparticle-enhanced Raman spectroscopy". Nature, Vol. 464, No. 7287, P. 392–395, 2010.

**15.** M. P. Cecchini, V. A. Turek, J. Paget, A.A. Kornyshev and J. B. Edel, "Self-assembled nanoparticle arrays for multiphase trace analyte detection", Nat Mater, Vol. 12, No. 2, P. 165–17, 2013.

**16.** F. De Angelis, F. Gentile, F. Mecarini , G. Das, M. Moretti, P. Candeloro, M. L. Coluccio, G. Cojoc, A. Accardo, C. Liberale, R. P. Zaccaria, G. Perozziello, L. Tirinato, A. Toma, G. Cuda, R. Cingolani and E. Di Fabrizio "Breaking the diffusion limit with super-

hydrophobic delivery of molecules to plasmonic nanofocusing SERS structures", Nat Photonics, Vol. 5, No.11, P. 682–687, 2011.

**17.** E. C. Lin, J. Fang, S. C. Park, F. W. Johnson, H. O. Jacobs, "Effective localized collection and identification of airborne species through electrodynamic precipitation and SERS based detection", Nat Commun, Vol. 4, No. 163, 2013.

**18.** E. L. Ru and P. Etchegion, "Principles of Surface Enhanced Raman Spectroscopy and related plasmonic effect", First edition, Elsevier, 2009.

**19.** S. Feng , J. Lin, Z. Huang, G. Chen, W. Chen, Y. Wang, R. Chen and H. Zeng, "Esophageal Cancer Detection Based on Tissue Surface-Enhanced Raman Spectroscopy and Multivariate Analysis", Appl. Phys. Lett., Vol. 102, No. 4, P. 043702–043704, 2013.

**20.** J. Chen, G. Qin, J. Wang, J. Yu, B. Shen, S. Li, Y. Ren, L. Zuo, W. Shen and B. Das, " One-step fabrication of sub-10-nm plasmonic nanogaps for reliable SERS sensing of microorganisms", Biosens. Bioelectron., Vol. 44, No. 191, 2013.

**21.** L. Guerrini, J. V. Garcia-Ramos, C. Domingo and S. SanchezCortes, " Sensing polycyclic aromatic hydrocarbons with dithiocarbamate-functionalized ag nanoparticles by surface-enhanced Raman scattering", Anal. Chem., Vol. 81, No. 3, 2009.

**22.** P.C. Lee, D. Meisel, "Adsorption and surface-enhanced Raman of dyes on silver and gold sols", Journal of Phys.Ch., Vol. 86, No. 17, 1982.

**23.** M. Fleischmann, P. J. Hendra and A. J. Mcquilla, "Raman spectra of pyridine adsorbed at a silver electrode", Chem Phys Lett., Vol. 26, P. 163-166, 1974.

**24.** M. A. Khan, T. P. Hogan and B. Shanker, "Metallic nanorods synthesis and application in surface enhanced Raman spectroscopy", Vol.1, No.1, 2009.

**25.** M. Birnbaum, "Semiconductor surface damage produced by ruby lasers", J. Appl. Phys., Vol. 36 , 1965.

**26.** Z. Guosheng, P. M. Fauchet, and A. E. Siegman, "Growth of spontaneous periodic surface-structures on solids during laser illumination", Phys. Rev. B, Vol. 26, No. 10, P. 5366−5381, 1982.

**27.** L. Bayera, M. Ehrhardta, P. Lorenza, M. Mäserb and K. Zimmera, "Large-area picosecond laser-induced periodic surface structure (LIPSS) on chromium", 9th International Conference on Photonic Tech., LANE 2016.

**28.** M. Hongo and Sh. Matsuo," Sub nanosecond-laser-induced periodic surface structures on prescratched silicon substrate", App. Ph. Exp., Vol. 9, 2016.

**29.** M. Fabiani, E. Rebollar, S. Perez, D. R. Rueda, M. C. García-Gutierrez, A. Szymczyk, Z. Roslaniec, M. Castillejo, and T. A. Ezquerra, " Laser-Induced Periodic Surface Structures Nanofabricated on Poly(trimethylene terephthalate) Spin-Coated Films", Langmuir, Vol. 28, P. 7938−7945, 2012.

**30.** J. Reif, O. Varlamova, M. Ratzke, M. Schade, H. S. Leipner, T. Arguirov, "Multipulse feedback in self-organized ripples formation upon femtosecond laser ablation from silicon", Appl. Phys. A-Mater. Sci. Process., Vol. 101, No. 2, P. 361−365, 2010.

**31.** M. Bolle, S. Lazare, M. Leblanc, A. Wilmes, "Submicron periodic structures produced on polymer surfaces with polarized excimer laser ultraviolet-radiation", Appl. Phys. Lett., Vol. 60, No. 6, P. 674− 676, 1992.

**32.** M. Csete, S. Hild, A. Plettl, P. Ziemann, Z. Bor, O. Marti, "The role of original surface roughness in laser-induced periodic surface structure formation process on poly-carbonate films", Thin Solid Films, Vol. 453, 2004.

**33.**K. L. Mittal, " Polymer surface modification: Relevance to adhesion", taylor and Francis group, Vol. 4, 2007.

**34.**C. V. Raman, K. Krishnan, "A new type of secondary radiation", Nature, Vol. 121, No. 3048, P.501- 502, 1928.

**35.**J. R. Ferraro and K. Nakamoto, "Introductory Raman Spectroscopy", Academic Press Ltd., 1994.

**36.**Q. wang, "Raman spectroscopic characterization and analysis of agricultural and biological systems", graduate theses and dissertations, paper 13019, 2013.

**37.**R. L. McCreery, "Raman spectroscopy for chemical analysis", Wiely-interscience, 2000.

**38.**H. A. Szymanshki, " Raman spectroscopy: Theory and practice" NewYork, NY, USA, Plenum Press, 1967.

**39.**K. M. Hamasha, "Raman spectroscopy for the microbiological characterization and identification of medically relevant bacteria", graduate theses and dissertations, 2011.

**40.**R. Singh, "Physics in perspective", Vol.4, P. 399- 420, 2002.

**41.**U. K. Sur, " Surface- enhanced Raman scattering (SERS) spectroscopy: a versatile spectroscopic and analytical technique used in nanoscience and nanotechnology", Advances in nano research, Vol. 1, No. 2, P. 111-124, 2013.

**42.**P.F. Liao, J.G. Bergman, D.S. Chemla, A. Wokaun, J. Melngailis, A.M. Hawryluk and N.P. Economou, "Surface-enhanced raman scattering from microlithographic silver particle surfaces", Vol. 82, P. 355-359, 1981.

**43.**R. E. Howard, P. F. Liao, W. J. Skocpol, L. D. Jackel and H. G. Craighead, " Microfabrication as a scientific tool", Vol. 221, P.117-121, 1983.

**44.**P Kambhampati, MC Foster and A Campion, "Two-dimensional localization of adsorbate/substrate charge-transfer excited states of

molecules adsorbed on metal surfaces", the Journal of che. Phy., Vol. 110, No. 1, P. 551-558, 1999.

**45.** G. C. Schatz, M. A. Young, and R. P. Van Duyne, "Electromagnetic Mechanism of SERS", Top. Appl. Phys., Vol. 103, P. 19-45, 2006.

**46.** J. R. Ferraro, K. Nakamoto and C. W. Brown, "Introductory Raman Spectroscopy", 2nd edition, Elsevier, 2003.

**47.** D. Bhandari, " Surface- enhanced Raman scattering: substrate development and applications in analytical detection", graduate theses and dissertations, 2011.

**48.** H. Xu, J. Aizpurua, M. Ka and P. Apell "Electromagnetic contributions to single-molecule sensitivity in surface-enhanced Raman scattering" Physical Review E 62(3): 4318-4324, 2000.

**49.** X. Huang and M. A. El-sayed," Gold nanoparticles: optical properties and implementations in cancer diagnosis and photothermal therapy", J. Adv. Res., Vo. 1, P. 13-28, 2010.

**50.** K. a. Willets and R. P. Van Duyne, " Localized surface Plasmon resonance spectroscopy and sensing" Ann. Rev. Phys. Chem., Vol. 58, P. 267- 297, 2007.

**51.** J. Brockman, B. Nelson, and R. Corn, "Surface Plasmon Resonance Imaging Measurements of Ultrathin Organic Films", Annual Review of Phys.Ch, Vol. 51, P. 41–63, 2000.

**52.** W. Knoll, "Interfaces and Thin Films as Seen by Bound Electromagnetic Waves", Ann. Rev of Phys. Ch., Vol. 49, P. 569–638, 1998.

**53.** K. Kelly, E. Coronado, L. Zhao, and G. Schatz," The Optical Properties of Metal Nanoparticles: The Influence of Size, Shape, and Dielectric Environment", Journal of Phys. Ch., Vol.107, P. 668–677, 2003

**54.** A. J. Haes, C. L. Haynes, A. D. McFarland, G. C. Schatz, R. P. Van Duyne and Sh. Zou, " Plasmonic Materials for Surface-Enhanced Sensing and Spectroscopy", MRS Bulletin, Vol. 30, P. 368–375, 2005.

**55.**V. Weber," Plasmonic nanostructures for the realization of sensors based on surface enhanced Raman spectroscopy", graduate theses and dissertations, 2013.

**56.**R. Aroca, "In Surface-Enhanced Vibrational Spectroscopy", John Wiley & Sons, Chichester, 2006.

**57.**C. Kavitha, K. Bramhaiah, N. S. John, B. E. Ramachandran, " Low cost, ultra-thin films of reduced graphene oxide–Ag nanoparticle hybrids as SERS based excellent dye", Chem. Phys. Lett., Vol. 629, P. 81-86, 2015.

**58.**C. Haynesand and R. P. Van Duyne, "Plasmon-Sampled Surface-Enhanced Raman Excitation Spectroscopy", Journal of Phys. Che. B, Vol. 107, P. 7426–7433, 2003.

**59.**D. Bhandari, S M. Wells, S. T. Retterer, and M. J. Sepaniak, "Characterization and Detection of Uranyl Ion Sorption on Silver Surfaces Using Surface Enhanced Raman Spectroscopy", Ana. Ch., Vol. 81, P. 8061–8067, 2009.

**60.**J. Oran, R. Hinde, N. Abu Hatab, S. Retterer, and M.Sepaniak, "Nanofabricated Periodic Arrays of Silver Elliptical Discs as SERS Substrates", Journal of Raman Spectroscopy, Vol. 39, P. 1811–1820, 2008.

**61.**S. A. Maier, " Plasmonic: Fundamentals and applications", springer, 2007.

**62.**E. C. Dreaden, A. M. Alkilany, X. Huang, C. J. Murphy, and M. A. ElSayed, " The golden age: gold nanoparticles for biomedicine", Chem. Soc. Rev., Vol. 41, No.7, 2012

**63.**J. A. Creighton, C. G. Blatchford and M. G. Albrecht, "Plasma resonance enhancement of Raman scattering by pyridine adsorbed on silver or gold sol particles of size comparable to the excitation wavelength", Chem. Soc. Faraday Trans. II, 1979.

**64.**A. Fojtik, A. Henglein and M. Giesig, "Formation of Nanometer-Size Silicon Particles in a Laser Induced Plasma in SiH4", Ber. Bunsenges. Phys. Chem., Vol. 97, 1993.

**65.**J. Nedderson, G. Chumanov and T. M. Cotton, " Laser Ablation of Metals: A New Method for Preparing SERS Active Colloids", Appl. Spectrosc., Vol.47, 1993.

**66.**S. Nie and S. Emery, "Probing Single Molecules and Single Nanoparticles by Surface-Enhanced Raman Scattering", Science Vol. 275, P. 1102–1106, 1997.

**67.**W. B. Cai. , B. Ren. , X. Q. Li. , .C. X. She, F. M. Liu, X. W. Cai, Z. Q. Tian ,"Investigation of Surface-Enhanced Raman Scattering from Platinum Electrodes using a Confocal Raman Microscope: Dependence of Surface Roughening Pretreatment", Surface Science Vol.406, P. 9–22, 1998.

**68.**Y. Xie, , D.Y.Wu, G. K. Liu, Z. F. Huang, B. Ren, J. W. Yan, Z. L. Yang and Z. Q. Tian, "Adsorption and Photon-Driven Charge Transfer of Pyridine on a Cobalt Electrode Analyzed by Surface Enhanced Raman Spectroscopy and Relevant Theories", Journal of Electro analytical Ch. Vol. 554, P. 417–425, 2003.

**69.**C. H. Munro, W. E. Smith, M. Garner, J. Clarkson, and P. C. White, "Characterization of the surface of a citrate-reduced colloid optimized for use as a substrate for surface- enhanced resonance Raman scattering", Langmuir, Vol.11, 1995.

**70.**D. J. White, "Nanostructured Optical Fiber for use as Miniature Surface-enhanced Raman Scattering Sensors", graduate theses and dissertations, 2008.

**71.**I. Khan, D. Cunningham, R. E. Littleford, D. Graham, W. E. Smith, and D. W. McComb, " From micro to nano: Analysis of surface-enhanced resonance Raman spectroscopy active sites via multiscale correlations", *Analytical Chemistry*, Vol. 78, No. 1, 2006.

**72.**M. Moskovits, "Surface-enhanced Raman spectroscopy: a brief retrospective", J. Raman Spectrosc., Vol. 36, 2005.

**73.**C. L. Haynes and R. P. Van Duyne, "Nanosphere Lithography: A Versatile Nanofabrication Tool for Studies of Size-Dependent Nanoparticle Optics". J. Phys. Chem. B, Vol. 105, P 5599–5611, 2001.

**74.**Q. Yu, P. Guan, D. Qin, G. Golden and P. M. Wallace, "Inverted Size-Dependence of Surface-Enhanced Raman Scattering on Gold Nanohole and Nanodisk Arrays", Nano Lett., Vol. 8, P. 1923–1928, 2008.

**75.**L. Gunnarsson, E. J. Bjerneld, H. Xu, S. Petronis, B. Kasemo and M. Käll, " Interparticle Coupling Effects in Nanofabricated Substrates for Surface-Enhanced Raman Scattering", Appl. Phys. Lett., Vol. 78, 2001.

**76.**J. D. Kim, "A study of structure formation on PET, PBT and PS surfaces by excimer laser ablation", graduate theses and dissertations, 2004.

**77.**H. G. Rubahn, "Laser applications in surface science and technology", John Wiley and sons, NY, 1999.

**78.**D. J. Elliot, "Ultraviolet laser technology and applications", Academic press Inc, San Diego, 1995.

**79.**C. P. Grigoropoulos" Transport in Laser Microfabrication: Fundamentals and applications", Cambridge University press, 2009.

**80.**M. Stafe, A. Marcu and N. N. Puscas, "Pulsed Laser ablation of solids basics theory and applications", Springer, Vol.53, 2014.

**81.**J. E. Andrew, P. E. Dyer, D. Forster, and P. H. Key, " Direct etching of polymeric materials", Appl. Phys. Lett., Vol. 43, No. 717, 1983.

**82.**R. Srinivasan and B. Braren, " Ablative photodecomposition of polymer films by pulsed far-ultraviolet (193 nm) laser radiation: dependence of etch depth on experimental conditions", J. Polym. Sci Polym. Chem., Vol. 22, 1984.

**83.**A. Miotello and P. M. Ossi, "Laser-Surface Interactions for New Materials Production, tailoring Structure and Properties", Springer Series in Materials Science, Vol.130, 2010.

**84.**S. Lazare and V.Granier, " Ultraviolet Laser Photoablation of Polymers: A Review and Recent Results", Vol. 10, No.1, 1989.

**85.**W. W. Duley, "UV Lasers: Effects and Applications in Materials Science", Cambridge University Press, Cambridge, 1996.

**86.**Denn, M. M., "Process Modeling, Longman", New York, 1986.

**87.**Vincelette, A. R., C. S. Guerrero, P. J. Carreau, and P. G. Lafleur, "A Model for Single Screw Plasticating Extruders", Int. Polym. Process, Vol. 4, P. 232–241, 1989.

**88.**A. Kumar, R. K. Gupta, "Fundamentals of polymer engineering", 2nd edition, MARCEL DEKKER, INC., 2003.

**89.**C. Gan, Y. Zhang, S.W. Liu, Y. Wang, M.Xiao," Linear and nonlinear optical refractions of CR39 composite with CdSe nanocrystals", Optical Materials, Vol. 30 , P. 1440–1445, 2008.

**90.**B. Sh. Jooybari, H. Afarideh, M. L. Rachti and M. Ghergherehchi, "Modification on chemical and optical properties of PADC polymer by ArF laser (193 nm) irradiation", Polym Eng, Vol. 34, No. 4, 2015.

**91.**P. E. Dyer, " Excimer laser polymer ablation: twenty years on ", Appl. Phys. A, Vol. 77, No.2, 2003.

**92.**P. E. Dyer, "Laser Ablation of Polymers, Photochemical Processing of Electronic Materials", ed. by I. W. Boyd and R. B. Jackman Academic London 1992.

**93.**R. Srinivasan and B. Braren, "Ultraviolet laser ablation of organic polymers", Chem. Rev., Vol. 89, No. 6, P.1303-1316, 1989.

**94.**M. Ozdemir and H. Sadikoglu, "Trends in Food Science and Technology", Vol. 9, 1998.

**95.**R. Srinivasan and W. J. Leigh, "Ablative photodecomposition: action of far-ultraviolet (193 nm) laser radiation on poly(ethylene terephthalate) films", *J. Am. Chem. Soc.*, Vol. 104, No. 24, P. 6784–6785, 1982.

**96.**J. Rabek, "Photodegradation of Polymers", Springer-Verlag, NY, 1996.

**97.** J. H. Brannon and J. R. Lankard, "Pulsed CO2 laser etching of polyimide", Applied Phys. Letters, Pulsed CO2 laser etching of polyimide", Vol.48, P.1226-1228. 1986.

**98.** P. E. Dyer, G. A. Oldershaw and J. Sidhu, "CO2 laser ablative etching of polyethylene terephthalate", APP. Ph. B Photophysics and Laser Ch., Vol. 48, No. 6, pp.489-493, 1989.

**99.** M. Rosenberger, S. Hessler, H. Pauer, M. Girschikofsky, G. L. Roth, B. Adelmann, H. Woern, B.Schmauss and R. Hellmann, " Polymer planner waveguide bragg gratings: fabrication, characterization, and sensing applications", Integrated Optics: Devices, Materials and Technologies XXI, Proc. of SPIE, 2017.

**100.** M. F. Zaki, " Gamma- induced modification on optical band gap of CR-39 SSNTD", Brazilian Journal of Phy., Vol. 38, No. 4, 2008.

**101.** V. Srinivasan, M. A. Smrtic and S. V. Babu, "Excimer laser etching of polymers", J. Appl. Phys., Vol. 59, No. 11, P. 3861-3867, 1986.

**102.** H. Schmidt, J. Ihlemann, B. Wolff-Rottke, K. Luther and J. Troe, " Ultraviolet laser ablation of polymers: spot size, pulse duration, and plume attenuation effects explained", Journal of App. Phys., Vol. 83, 1998.

**103.** F. P. Incropera and D. P. Dewitt, "Introduction to heat transfer", Wiley, NY, 1st edition, 1985.

**104.** P.E. Dyer, S.D. Jenkins and J. Sidhu, "Development and origin of conical structures on XeCl laser ablated polyimide", Appl. Phys. Lett., Vol. 49, 1986.

**105.** C. Wochnowski, S. Metev and G. Sepold, "UV-laser-assisted modification ofthe optical properties of poly methyl methacrylate", Appl. Surf. Sci., 2000.

**106.** S. Cockcroft, P.E. Dyer, C. Moore, C.D. Walton and R. Zakaria, "Ablation of pristine and radiation exposed CR-39 polymer using a 157

nm laser", in: CLEO/Europe and EQEC 2009 Conference Digest, Munich, 2009.

**107.** B. Hopp, Z.S. Bor, E. Homolya and E. Mihalik, Investigation of conical structures created by ArF excimer laser irradiation of polycarbonate, Appl. Surf. Sci., 1997.

**108.** A. Costela, I. Garcı a-Moreno and F. Florido "Laser ablation of polymeric materials at 157 nm", J. Appl. Phys., Vol. 77, 1995.

**109.** C. Paterson, A.S. Holmes and R.W. Smith, "Excimer laser ablation of microstructures: a numerical model", J. Appl. Phys., Vol. 86, 1999.

**110.** I. Ta chang, "Excimer laer ablation of polymer- clay nanocomposites", graduate theses and dissertations, 2012.

**111.** J. Rabek, "Photodegradation of Polymers", Springer-Verlag, NY, 1996.

**112.** F. Kokai, H. Saito and T. Fujioka, "Micromolecules", Vol. 23, 1993.

**113.** E. Sancaktar and H. Lu, "The effects of excimer laser irradiation at 248 nm on the surface mass loss and thermal properties of PS, ABS, PA6, and PC polymers," J. Appl. Polym. Sci., Vol. 99, 2006.

**114.** A. Rodriguez-Rodriguez, E. Rebollar, M. Soccio, T. A. Ezquerra, D. R. Rueda, J. Vicente Garcia-Ramos, M. Castillejo and M. C. Garcia-Gutierrez, "Laser-Induced Periodic Surface Structures on Conjugated Polymers: Poly(3-hexylthiophene)", Macromolecules, Vol. 48, No. 12, P. 4024-4031, 2015.

**115.** E. Rebollar, S. Pérez, J.J. Hernández, I. Martín-Fabiani, D.R. Rueda, T.A. Ezquerra and M. Castillejo, "Assessment and formation mechanism of laser-induced periodic surface structures on polymer spin-coated films in real and reciprocal space", Langmuir, Vol. 27, 2011.

**116.** M. Csete and Z. Bor, "Laser- induced periodic surface structure formation on polyethylene-tere phthalate", Appl. Surf. Sci., Vol. 133, No. 5, 1998.

**117.** P. Slepicka, E. Rebollar, J. Heitz and V. Svorcík, "Gold coatings on polyethyleneterephthalate nano-patterned by F2 laser irradiation Appl. Surf. Sci., Vol. 254, No. 11, 2008.

**118.** E. Rebollar, I. Frischauf, M. Olbrich, T. Peterbauer, S. Hering, J. Preiner, P. Hinterdorfer, C. Romanin and J. Heitz, " Proliferation of aligned mammalian cells on laser-nanostructured polystyrene", Biomaterials, Vol. 29, No. 12, 2008.

**119.** D. Bäuerle, " Laser processing and chemistry", Springer-Verlag, Berlin, 2000.

**120.** M. Castillejo, P. M. Ossi and L. higiler editors, "Laser in materials science", Springer, Vol. 191, 2014.

**121.** Chen, J.; Qin, G.; Wang, J.; Yu, J.; Shen, B.; Li, S.; Ren, Y.; Zuo, L.; Shen, W.; Das, B. Biosens. Bioelectron. 2013, 44, 191.

**122.** X. Zhang, C. R. Yonzon, M. A. Stuart and R. P. Van Duyne, " Surface-enhanced raman spectroscopy biosensors: excitation spectroscopy for optimization of substrates fabricated by nanosphere lithography", IEE Proc. Nanobiotechnol, Vol. 152, No. 6, 2005.

**123.** J. Sylvia, J. Janni, J. Klein, & K. Spencer, " Surface-Enhanced Raman Detection of 1,4-Dinitro Toluene Impurity Vapor as a Marker to Locate Landmines", Analytical Chemistry, Vol. 72, P. 5834–5840, 2000.

**124.** S. Cinta-Pinzaru, N. Peica, B. Kustner, S. Schlucker, M. Schmitt, T. Frosch, J. H. Faber, G. Bringmann and J. Popp, "FT-Raman and NIR-SERS Characterization of the Antimalarial Drugs Chloroquine and Mefloquine and their Interaction with Hematin", Journal of Raman Spectroscopy, Vol. 37, P. 326–334, 2006.

**125.** J. Binoy, I. Joe, V. Jayakumar, O. Nielsen, and J. Aubard, "DFT Based Relaxed PES Scan Studies and SERS of Anti-Cancer Drug, Combretastatin A-4", Laser Physics Letters, Vol. 2, P. 544–550, 2005.

**126.** A. V. Szeghalmi, L. Leopold, S. Pinzaru, V. Chis, I. S. Dumitrescu, M. Schmit, J. Popp and W. Kiefer "Adsorption of 6-Mercaptopurine

and 6-Mercaptopurine Riboside on Silver Colloid: a pH Dependent Surface Enhanced Raman Spectroscopy and Density Functional Theory Study", Part I. 6-Mercaptopurine, Journal of molecular structures, Vol. 735, P. 103–113, 2005.

**127.** A. V. Szeghalmi, L. Leopold, S. Pinzaru, V. Chis, I. S. Dumitrescu, M. Schmit, J. Popp and W. Kiefer, " Adsorption of 6-Mercaptopurine and 6-MercaptopurineRiboside on Silver Colloid: A pH-Dependent Surface-Enhanced Raman Spectroscopy and Density Functional Theory Study", II. 6-Mercaptopurine Riboside, Biopolymers, Vol. 78, P. 298–310, 2005.

**128.** K. C. Bantz, "Recent progress In SERS biosensing", Phys. Chem. Chem. Phys., Vol. 13, P. 11551- 11567, 2011.

**129.** A. Tereshchenko, " Optical biosensors on ZnO nanostructures: advantages and perspectives. A review", Sensors and actuators B, chemical, Vol. 229, P. 664- 677, 2016.

**130.** F. Long, A. Zhu, H. Shi, " Recent advances in optical biosensors for environmental monitoring and early warning", sensor, Vol. 13, P. 13928- 13948, 2013.

**131.** R. P. Singh, "Prospects of nanobiomaterials for biosensing", Int. J. of Electrochemistry, 2011.

**132.** K. T. Carron and L. G. Hurley, "Axial and azimuthal angle determination with surface-enhanced Raman spectroscopy: Thiophenol on copper, silver and gold metal surfaces", J. Phys. Chem., Vol. 95, No. 24, 1991.

**133.** S. Sriram, M. Bhaskaran, S. Chen, S. Jayawardhana, P. R. Stoddart, J. Z. Liu, N. V. Medhekar, K. Kalantar-Zadeh, and A. Mitchell, “Influence of electric field on SERS: frequency effects, intensity changes, and susceptible bonds.,” J. Am. Chem. Soc., Vol. 134, pp. 4646–53, 2012.

**134.** F. Schreiber, "Structure and growth of self-assembling monolayers", Prog. Surf. Sci., Vol.65, 2000.

**135.** C. M. Whelan, M. R. Smyth and C. L. Barnes, "HREELS, XPS, and electrochemical study of benzenethiol adsorption on Au(111)", Langmuir, Vol. 15, 1999.

**136.** M. J. Focazio, D. W. Kolpin, K. K. Barnes, E. T. Furlong, M. T. Meyer, S. D. Zaugg, L. B. Barber and M. E. Thurman, "A National Reconnaissance for Pharmaceuticals and other Wastewater Contaminants in the United States - II) Untreated Drinking Water Sources", Science of the Total Environment, Vol. 402, P. 201–216, 2008.

**137.** J. McLachlan, "Environmental Signaling: What Embryos and Evolution Teach us about Endocrine Disrupting Chemicals", Endocrine Reviews, Vol. 22, P. 319–341, 2001.

**138.** D. Sedlak, J. Gray, and K. Pinkston," Contaminants in Recycled Water", Environmental Science & Technology, Vol. 34, P. 509A–515A, 2000.

**139.** US national library of medicine, https://pubchem.ncbi.nlm.nih.gov/compound/methylene_blue#section=Top.

**140.** M. Oz, D. E. Lorke, M. Hasan, and G. A. Petroianu, " Cellular and molecular actions of methylene blue in the nervous system", Medicinal Research Reviews, Vol. 31, No. 1, 2011.

**141.** R. Suwanarusk, B. Russell, A. Ong, K. Sriprawat, CS Chu, A. Pyaephyo, B. Malleret, F. Nosten and L. Renia " Methylene blue inhibits the asexual development of vivax malaria parasites from a region of increasing chloroquine resistance", Journal of Antimicrobial chemotherapy, Vol. 70, No. 1, 2015.

**142.** FDA communication, "Risk of methemoglobinemia in the medicine cabinet", Pharmacy today, 2012.

**143.** BC cancer agency cancer drug manual, drug name (Ifosfamide), developed 1994, revised 2010.

**144.** A. A. Moosa, A. M. Ridha, N. A. Kadhim, "Use of biocomposite adsorbents for the removal of methylene blue dye from aqueous solution", American journal of materials science, Vol. 6, No. 5, 2016.

**145.** E. Rebollar , G. Bounos , M. Oujja, S. Georgiou and M. Castillejo, "Effect of Molecular Weight on the Morphological Modifications Induced by UV Laser Ablation of Doped Polymers", J. Phys. Chem. B, Vol. 110, No. 33,p. 16452–16458, 2006.

**146.** P. Slepička, J. Heitz, J. Siegel, M. Spirkova and V. Svorcik, "F2-Laser Angle Nanomodification of PET", Materials Science Forum, Vols. 567-568, p. 257-260, 2008.

**147.** J. Siegel, P. Slepicˇka, J. Heitz, Z. Kolska, P. Sajdl, V. Sˇvorcˇı´k, " Gold nano-wires and nano-layers at laser-induced nano-ripples on PET", Appl. Surface Science, Vol. 256, 2010.

**148.** J. Heitz B. Reisinger, S. Yakunin, N. H. Voelcker, Q. Peng, A. L. Hook, Ch. Romanim and M. Fahrner, "Laser-Induced Micro- and Nanostructures at Polymer Surfaces for Applications in Cell Biology", IEEE, 2011.

**149.** K. T. Kim, J. Y. oh, B. S. Shin and D. S. Park," Surface treatment of polyimide film by pulsed UV laser ablation and its effect on the electrochemical characteristics", Bull. Korean chem. Soc., Vol. 33, No. 12, 2012.

**150.** S. Perez, E. Rebollar, M. Oujja, M. Martín and M. Castillejo, "Laser-induced periodic surface structuring of biopolymers", Appl. Phys. A, Vol.110, No. 3, 2013.

**151.** C. Dorronsoro, J. Bonse, and J. Siegel," Self- assembly of a new type of periodic surface structures in a copolymer by excimer laser irradiation above the ablation threshold", Journal of Appl. Phys., Vol. 114, 2013.

**152.** R. A. Barb, C. Hrelescu, L. Dong, J. Hritz, J. Siegel, P. Slepicka, V. Vosmanska, V. Svorcik, B. Magnus, R. Marksteiner, M. Schernthaner and k. Groschner, "Laser induced periodic surface structures on polymers for formation of gold nanowires and activation of human cells", Appl. Phys. A, Vol.117, 2014.

**153.** J. Jacob, P. Shanmugavelu, R.Balasubramaniam and R. K.Singh, "Study and analysis of thermal effects during the excimer laser ablation of polymers in different gaseous environment", AIMTDR, 2014.

**154.** B. Shakeri Jooybari, " ArF laser ablation of CR-39 polymer: Effect of irradiation on cone structure formation", Physics Procedia, Vol. 80, P. 155-158, 2015.

**155.** I. Michaljanicova, P. Slepicka, J. Heitz, R. A. Barb, P. Sajdi and V. Svorcik "Comparison of KrF and ArF excimer laser treatment of biopolymer", Appl. Surface science, Vol. 339, P. 144-150, 2015.

**156.** S. Behrouzinia "Hydrophobic investigation of Excimer Laser effects on poly(Ethylene Terephthalate)", IJFPS, Vol. 6, No.2, p. 4-8, 2016.

**157.** A. Pospori, C. A. F. Marques, O. Bang, D. J. Webb, and P. André." Polymer optical fiber bragg grating inscription with a single UV laser pulse", Optics express, Vol.25, No. 8, 2017.

**158.** ANSYS v11 multiphysics software, Release 11.0sp1 UP20070830.

**159.** ASM international, "Characterization and failure analysis of plastics", ASM international, materials park, OH, 2003.

**160.** M. J. Weber, "Handbook of Optical Materials", CRC Press, 2002.

**161.** W. Kam, Y. S. Ong, W. H. Lim, R. Zakaria, "Laser ablation and waveguide fabrication using CR39 polymer", Optics and lasers in Eng., Vol. 55, P. 1-4, 2014.

**162.** R. S. Kappes, F. Schonfled, C. Li, A. A. Goleiz, M. Nagel, Th. Lippert, H. J. Butt and J. S. Gutmann " A study of photothermal laser ablation of various polymers on microsecond time scales", springer plus, Vol. 3, 2014.

**163.** C-R Yang, Y. S. Hsieh, G. Y. Hwang and Y. D. Lee, " Photoablation characteristics of novel polyimides synthesized for high-aspect-ratio excimer laser LIGA process", J. Micrmech. Microeng, Vol. 14, No.4, 2004.

**164.** P. Parvin " Regular self-microstructuring on CR39 using high UV laser dose", Appl. Surface Science, Vol. 292, 2014.

**165.** R. Zakaria, "157 nm $F_2$ laser characterization and application to polymer ablation", graduate theses and dissertations, 2009.

**166.** M. Li, "Effects of post- thermal treatment on preparation of surface microstructures induced by polarized laser on polyimide film", Mater. Chem Phys., Vol. 77, No.3, 2002.

**167.** M. Csete, O. Marti and Z. Bor, "Laser-induced periodic surface structures on different poly-carbonate films", Appl. Phys. A, Vol. 73, P. 521-526, 2001.

**168.** E. N. Saad, M. F. Eissa, E. A. Badawi and M. A. K. El-Fayoumi, "Investigation of the physical properties of polymeric materials induced by alpha radiation", Int. Journal of adv. Research, Vol.2, No.12, 2014.

**169.** E. Rebollar " Physicochemical modifications accompanying UV laser induced surface structures on poly(ethyleneterephthalate) and their effect on adhesion of the mesenchymal cells", phys. Chem. Chem. Phys., Vol. 16, 2014.

**170.** E. Rebollar, S. Perez, J. J. Hernandez, I. Martin-Fabiani, D. R. Rueda, T. A. Ezquerra, and M. Castillejo, "Assessment and formation mechanism of laser-induced periodic surface structures on polymer spin-coated films in real and reciprocal space", Langmuir, Vol. 27, No.9, 2011.

**171.** J. Bonse, M. Munz, and H. Sturm, "Structure formation on the surface of indium phosphide irradiated by femtosecond laser pulses", Journal of Appl. Phys., Vol. 97, 2005.

**172.** M. Huang, F. Zhao, Y. Cheng, N. Xu, and Z. Xu, "The morphological and optical characteristics of femtosecond laser-induced large-area micro/nanostructures on GaAs, Si, and brass", Optics Express, Vol. 18, 2010.

**173.** J. ZENG and A.N. NETRAVALI, "KrF excimer laser surface modification of ultrahigh molecular weight polyethylene fibers for improved adhesion to epoxy resins", Polymer Surface Modification: Relevance to Adhesion, Vol. 3, pp. 159-182 Ed. K.L. Mittal, 2004.

**174.** S. Mihailov, W. Duley, "Laser beam surface treating and coating", Proc. SPIE , Vol. 957, P. 111-120, 1988.

**175.** NA Borisevich, NN Khovratovich , Opt. Spectrosc., Vol.10, P. 309-313, 1961.

**176.** P. Slepička, A. Chaloupka, P. Sajdi, J. Heiz, V. Hnatowicz and V. Svorcik "Angle dependent laser nanopatterning of poly(ethylene terephthalate) surfaces" , Applied Surface Science, Vol. 257, P. 6021-6025, 2011.

**177.** P. Slepi!ka1, O. Ned"la, J. Siegel, R. Krajcar, Z. Kolská and V. vor!ík, "Ripple polystyrene nano-pattern induced by KrF laser", Express Polymer Letters, Vol. 8, P. 459-466, 2014.

**178.** A. Johansson, S. Stafstrom, "Interactions between molecular wires and a gold surface",Chem.Phys.Lett., Vol. 322, 2000.

**179.** T. H. Joo, M. S. Kim and K. Kim, "Surface-enhanced Raman scattering of benzenethiol in silver sol", J. Raman Spectrosc., Vol. 18, No.1, 1987.

**180.** G. Xue, M. Ma, J. Zhang, Y. Lu and K. T. Carron, "SERS and XPS studies of the molecular orientation of thiophenols from the gaseous state onto silver". Journal of Colloid and Interface Science, Vol. 150, No. 1, 1992.

**181.** L. A. S. Pereira "Micro- Raman spectroscopy characterization of a CR-39 detector", Appl. Spectr., Vol. 67, No.4, 2013.

**182.** H. Wackerbarth “Hierarchical self-assembly of designed 2´2-a-helix bundle proteins on Au(111) surfaces”, Langmuir, Vol. 22, 2006.

**183.** H. Wackerbarth, M. Grubb, J. Zhang, AG. Hansen and J. Ulstrup "Long-range order of organized ligonucleotide monolayers on Au(111) electrodes", Langmuir, Vol. 20, 2004.

**184.** M. Schwartzkopf, "From atoms to layers: in situ gold cluster growth kinetics during sputter deposition", Nanoscale, Vol. 5, No.11, 2013.

**185.** M. Couillard. "Subsurface modifications in indium phosphide induced by single and multiple femtosecond laser pulses: A study on the formation of periodic ripples", Journal of Appl. Phys., Vol. 101, No.3, 2007.

**186.** C. J. Sandroff and D. R. Herschbach, " Surface- Enhanced Raman study of organic sulfides adsorbed on silver: facile cleavage of sulfur-sulfur and carbon- sulfur bonds", J. of Phys. Ch., Vol. 86, No. 17, 1982.

**187.** E. Rebollar, " Gold coating on polymer laser induced periodic surface structures: Assessment as substrates for surface- enhanced Raman scattering", Phys. Ch. Ch. Phys., Vol. 14, 2012.

**188.** A. Gopinath, S.V. Boriskina, B.M. Reinhard and L.D. Negro, "Deterministic aperiodic arrays of metal nanoparticles for surface-enhanced Raman scattering (SERS)", Opt. Express vol. 17, p. 3741-53, 2009.

**189.** D. McFarland, M. A. Young, J. A. Dieringer, and R. P. Van Duyne, “Wavelength-Scanned Surface-Enhanced Raman Excitation Spectroscopy,” A., *J. Phys. Chem. B.,* Vol. 109, P. 11279-11285, 2005.

**190.** E. Rebollar, " laser- induced surface structures on gold- coated polymers: Influence of morphology on surface- enhanced Raman Scattering enhancement", J. of appl. Pol. Science, 2015.

**191.** E. C. Le RU, E. Blackie, M. Meyer and P. G. Etchegoin, " Surface Enhanced Raman Scattering Enhancement factors: A comprehensive study", J. Phys. Chem., Vol. 111, 2007.

**192.** R. Buividas, P.R. Stoddart and S. Juodkazis, "Laser fabricated ripple substrates for surface-enahnced Raman scattering", Ann. Phys., Vol. 524, No.11, 2012.

**193.** A. Chou, E. Jaatinen, R. Buividas, G. Seniutinas, S. Juodkazis, E.L. Izake and P.M. Fredericks, "SERS substrate for detection of explosives", Nanoscale, Vol.4 , No. 23, P.7419–7424, 2012.

**194.** T. Gunnarsson, T. Rindzevicius, J. Prikulis, B. Kasemo, M. Kail, S. Zou, G.C. Shatz, 'Confined plasmons in nanofabricated single silver particle pairs: experimental observations ofstrong interparticle interactions", J. Phys. Chem. B vol. 109, p. 10791087, 2005.

**195.** W. Rechberger, A. Hohenau, A. Keitner, J.R. Krenn, B. Lamprecht, F.R Aussenegg, "Optical properties oftwo interacting gold nanoparticles", Opt. Commun, vol. 220, p. 137-141,2003.

**196.** R.M. Bakker, A. Boltasseva, Z. Liu, R.H. Pedersen, S. Gresillon, A.V. Kildishev, V.P. Drachev, V.M. Shalaev, "Near-field excitation ofnanoantenna resonance", Opt. Express, vol. 15, p. 13682-13688,2007.

**197.** G. N. Xiao, S. Q. Man, " Surface enhanced Raman scattering of Methylene blue adsorbed on cap-shaped silver nanoparticles" Chem. Phys. Lett, Vol. 447, 2007.

وزارة التعليم العالي والبحث العلمي
جامعة بغداد
معهد الليزر للدراسات العليا

# دراسة سطح CR39 المعدل بليزر فلوريد الاركون كمتحسس لتشتت رامان

أطـروحة مقدمة الى

معهد الليزر للدراسات العليا/جامعة بغداد/لاستكمال متطلبات نيل شهادة دكتوراه فلسفة في الليزر/ الهندسة الالكترونية والاتصالات

من قبل

**رنا محمد طه البياتي**

بكالوريوس هندسة الليزر و الالكترونيات البصرية – 2001
ماجستير هندسة الليزر و الالكترونيات البصرية – 2004

بإشراف

الأستاذ المساعد الدكتور حسين علي جواد

1439هـ 2017 م

**الخلاصة**

ان تطور المتحسسات البايولوجية عالية التحسس والكشف السريع وتشخيص مستوى التأثر للملوثات الطبية الحيوية في الطبيعة اصبحت من المجالات الفعالة للبحوث. تعتبر اطياف رامان من التقنيات الفعالة في التوصيف الجزيئي ولكن لسوء الحظ تكون الاشارة المسجلة ضعيفة. ان تحسين السطح في تشتت رامان يسهل عملية التسجيل الجزيئي لانها تحسن الاشارة الضعيفة بشكل ملحوظ.

في هذا البحث, تم استخدام نموذج العنصر المحدد ثنائي الاتجاه لفهم افضل للسلوك الفيزيائي المصاحب لعملية استئصال البوليمر بالليزر ثم تم اجراء الابحاث العملية لانتاج قاعدة تحسن تشتت رامان باستخدام عملية الاستئصال بالليزر.

ليزر الاكسيمر ذو الطول الموجي 193 نانومتر فلوريد الاركون بطاقة قصوى 330 ملي جول, امر نبضة 15 نانوثانية ومعدل تكرارية 1 هيرتز قد تم استخدامه لتشعيع نماذج البوليمرات من نوع CR39. ان مادتي الثايوفينول والمثيلين الازرق تم توظيفهما للتحقق من التشخيص والتحسس للمواد المستخدمة المحسنة لتشتت رامان.

ان المواد التي تم تصنيعها لتكون جاهزة لتقوية تشتت رامان تمثل تركيب سطحي دوري يسمى عادة " التراكيب السطحية الدورية المحتثة بالليزر" وبثلاثة تشكيلات مختلفة وهي (السلاسل النانوية, الشكل المحيطي, الاخاديد) على سطح البوليمر CR39 مع فترة تعاقب من 630 – 822 نانومتربكثافة طاقة فوق عتبة الاستئصال المسجلة (250 ملي جول/سم$^2$). ان عتبة الاستئصال المسجلة كانت بشكل مقارب جدا لما سجل في نتائج التمثيل النظري في حالة تكرارية نبضات الليزر.

السطوح نانوية التركيب المصنعة تم اكساؤها بطبقة من مادة الذهب وباسماك مختلفة. ان امكانية المادة المصنعة في تقوية تشتت رامان تم تقييمها من خلال مادة اختبارية وهي الثايوفينول

كجزيئة محللة. وقد لوحظ ان التركيب المصنع ذو الشكل الاخدودي المطلي بسمك 30 نانومتر من الذهب اعطى افضل معامل تحسين بحدود $0.9*10^{8}$ الى $2*10^{8}$ وهو مناسب لكشف جزيئة منفردة.

ان كفاءة المادة المنتجة كمتحسس للمواد الحيوية قد تم فحصها باستخدام مادة المثيلين الازرق. ان حساسية جهاز المتحسس للمواد الحيوية قد وصفت من خلال كشف تركيز منخفض لمادة المثيلين الازرق ولمدى كشف قدره 0.1 مايكرومولر.